Sensor Arrays for the Measurement of Dispersive, Flexural Waves in Structures for Signal-to-Noise Ratio Enhancement and Angle of Arrival Determination

by

Carol Jaeger Wynn

Dissertation submitted to the Faculty of the

Virginia Polytechnic Institute and State University

in partial fulfillment of the requirements for the degree of

Doctor of Philosophy

in

Mechanical Engineering

APPROVED:

Alfred L. Wicks, Chairman

Harry H. Robertshaw

Robert G. Leonard

William T. Baumann

William R. Saunders

Harley H. Cudney

September, 1993
Blacksburg, Virginia

Sensor Arrays for the Measurement of Dispersive, Flexural Waves in Structures for Signal-to-Noise Ratio Enhancement and Angle of Arrival Determination

This work examines the application of sensor arrays to structures. The wave equation solution of Euler–Bernoulli beam theory provides the structural model for this study. A review of basic array theories for the enhancement of signal-to-noise ratio (SNR) and determination of angle of arrival (AOA) leading to source localization is given. Array techniques are considered with applications to dispersive flexural waves where the propagation velocity is not constant but dependent on frequency.

The theory is validated through experiments with harmonic and broad band applications. The test apparatus consisted of a long thin beam with anechoic terminations to emulate an infinite beam for frequencies above 300 Hz and a finite beam below 200 Hz. The beam was excited by a shaker (with a force transducer) mounted on one end of the beam. Measurements were taken with accelerometers and a laser velicometer at the other end of the beam. The infinite beam case was used to isolate the travelling wave response to single harmonic excitation. The finite case was used to consider transient response of the beam to an impulse.

The harmonic response experiments on the infinite beam is used to demonstrate two things. First they show that the SNR increases by the square root of the number of sensors. Secondly they show that AOA can be determined explicitly from the phase between sensors for single frequency applications. The measured values of AOA were within ± 3 degrees for these experiments. This technique applies to harmonic signals in a highly damped medium.

The technique developed for transient applications uses the magnitude and the variance of the correlation coefficient of a densely populated array to determine AOA. This technique is based on correlation between measurements along a wave front. It does not assume a phase relationship between sensors but instead exploits the spread of the signal as it travels. The spread is characteristic of a dispersive medium. This resolution of this technique is directly linked to the population of the array and the angular relationship between elements. The experiments verified that this technique measures the AOA for within the resolution of the array. For arrays from 3x4 to 7x10 resolution of $\pm$ 6 to 9 degrees was possible.

This work has developed array theory for application to dispersive waves in structures. It highlights the differences in the phase relationship between elements for dispersive versus non dispersive media. It shows improvement of SNR using structural arrays. The potential for AOA determination on highly damped structures using harmonic signals was demonstrated. AOA determination was also shown for finite structures using impact excitation.

Acknowledgements

I would like to thank those who have helped me in this endeavor, first my advisor, Dr. Alfred Wicks, particularly for his help of late. Also thanks to my other committee members, Dr. H. H. Robertshaw, Dr. R. G. Leonard, Dr. W. R. Saunders, Dr. W. T. Baumann, and Dr. H. H. Cudney for their support.

Thanks to the department for its financial support.

Thanks to all my friends and colleagues for their assistance.

Thanks go to my parents and family for their love and support in this undertaking.

Most of all thanks go to my husband, Robert, AROU.

Contents

List of Figures

List of Tables

Nomenclature

Lower case

Symbol	Definition	Unit
a	location of input force	$in.$
c	wave speed in medium	$in./sec$
c_0	velocity	$in./sec$
c_Q	velocity	$in./sec$
d_i	distance from source to sensor i	$in.$
f	frequency	Hz
i	imaginary operator,$\sqrt{-1}$	
k	structural wave number	$in.^{-1}$
m	sensor index	
m_s	number of sensors	
n_i	noise at element i	volts,V
s	sensor separation in x direction	$in.$
s_{xy}	sensor separation between sensors x and y	$in.$
$u_i(t)$	signal from source i	
v	wave velocity	$in./sec$
w_i	weighting of sensor i	
x, y, z	cartesian coordinates	$in.$

Upper case

Symbol	Definition	Unit
A	cross sectional area	$in.^2$
AG	array gain	dimensionless or dB
E	Young's modulus	psi
$E[\,]$	expected value operation	
F	applied force	lbf
$\mathcal{F}^{-1}$	Inverse Fourier Transform	
I	area moment of inertia	$in.^4$
J	mass moment of inertia	$lbm - in.^2$
K	wave number	in^{-1}
$\mathcal{K}$	shear stiffness	lbf
$\mathcal{M}$	mass	lbm
M	moment	$lbf - in.$
$P_x x$	power spectra of x	
$P_x y$	cross spectra of x and y	
R^2	area moment of Inertia per unit Area(I/A)	$in.^2$
$\mathbf{R_x}$	covariance matrix of x	
$S(i)$	output of array element i	volts,V
SNR	signal to noise ratio	
$\mathcal{X}$	shear distribution parameter	
V	shear	$lbf/in.^2$
W	magnitude of incident wave	

Greek Symbols

Symbol	Definition	Unit
γ	shear strain	
$\gamma(z)$	true variation of shear strain	
δ	dirac delta function	
λ	wavelength	$in.$
ν	Fourier variable (Appendix A)	
ν	Poisson's ratio (Chapter1)	
ϕ	phase lag or time delay	radians or seconds
ρ	density	$lbm/in.^3$
σ^2	variance	V^2
σ	standard deviation	V
θ	Angle of Arrival	rad
υ_i	uncertainty in measurement i	
ζ	sensor separation along propagation axis	$in.$
ω	angular frequency	rad/sec
Θ'	mass moment of inertia of beam	$lbm - in.^2$

Chapter 1

Introduction

The use of sensor arrays has long existed in sonar, radar, ultrasound, and satellites, just to mention a few applications. However, these applications have been limited to materials where propagation is through a known fluid such as water, or air. Applications of sensor arrays for structures also have great potential as a measurement tool.

The advantages of sensor arrays in structures (over single element sensors) are similar to the advantages found in the above mentioned applications. There is an enhancement in signal to noise ratio - usually quantified by the term array gain (AG). The direction or angle of arrival (AOA) of the signal can be determined if the wave propagation speed is known. With different wave types (flexural, shear, or longitudinal), the arrival times can be used to give range measurements. The techniques used in arrays can be applied directly to harmonic excitation of structures.

There are many possibilities for array concepts that have been untried in other applications but would enhance performance here. If piezoelectrics were used, they could be used as actuators as well as sensors. Phase and amplitude variation will

allow beamforming actuation and the generation of complex excitations by simply changing the weights and phases of the inputs.

It is the purpose of this work to explore the use of array sensors as they apply to structures. The first chapter develops the theory for vibrations of beams. It presents different models specifying the criteria of validity for each. It also presents the differences between infinite and finite structures and appropriately between travelling and standing waves.

Chapter two develops the theories used in array processing. It explains how arrays can improve signal-to-noise ratio and determine direction of arrival or range and depth information about sources.

Chapter three develops the application of array processing to structures. It details how the array processing applies to travelling waves in beams as a first approximation to structures. In particular, it considers the complications of dealing with the dispersive nature of flexural waves.

Chapter four gives the experimental results of applying array processing to an infinite beam (travelling waves). It discusses the instrumentation and resolution considerations involved in developing a system.

Chapter five gives the experimental results of applying array processing to transient signals on a finite beam (broad band applications).

The analysis uses the response of sensors on a beam to prove enhanced signal to noise ratio and source localization determination. Other advantages and actuation applications will be discussed.

1.1 Beam Theory

Vibrations in structures have been studied in great detail. Many authors have surveyed the subject, for a more in-depth review of the material see (Abramson, 1957; Abramson *et al.,* 1958; Miklowitz 1960). In general, two approaches to modelling vibrations are taken. Modal models represent the vibrations as a summation of orthogonal mode shapes. In most applications, with the exception of structural acoustics, modal models are generally used over wave models; but they are inaccurate for sharp impacts or infinite structures. Infinite structures are those structures which absorb most or all energy before that that energy can reach a terminus and reflect. This is indicative of heavily damped systems.

Wave models are used in (though not limited to) acoustics as well as infinite structures. An infinite beam, for example, has no natural modes so a mode shape solution would be impossible. Wave models represent the vibrations as a summation of vibrations with both near-field and far field terms. Near-field waves are waves that exist close to the source; far-field terms refer to those that have propagated away from the source.

1.2 Beam Theories and Approximations

The study of beams is generally a first step in the study of structures since beams represent the simplest of structures, (Abramson, *et al.,* 1958). While beams are simple structures, the boundaries complicate beam analysis by causing reflections. An infinite beam is simpler because it has no end conditions/boundaries; and, therefore, produces no reflections It is an ideal medium for studying the propagation of travelling waves.

Because of the complicated nature of continuous media and the discontinuity at boundaries, beam equations are not simple. These complicated equations have led many theorists (including Euler, Bernoulli, Saint Venant and Timoshenko) to develop simplifying assumptions and solutions to the beam equation.

1.2.1 Euler and Bernoulli

Beam equations fall into a three categories: elementary, approximate, and exact theory. Elementary beam theory has been developed by Bernoulli and Euler and has the governing equation

$$EI \frac{\partial^4 y}{\partial x^4} + \rho A \frac{\partial^2 y}{\partial t^2} = 0 \tag{1.1}$$

where E is Young's modulus, I is the area moment of inertia, ρ is the density, x is the axis variable along the beam width and y is the variable along flexural displacement. This equation is fully developed in appendix A and the Fourier solution of the equation applied to an infinite beam is included there.

A general solution to this equation is the form

$$y = A\sin\beta x + B\cos\beta x + C\sinh\beta x + D\cosh\beta x. \tag{1.2}$$

A wave form solution can also be assumed,

$$y(x,t) = A\cos\frac{2\pi}{\lambda}(x - ct) \tag{1.3}$$

where c is the wave velocity and λ is the wavelength. A full wave solution of the Euler – Bernoulli equation for an infinite beam is given in Appendix A. The assumptions for its validity are given there as well.

Combining equation 1.3 with equation 1.1 yields

$$c = \frac{2\pi}{\lambda}\sqrt{\frac{EI}{\rho A}}. \tag{1.4}$$

From equation 1.4 the propagation velocity is inversely proportional to the wavelength (Meirovitch, 1967). If a disturbance which consists of multiple frequencies, is impacted on the beam, each harmonic component would travel at its corresponding wave velocity effectively dispersing the impact. Unlike deep water and air, a beam is a dispersive medium; a medium where the wave velocity is not constant, but dependent on the wavelength and thus the signal content spreads as it travels.

This inverse relationship, in the limit, also leads to the physically impossible notion that very short wavelengths travel instantaneously along the beam. This is one of the troublesome problems of elementary beam theory and was discovered seemingly

first by Lamb (1917), showing why the elementary theory does not work for sharp impacts. Rayleigh (1894) and Timoshenko (1921, 1922) corrections develop intermediate theory that is more robust than elementary theory.

1.2.2 Rayleigh Approximation

Rayleigh corrected for the effects of rotary inertia and Timoshenko corrected for the transverse deformation from shear. The Rayleigh correction gives a differential equation of the form

$$c_0^2 R^2 \frac{\partial^4 y}{\partial x^4} - R^2 \frac{\partial^4 y}{\partial x^2 \partial t^2} + \frac{\partial^2 y}{\partial t^2} = 0. \tag{1.5}$$

The corresponding velocity and dispersion is related by

$$c = c_0 \sqrt{\frac{\frac{4\pi^2 R^2}{\lambda^2}}{1 + \frac{4\pi^2 R^2}{\lambda^2}}} \tag{1.6}$$

where R^2 is the ratio of the area moment of inertia to the cross-sectional area

$$R^2 = I/A \tag{1.7}$$

and

$$c_0 = \sqrt{\frac{E}{\rho}}. \tag{1.8}$$

1.2.3 Timoshenko Equations

The Timoshenko equation is useful because it is a balance between the simple equation of the elementary theory and the complex equations of the exact theory. Because shear deformations have greater effects on the accuracy of beam model then do rotary inertia effects, Timoshenko corrections are generally chosen as the intermediate model between Euler–Bernoulli and exact theory. The Timoshenko equation is given by

$$\frac{\partial^4 M}{\partial x^4} - \left(\frac{1}{c_0^2} + \frac{1}{c_Q^2}\right)\frac{\partial^4 M}{\partial x^2 \partial t^2} + \frac{1}{c_0^2}\left(\frac{1}{c_Q^2}\frac{\partial^4 M}{\partial t^4} + \frac{1}{c_0^2 R^2}\frac{\partial^2 M}{\partial t^2}\right) = 0 \qquad (1.9)$$

where:

$$c_Q = \frac{GA_s}{\rho A} \quad ; A_s = \int\int \gamma(z) dA \qquad (1.10)$$

G = shear modulus, M = moment , and $\gamma(z)$ = true variation of γ , the shear strain, over the area.

Unlike the other theories it is impossible to write an explicit expression for c, but by solving the equations above an expression for c is given by

$$1 - \left(\frac{c^2}{c_0^2} + \frac{c^2}{c_Q^2}\right) + \frac{c^4}{c_Q^2 c_0^2} - \frac{c^2}{R^2 c_0^2 k^2} = 0 \qquad (1.11)$$

1.3 Literature Review

Many reviews of the literature of vibrations as they apply to beams exist. Miklowitz (1960) has an excellent review of the study of elastic wave propagation. Miklowitz

concentrates on transient wave propagation in homogeneous, isotropic, linear elastic solids. He considers these as they apply to rods, plates, circular cylindrical shells, half space and infinite mediums.

Abramson *et al.,* (1958) reviews the theories, assumptions and limitations of stress wave analysis in beams and rods. The authors consider longitudinal and flexural waves, both plastic and elastic. The review begins with the elementary theory, continues through the intermediate theories of Timoshenko, and is compared to the performance of the exact theory.

While much work has obviously been done in the area, many publications are of particular note for how they relate to this work. The application of the many different forms of the beam equations has seen much attention in the literature.

Schaechter (1982) uses elementary theory in his work for demonstrating the hardware controlling flexible beams. His solution is a modal solution as opposed to a wave solution. It is more common to see wave solutions in acoustic applications like power flow measurement, but control and measurement can be achieved with wave models as well. Meirovitch and Norris (1984) and Meirovitch *et al.,* (1984) discuss the use of modal models in the modelling and control of distributed systems.

Von Flotow and Schafer (1986) consider the merits of modal versus wave models, particularly in how they apply to control applications. They purport that an alternative to low authority feedback controllers (when high authority, full state feedback is impossible from lightly damped modes and model uncertainty) is an approach based

on wave models. This view is considered appropriate for large spacecraft structures where major forces are spatially and temporally localized. The paper then continues using elementary beam theory to develop a wave absorbing controller.

Carroll (1987) uses Bernoulli theory in his study of structural response and power flow measurements. The emphasis of his dissertation was using quadrature for discriminating against reverberation so he studies the one-dimensional case of flexural wave propagation in a finite beam.

Gonidou (1988) uses Bernoulli-Euler theory solved using fourier transforms for infinite, semi-infinite, and finite beams. Gonidou studies the active control of flexural power flow in thin beams. Guigou (1992) also uses Bernoulli-Euler theory solved via fourier transforms to solve for semi-infinite and finite beams.

Jones (1955) uses Timoshenko theory to explore transient flexural stresses in an infinite beam. The solution is obtained by means of fourier transforms, from asymptotic approximations. The results are of the numerical form unlike the similar paper by Dengler and Goland (1952) where their solutions are of the integrand form. Dengler and Goland also use the Timoshenko equations to solve for transverse impact of long beams and also offer corrections to a similar solution by Uflyand (1950).

Boley and Chao (1955) study transverse impacts using Timoshenko equations, but they use Laplace transforms to solve the equations. The solutions are again given in integral forms and must be evaluated numerically.

Anderson (1954) considers how Timoshenko equations determine the wavelength distribution of the bending-moment and shear-force responses to both a force impulse (transverse) and a moment impulse. The solution is for infinite beams.

Miklowitz (1953) solves coupled Timoshenko equations (as opposed to a single variable equation) representing rotational and translatory motions of the beam using Laplace transforms. Miklowitz's work shows agreement with the solution of Dengler and Goland (1952). The derivation of transforms for both finite and infinite beams is presented.

Plass (1958) provides a collection of numerical solutions to the Timoshenko beam equations. He solves various end conditions with half-sine wave impacts numerically and one by Laplace transforms as well. Oliver (1957) looks at the response of cylindrical rods to short pulses.

Some work has also been done with the exact theory. Abramson (1957) uses the analysis as outlined by Love (1927) to study flexural waves in beams of circular cross section. Devault and Curtis (1959) outline a procedure for formulating exact theory solutions of elastic cylindrical rods.

What can be seen from all of this is that appropriate theories can be used depending on the application. If rotary inertia and shear effects are truly negligible then Euler-Bernoulli models are adequate. This is true when the following assumptions are met

- cross-sectional dimensions are small compared to the length
- transverse sections remain planar and normal to the length in bending

- rotary inertia effects are negligible
- shear deformations are small compared to flexural deformations.

The necessity of going to a more complex model, such as the Timoshenko equation is mandated by the accuracy of the model to a particular application. In applying sensor arrays to structures, the critical consideration is the propating velocity of the wave for it defines the phase relationship between array elements. As long as the theory predicts the velocity with acceptable accuracy, elementary theory is applicable. For simplicity sake in this experiment, the structure and frequencies of interest have been chosen so that Euler – Bernoulli theory is appropriate. The work can be applied to different structures, simply by using the wave velocity, wave length, etc., indicated by the application. Applications to plates and more complicated structures can be done as well. It is interesting to note that the difference between an Euler – Bernoulli beam equation and the plate equation is that E is replaced with $E(1-\nu)$ because elasticity is constrained in width as well as length, (Cremer *et al.*, 1988).

While it is obvious that much has been done in this field, the work of Carroll (1987), Gonidou (1988), and Guigou(1992) apply directly. The powerflow models by Carrol (1987) and Gonidou(1988) and solutions presented by Guigou (1992) were the models and solutions used in this work. These provide a fourier wave solution to the Euler-Bernoulli model of flexural vibration. The other work presented in this review can be used to develop different wave models when the simplifying assumptions of Euler-Bernoulli theory are not met.

Chapter 2

Sensor Array Processing

Array Processing Introduction

Now that the foundation for structures is established, the next step is to consider how array processing can be applied to the measurement of vibrations. First, the author wishes to introduce and review the vast body of array literature as it already exists in other applications and then bring the reader to an understanding of how these techniques can be applied to structures.

There are at least two ways to consider the array literature that exists. One is to consider the literature and techniques within the applications for array processing; the other is to consider the types of analysis that are available. A little of both is done here. A review of techniques is given first with an in-depth look at what can be accomplished and how. Then a few paragraphs are provided to acquaint the audience with the gamut of applications of array processing.

A look at the techniques follows.

2.1 Array Processing

Nicholas and Vezzosi (1991) give a summation of the history of the development of array processing techniques. "In recent years, an extensive body of theory and practice has been developed for spatial array processing. The need for higher resolution of the source field image, has led to an evolution in these techniques, from classical beamforming to the Capon estimator, autoregressive methods and finally the high resolution methods based on the eigen decomposition of the cross spectral matrix measured at the array output." The following is a review of the literature of the present usage of these techniques as they apply to some of the usages detailed above.

2.1.1 Basic Array Theory

To gain an understanding of basic array properties, an investigation into a simple array pattern(s) is useful.

The simplest, and one of the most common array patterns is the uniform linear array (ULA). Bendat and Piersol (1986), among others, described the basics of linear arrays. Figure 2.1 shows the geometry of a typical linear array.

Assume that a wave source exists in (or on) a medium and that the sensors are positioned such that the distance from the source to the sensors is much greater than the separation between sensors. For a wave propagating normal to the array in a homogeneous medium, the signal can be estimated to hit the array as a planar wave. When the wave impacts the sensors as a planar wave, the signal history at

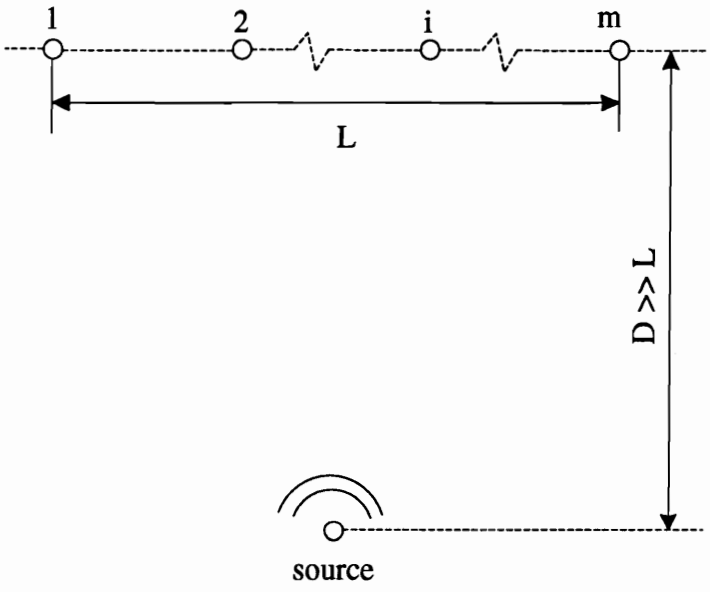

Figure 2.1: Schematic of Simple Linear Array

each sensor has the same deterministic content, the signal content is the same except for noise. For example, if the model in figure 2.1 is a linear array of m_s sensors, the output of each sensor can be written

$$S_i(t) = f(x(t)) + n_i(t). \tag{2.1}$$

If the model further assumes that the noise for each sensor, $n_i(t)$, is zero mean, statistically independent, and of the same variance (i.e. each sensor is equally noisy), then the array's gain can be quantified. Array gain is a measure of the signal to noise ratio improvement.

If the output of each element is qualified by Eq. 2.1 then the array output given by the average of the sensors is

$$\bar{S}(t) = \frac{1}{m_s} \sum_{i=1}^{m} [f(x(t)) + n_i(t)] \tag{2.2}$$

or equivalently

$$\bar{S}(t) = f(x(t)) + \frac{1}{m_s} \sum_{i=1}^{m} n_i(t). \tag{2.3}$$

Using the statistical relationship $\sigma_{\bar{x}}^2 = \frac{\sigma_x^2}{N}$ where N is the number of samples the variance of the array is given by

$$\sigma_{\bar{s}}^2 = \sigma_f^2 + \frac{\sigma_n^2}{m_s} \tag{2.4}$$

where m_s is the number of sensors, $\sigma_{\bar{s}}^2$ is the variance of the array average, σ_f^2 is the

variance of the correlated signal, and σ_n^2 is the variance of the noise on a sensor. The signal to noise ratios (both in and out) are then given by

$$(\text{SNR})_{in} = \frac{\sigma_f}{\sigma_n} \tag{2.5}$$

$$(\text{SNR})_{out} = \frac{\sigma_f}{\sigma_n/\sqrt{m_s}} = \sqrt{m_s}\ (\text{SNR})_{in}. \tag{2.6}$$

This relationship shows that the output signal to noise ratio is increased by a factor of $\sqrt{m_s}$. This is usually referred to as the array gain and is often give in decibels.

2.1.2 Directivity

The above relationships are true only when the source is normal to the array. This is because the array has directivity. As the source moves off normal, the planar wave hits the array at an angle, see figure 2.2. As the angle of incidence increases, the sensors no longer receive coincidently; a pure time delay occurs between adjacent sensors. If the spacing between sensors is uniform, then the time delay between the sensors is the same.

A standard method of quantifying the directivity of an array is to develop the directivity pattern. A directivity pattern characterizes the behavior of the array for all angles. For a ULA assuming a harmonic source, the signal reaching the center element of the array can be expressed as $S_0(t) = \sin(wt)$. The other sensors' equations are given by $S_m(t) = \sin(wt + m\phi)$ where ϕ is the phase lag (or time delay) and m is

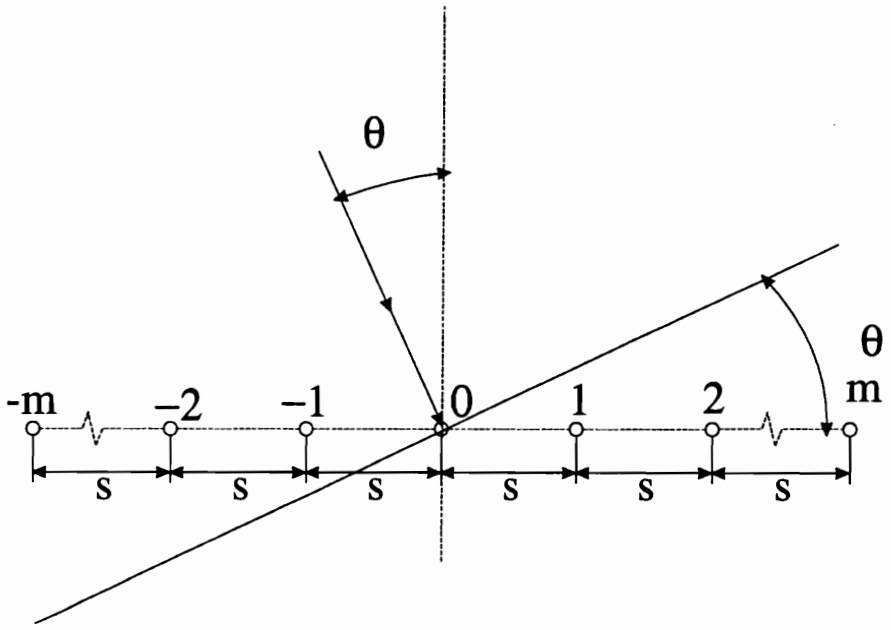

Figure 2.2: Angle of Arrival and Time Delay Schematic for Linear Array

the sensor index. If the propagation velocity, c, is constant, then $m\Delta t = ms\sin\theta/c$ and $m\phi = Kms$; where s is the spacing between sensors and the trace wave number, $K = \frac{2\pi f}{c}\sin(\theta)$. A typical pattern is given in figure 2.3. For a uniform linear array the directivity pattern can be described by the following equation.

$$AG = \frac{\sin(m_s K \sin\theta s/2)}{m_s \sin(K \sin\theta s/2)} \tag{2.7}$$

What can be seen from the beam pattern is that the response of the array is dependent on the spacing of the sensors relative to the wavenumber as well as on the AOA. As ks decreases (and equivalently s/λ decreases) the array loses its directivity. The output of the array becomes omnidirectional.

In a beam, where the propagation is not constant $m\Delta t = ms\sin\theta/c$ and $m\phi = kms\sin(\theta)$, where k is the structural wave number (as given by eq. A.13). The time delay between sensors is not the same at different frequencies as c is not the same at different frequencies. If the phase lag between sensors is known, the angle of incidence, commonly called angle of arrival (AOA), can be calculated. Thus with an array, and the phase information provided, source localization can be accomplished.

The inverse problem is also true for arrays. If the incoming wave's direction can be determined by the phase lag between sensors, then a directional wave could be created from an actuator array if the proper phase relationships are held. In active sonar and radar this is what is known as beamforming. Beamforming allows radar and sonar to send out a signal in a particular direction and watch/listen for reflec-

tions/echoes.

What can be seen with arrays is an improvement in performance that is quantified by the array gain (AG). For uniform linear arrays (ULA) the AG is $\sqrt{m_s}$ when the incoming signal is normal to the array so that the signals arrive coincidently; but when the signal is not incident normal to the array the phasing cause the AG to diminish. The beam pattern describes the array's performance for all angles of incidence, for a given relationship between wavenumber and spacing. The fact that the array's output is maximized along an axis suggests the array's directivity. This directivity can be exploited to determine the source's direction, relative to the array. The determination of AOA is the emphasis of much array processing.

2.1.3 Beamforming

The beamformer is an array processing technique that defines a set of weights for each element that allows the array to steer its directivity pattern. The main lobe of the array can be tuned to an angle where before it was fixed at normal to the array. The set of weights are the phase delays required to steer the beam (or main lobe) along a direction.

It is standard practice to write the beamformer equations denoting one sensor as a reference element. If s_{ir} = the distance between the reference sensor and sensor i, the weight of each sensor is then given by

$$w_{ir} = \frac{1}{m_s} e^{-i2\pi s_{ir} \sin\theta/\lambda}. \tag{2.8}$$

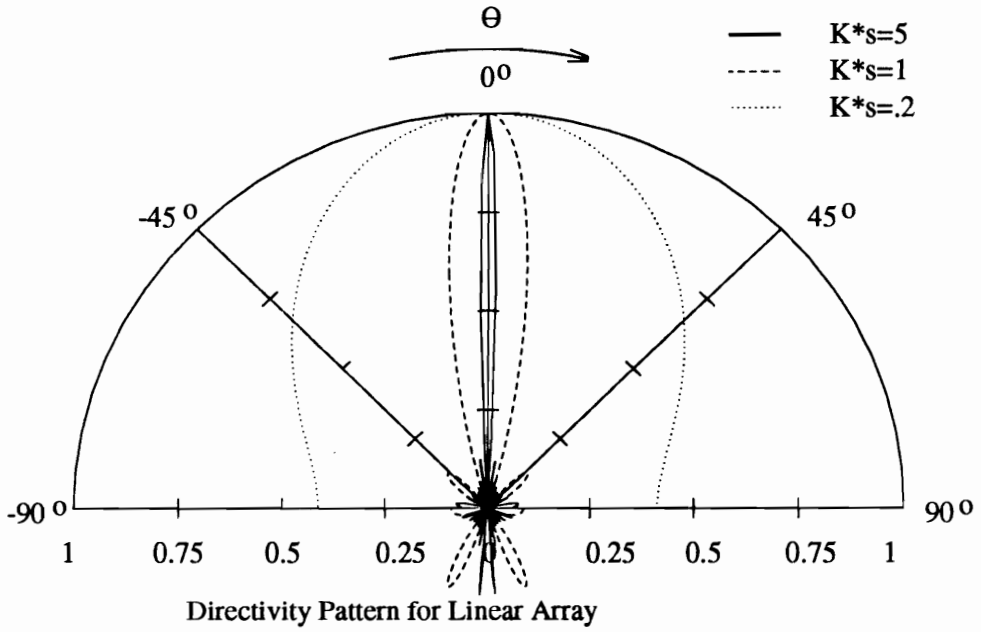

Figure 2.3: Beam Pattern for a linear array

For structures it is convenient to rewrite this as

$$w_{ir} = \frac{1}{m_s} e^{-iks_{ir}\sin\theta}. \tag{2.9}$$

where k is the structural wave number. The output of the array can be expressed as

$$y(t) = \sum_{1}^{m_s} w_i(\theta) x_i(t), \tag{2.10}$$

which can be more conveniently written in vector notation as

$$y(t) = \mathbf{w}^T(t)\mathbf{x}(t). \tag{2.11}$$

The classic beamformer gives the same directivity pattern as seen in figure 2.3, only shifted to the look direction. The output power of the classic beamformer is given by the expression

$$P(\theta) = E[|y(t)|^2] = \mathbf{w}^H(t)\mathbf{R}\mathbf{w}(t). \tag{2.12}$$

If one looks at the performance of a conventional beamformer, one sees that the main lobe is fairly wide and that side lobes exist as well. Thus if more that one source is present, the contributions from the other source(s) will cause bias error in the estimator output in the direction of the other source(s) direction(s). Because of the side lobe interference much emphasis has been made in creating high resolution techniques.

2.2 High Resolution Passive Array Processing

High resolution processing encompasses a series of technique to enhance the resolution of passive techniques, usually with reference to directional information. Bienvenu and Owsley (1991) give an overview of the principles of high resolution array processing. High resolution processing is the performance key to passive sonar, trying to create the sharpest image from the information that is receivable.

LeCadre and Ravazzola (1991) detail the extension of high resolution methods to realistic cases. They consider the noise models and the consequences of correlated noise sources, estimation of the additive noise models, noise whitening procedures and state space representations. They consider how these affect responses of the system dependent on the modelling types including ARMA, MUSIC, Maximum likelihood and maximum entropy techniques, eigendecomposition and iterative methods. Shang (1989) considers a high-resolution method of source localization processing in mode space.

2.2.1 Capon Estimator

To minimize biasing from side lobes of the conventional beamformer, Capon (1969) developed what is now referred to as the Capon estimator. This estimator minimizes the power of the estimator while keeping the gain in the steer direction constant. The weights can then be found to be

$$\mathbf{w}_C = \frac{\mathbf{R}^{-1}\mathbf{w}_B}{\mathbf{w}_B^H \mathbf{R}^{-1}\mathbf{w}_B}, \tag{2.13}$$

where $\mathbf{R}$ is the covariance matrix of $\mathbf{x}$ if $\mathbf{R}$ is a hermetian and positive definite matrix. $\mathbf{w}_B$ are the weights given by the classical beamformer.

Figure 2.4 shows the effects of the higher resolution of the Capon estimator. The output of the estimator is given for two signals at 60 and 100° with a SNR of 20 dB on a 7 element uniform array. Sample covariance was used to calculate the values of the Capon estimator (as it is unlikely that the true covariance of unknown sources would be known). The outputs are normalized by the maximum output.

2.2.2 Linear Predictor Models – AR

Linear Predictor Models were first introduced by Burg in connection with the maximum entropy estimator (1972). The linear predictor uses the covariance matrix to predict one sensor as a linear combination of the remaining sensors. The weights of the estimator are chosen so as to minimize the squared error between the sensor and the estimates.

If $\hat{x}_n$ is the predicted value it is written

$$\hat{x}_n = -\sum_{i=1}^{m_s-1} a_i x_{n-i} \tag{2.14}$$

This process is termed autoregressive as x_n is expressed in terms of itself. The error is then given by

$$\epsilon_n = x_n - \hat{x}_n = \sum_{i=0}^{m_s-1} a_i x_{n-i}; a_0 = 1 \tag{2.15}$$

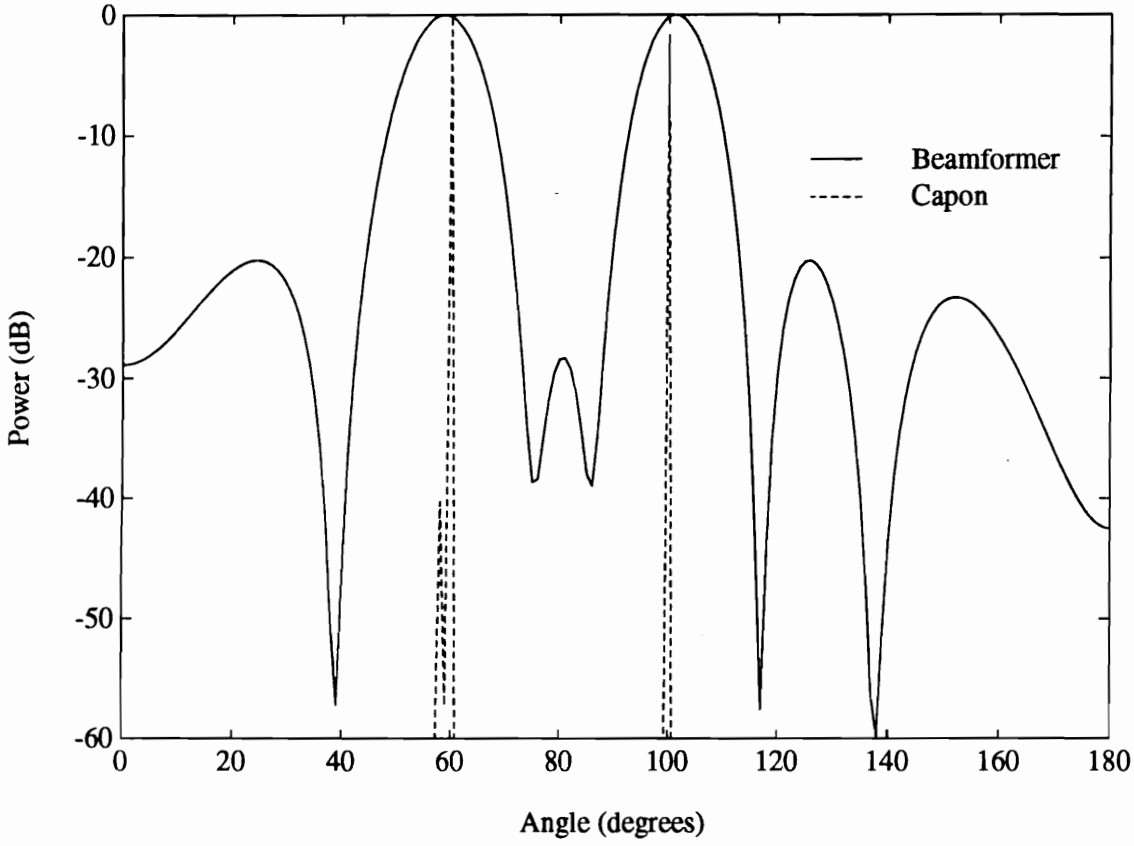

Figure 2.4: Power Output of Beamformer vs. Capon Estimator

the mean square error (MSE) is given by

$$\sum_{i=0}^{m_s-1} a_i E[x_{n-i} x_n^H].$$

In practice for a uniform linear array with uncorrelated sources

$$E[x_{n-i} x_{(n-i)}^H] = r(k-i) = r^*(i-k).$$

minimization of the error leads to the linear predictor which solves the equation

$$\begin{bmatrix} r(0) & r(1) & \dots & r(M-1) \\ r^*(1) & r(0) & \dots & r(M-2) \\ \vdots & \vdots & \ddots & \vdots \\ r^*(M-1) & r^*(M-2) & \dots & r(0) \end{bmatrix} \begin{bmatrix} a_{M-1} \\ a_{M-2} \\ \vdots \\ a_1 \\ 1 \end{bmatrix} = \begin{bmatrix} 0 \\ 0 \\ \vdots \\ 0 \\ \delta_{M-1} \end{bmatrix} \tag{2.16}$$

where δ_{M-1} is defined to be the mean square error of the observed minus the predictor, (Pillai, 1989).

While this methodology appears simple and straight forward, it is important to realize that the cross correlations, r(i), are not known and must be estimated from the sample. The implementation of AR models, and the determination of coefficients is quite involved and beyond the scope of this work. The application of this technique will be discussed in the broader case of ARMA modelling.

2.2.3 ARMA

A broader model uses a transfer function model. An input sequence and output sequence, $u(n)$ and $x(n)$ respectively, are related by the equation

$$x_n = -\sum_{j=1}^{p} a(j)x(n-j) + \sum_{k=0}^{q} b(k)u(n-k) \tag{2.17}$$

This is referred to as an autoregressive moving average (ARMA) model. In transfer function form (between input $u(n)$ and $x(n)$) it is expressed as

$$H(z) = \frac{B(z)}{A(z)}.$$

$A(z)$ is the autoregressive branch and $B(z)$ is the moving average branch. For stability in the z-plane it is assumed that $A(z)$ has its zeros within the unit circle.

AR and ARMA define transfer functions based on an input of white noise. This z-plane transfer function can be exploited to determine AOA. The auto regressive part of the model relates the values of a sensor based on other sensors. The coefficients thus contain information that models the relationship from sensor to sensor. The z^{-1} operator is a pure time delay and is defined $z = e^{j\phi}$. In radar ϕ is referred to as the electrical phase angle and is defined by

$$\phi = \frac{2\pi s}{\lambda} \sin\theta \tag{2.18}$$

where s is the separation between sensors, λ is the wavelength, θ is AOA. By evaluating the transfer function at z values corresponding to the range of AOA's, the

response of the array can be evaluated at all angles. A peak in the transfer function will be seen at the AOA, assuming the ARMA model is estimates the transfer function. The complications of determining the phase angles (from the pure time delay of the z operator) in dispersive media will be considered later.

2.2.4 Eigenvector Based Techniques – MUSIC

Another body of techniques for AOA detection includes eigenvector based algorithms. For a linear array of m_s sensors detecting signals from K independent sources, the signal at any detector can be expressed as

$$x_j(t) = \sum_{k=1}^{K} u_k(t) e^{-ikd_j \sin\theta} + n_j(t), \tag{2.19}$$

where d_j is the distance between source and sensor j; $u_1,\ u_2,\ \ldots\ , u_K$ are the signals of the sources, $\theta_1, \theta_2, ..., \theta_K$ are the AOA of the sources and $x_j(t)$ is the signal seen at the ith sensor location.

Letting $\mathbf{a}(\theta) = e^{-ikd_j \sin\theta}$, this can be written in vector notation as

$$x_j(t) = \mathbf{u}(t)\mathbf{a_j}(\theta) + \mathbf{n}(t) \tag{2.20}$$

where $\mathbf{u} = [u_1, u_2, ..., u_K]^T$, $\mathbf{x} = [x_1(t), x_2(t), ..., x_{m_s}(t)]$

or more succinctly

$$\mathbf{x}(t) = \mathbf{A}\mathbf{u}(t) + \mathbf{n}(t) \tag{2.21}$$

where $\mathbf{A} = [\mathbf{a}(\theta_1), \mathbf{a}(\theta_2), ...\mathbf{a}(\theta_K)]$

The output covariance

$$\mathbf{R} = E[\mathbf{x}(t)\mathbf{x}^H(t)] = \mathbf{A}\mathbf{R}_\mathbf{u}\mathbf{A}^H + \sigma^2\mathbf{I} \tag{2.22}$$

where $\mathbf{R}_\mathbf{u} = E[\mathbf{u}(t)\mathbf{u}^H]$ is the source covariance matrix. Assuming independent (non-coherent) sources, yields that $\mathbf{R}_\mathbf{u}$ is full rank , and from the independence of the direction vectors $\mathbf{A}$ is full rank; yielding that $\mathbf{A}\mathbf{R}_\mathbf{u}\mathbf{A}^H$ is of rank m_s.

Letting $\mu_1, \mu_2, ..., \mu_K$ be the non-zero valued eigenvalues of $\mathbf{A}\mathbf{R}_\mathbf{u}\mathbf{A}^H$, then the eigenvalues of $\mathbf{R}$ are

$$\boldsymbol{\lambda}_R = \begin{cases} \mu_k + \sigma^2 & \text{for } k = 1, 2, .., K \\ \sigma^2 & \text{for } k = K+1, K+2, ..., m_s \end{cases} \tag{2.23}$$

Letting $\mathbf{v}$ be equal to the associated eigenvectors,

$$\mathbf{R} = \boldsymbol{\lambda}\mathbf{v}\mathbf{v}^H = \mathbf{v}\boldsymbol{\Lambda}\mathbf{v}^H. \tag{2.24}$$

For eigenvalues $\boldsymbol{\lambda}_k$ where $k > m_s$,

$$\mathbf{R}\mathbf{v}_i = \sigma^2\mathbf{v}_i = (\mathbf{A}\mathbf{R}_\mathbf{u}\mathbf{A}^H + \sigma^2\mathbf{I})\mathbf{v}_i \tag{2.25}$$

which means

$$\mathbf{A}\mathbf{R}_u\mathbf{A}^H\mathbf{v}_i + \sigma^2\mathbf{I}\mathbf{v}_i = \sigma^2\mathbf{v}_i \tag{2.26}$$

meaning that

$$\mathbf{A}\mathbf{R}_u\mathbf{A}^H = 0. \tag{2.27}$$

This last statement leads to the conclusion that for those values of the eigenvalues (the low repeating values) the corresponding eigenvectors are orthogonal to the direction vectors that dictate the AOA. From Schmidt (1979) this procedure is referred to as MUltiple SIgnal Classification or MUSIC. While MUSIC does not estimate the power of the signals for each AOA, it does guarantee that the peaks of

$$\frac{1}{\sum_{k=K+1}^{M} |\mathbf{v}_i^H\mathbf{a}(\theta)|^2} \tag{2.28}$$

correspond to the true AOA given that the array output covariance $\mathbf{R}$ is known exactly with uncorrelated, identical noise conditions, (Pillai, 1989).

Yang (1990) uses eigenvector decomposition to extract mode amplitudes for data from a vertical array. The product of normal mode amplitudes with steering vectors is a maximum for true source ranges and correlation of decomposed modes with theoretically calculated mode amplitude is maximized at the source depth. Thus source depth and range estimates can be determined. This method is well suited for position uncertainty (slight tilt) of the sensors of a vertical array, but is performance dependant on the ability to measure modes.

2.2.5 Maximum Likelihood Estimation

Most of the high resolution techniques assume that certain parameters are known, and these methods succeed or fail based on how well these parameters are known or how well they can be estimated. This opens the avenue for estimation of these parameters. When these are not known Maximum Likelihood (ML) techniques are often employed.

Maximum likelihood estimation (MLE) and maximum likelihood methods (MLM) estimate a parameter, say γ, by choosing that value of γ that maximizes the probability density function of $y(\gamma)$ using the observed value of y. The logic here being that as y was an observed value it is also a likely value. And this likely (observed) value is probably close to the true value. This value of y can then be used to predict γ.

The advantages of MLE is that if an estimator exists that is unbiased and attains the Cramer-Rao (is efficient) bound, then ML will produce it (Kay, 1988). For sufficiently large data sets ML is unbiased and has a Gaussian distribution. For many linear models the MLE is equivalent to the least squares estimator (LSE). If a system can be described by

$$\mathbf{y} = \mathbf{A}\mathbf{x} + \mathbf{n}, \tag{2.29}$$

where $\mathbf{A}$ is known, $\mathbf{y}$ is the observed data, and $\mathbf{n}$ is zero mean Gaussian noise; then $\mathbf{x}$ can be estimated by

$$\mathbf{x} = (\mathbf{A}^H\mathbf{A})^{-1}\mathbf{A}^H\mathbf{y}. \tag{2.30}$$

This is equivalently the MLE and the LSE. The MLE is not equivalent to the LSE when $\mathbf{A}$ is random or if $\mathbf{n}$ is not mean zero Gaussian noise. However, for nonlinear systems the MLE can require iterative methods to determine a solution.

For AOA applications the problem is to obtain estimates of θ_i from the information received which is $\mathbf{x}$. The data are related as given in equation 2.21. This is a nonlinear problem, and thus the thrust of the research is the maximization and constraint realization. Watanabe *et al.,* (1991) employ MLE techniques using quasi-Newton methods. The computational cost for ML bearing estimation using uniform arrays is low. Lin and Barkat (1991) use dynamic programming to estimate the sources and AOA with the Maximum Likelihood Estimator (MLE). Goryn and Kaveh (1991) show that if there is *a priori* information about the number of sources a conditional ML solution can be obtained. They also present a suboptimal estimator that requires no *a priori* knowledge about the number of signals. They develop competitive feedback network solutions for narrow band direction finding.

MAP(Maximum a posteriori)

A priori refers to those maximizing routines where a knowledge of something is assumed ahead of time. Wahlberg, *et al.,* (1991) consider a robust signal parameter estimation technique to make the estimation less sensitive to perturbations in the array manifold. Since the techniques for parametric estimation have models

that assume perfect knowledge of the arrays reaction to stimuli, the results degrade when the actual array differs from the assumed one. Wahlberg, et. al., offer a MAP (maximum a posteriori estimator) that achieves the Cramer Rao bounds even for moderate sample sizes.

2.2.6 Subarray Processing – ESPRIT

Subarray processing exploits the relationship among subarrays of the full sensor array. There are forward and reverse smoothing routines that are used for coherent or correlated noise scenarios, but probably the most noteworthy of the subarray routines is the ESPRIT routine. Estimation of Signal Parameters via Rotational Invariance Techniques (ESPRIT) uses the relationship to estimate the AOA based on the displacement between the subarrays.

The most common development of the ESPRIT algorithm is for the uniform linear array (ULA). Consider two subarrays

$$\begin{aligned} \mathbf{x}_1^s(t) &= [x_1(t), x_2(t), ..., x_K(t)] \\ \mathbf{x}_2^s(t) &= [x_{m_s-K+1}(t), x_{m_s-K+2}(t), ..., x_{m_s}(t)] \end{aligned} \tag{2.31}$$

these can also be expressed in vector notation as

$$\begin{aligned} \mathbf{x}_1^s &= \mathbf{A}\mathbf{u}(t) + \mathbf{n}_1(t) \\ \mathbf{x}_2^s &= \mathbf{A}\mathbf{B}\mathbf{u}(t) + \mathbf{n}_1(t) \end{aligned} \tag{2.32}$$

where $\mathbf{A}$ is the matrix of direction vectors for the first subarray as developed previ-

ously, see equations 2.19 through 2.21. For ULA, **A** is a Vandermonde matrix.

$$\mathbf{B} = diag[e^{-jk\Delta \sin\theta_1}, e^{-jk\Delta \sin\theta_2}, ..., e^{-jk\Delta \sin\theta_K}].$$

Where Δ is the separation between the subarrays.

In a non coherent signal environment the noise can be found using standard eigenstructure and eliminated. Looking at the covariance and cross variance without the noise one determines

$$\begin{aligned} \mathbf{C}_{x_1^s x_1^s} &= E[\mathbf{x}_1^s \mathbf{x}_1^s] &&= \mathbf{A}\mathbf{R}_\mathbf{u}\mathbf{A}^H \\ \mathbf{C}_{x_1^s x_2^s} &= E[\mathbf{x}_1^s \mathbf{x}_2^s] &&= \mathbf{A}\mathbf{R}_\mathbf{u}\mathbf{B}\mathbf{A}^H \\ \mathbf{C}_{x_1^s x_1^s} - \gamma \mathbf{C}_{x_1^s x_2^s} &= \mathbf{A}\mathbf{R}_\mathbf{u}(\mathbf{I}_\mathbf{K} - \gamma\mathbf{B})\mathbf{A}^H \end{aligned} \tag{2.33}$$

Since both **A** and $\mathbf{R}_\mathbf{u}$ are full rank singular values are given by the roots of

$$|\mathbf{I}_K - \gamma \mathbf{B}^H| = 0 \gamma_k = \mathbf{B}_{kk} = e^{-jk\Delta \sin\theta_k} \tag{2.34}$$

Bas Ober *et al.,* (1991) use an ESPRIT-like algorithm to determine with high resolution angle of arrival information (AOA).

2.2.7 Matched Field Processing (MFP)

Matched field processing is accomplished by comparing the expected response of the array for all source locations within the measured field (Baggeroer *et al.,*, 1988). This is a computationally intense routine, so much of the literature considers means of lowering the computational cost or quantifying the effects of limiting factors. Cox

et al., (1990) create a subarray technique that allows simple planar beamforming techniques to be used where refraction and multipath effects make planar assumptions inapplicable. This method seems to have possibilities in reflected structural waves as well. This method can be applied to MFP while keeping the computational intensity down. Matched field processing is well suited to those applications where reflection and refraction add to the propagation signature of the region, as long as the propagation field is well known.

Tran and Hodgkiss (1991) use matched-field processing at 200 Hz for source detection and localization for a 120 hydrophone array. Livingston and Diachok (1989) use matched-field processing techniques to estimate under-ice reflection amplitude and phase information from continuous wave (CW) sources. These computations were varied iteratively to achieve maximum matched-field processor gain with minimum range and depth errors. Hamson and Heitmeyer (1989) present simulated and experimental results on source localization in shallow water by matched-field processing. Perkins and Kuperman (1990) consider matched field processing in three dimensions to give localization in bearing as well as in range and depth and is demonstrated by a simulation. Nicholas and Vezzosi (1991) show the feasibility of the localization of sources with an array of unknown geometry under a series of conditions. The simulations quantify the validity of the model. Schmidt *et al.*, (1990) develop a matched field beamformer that accommodates some mismatching in the environment while suppressing sidelobes. They derive a multiple constrain matched field processor (MCM).

2.3 Array Processing Summary

As is now evident, the array literature is voluminous. With simple array processing the quality of signals can enhanced. By beamforming through the look directions, signal direction can be estimated. With multiple signals, the Capon estimator, MUSIC, ESPRIT, ARMA, or other complex signal processing can be applied for higher resolution of AOA determination. Estimation techniques, like MLE, can be applied when a needed quantity is unknown. As suspected, the more that is known the better the performance will be. Certain techniques are better suited for a particular set of knowns and unknowns, so smart application of the wealth of techniques is necessary. These techniques are limited by what is known, what is measured, and the quality of the measurement.

These array techniques have obvious applications to structures. The quality of a vibrational measurement can be improved be array processing techniques, but some adaptations meed to be made. For flexural waves a beam is a dispersive media; so when beamforming is done, tuning of the array needs to occur both in frequency and in angle. Thus many of the equations of the algorithms have a phase dependency in two variables.

In structures also the choice of algorithms will depend on what is known, what is measured, and how well it can be measured. Generally with little *a priori* information the incoming signal can be enhanced. For travelling waves in a structure, AOA determination can be accomplished with a knowledge of the phase and spacing among sensors and knowledge of the frequency. With transient waves of different

propagating velocities, range determination can be made.

2.4 Applications of Array Processing Review

As the processing techniques have been introduced, a review of the applications of array techniques is needed.

The use of arrays outside of structures has existed for a long period of time and has many applications. Haykin (1985) gives an overview of array processing techniques and applications included below. A full review of array applications is not possible here, because of size considerations; and because such reviews already exist; if more information is needed Pillai (1989), Bienvenu and Owsley (1991), Kock (1973), Urick (1975) give reviews of the literature and history of arrays as they apply to their works.

Sonar

There are many applications of arrays, one of the most common is sonar. Sonar, both active and passive, uses sound pressure transducers – hydrophones – to determine the spatial and temporal characteristics of an area and create a map of the area of interest. The military application, which is generally a passive technique (listen only) seeks information about other vessels in the vicinity. Active sonar is used to map the ocean floor, by listening for reflections. Very simply, active sonar sends out a signal and listens for the reflections. By measuring the time delay between the sending of the signal and the return of the echo and knowing the wave propagation

speed, the distance to the target can be determined. Using the phase relationship between sensors as discussed above, the direction of the source can likewise be determined.

Preston *et al.*, (1990) use both towed and suspended arrays (horizontal and vertical respectively) to obtain baseline backscattering data of the Tyrrhenian Sea. They use frequency domain beamforming techniques to reduce their data. The work had two purposes: to measure the basin reverberation and backscattering and to compare explosive induced backscatter on both a horizontal and a vertical array. Sergiopoulos and Sullivan (1989) extend the aperture of the physical towed array by coherently combining the acoustic signals arriving at the hydrophones with compensation through a factor that corrects for the phase irregularities in the flow path, the overlap correlator. The overlap correlator uses redundant information to overlap data from a moving array effectively allowing it to perform as subarrays combining to form a larger array.

Stein (1988) uses hydrophones to study a few transient ice events to see how background levels are created in the Arctic Ocean. This work in ice is perhaps most demonstrative of how sensor techniques can be applied to structures. Stein considers three types of wave radiation in ice: flexural, longitudinal, and acoustic. Only flexural waves are dispersive. Stein uses the arrival times of the different wave types to determine the distance to the source. In structures, longitudinal waves travel at a constant velocity while flexural waves travel at speeds determined by their frequency content. If an event creates more than a single wave type, then the arrival times could likewise be used to determine range measurements.

Exploration Seismology

Exploration seismology is an active technique where signals flood an area with wave activity, usually a series of explosions. Then by listening to reflections, refractions, and diffractions, the seismologist determines the physical characteristics of the underground area. This is used to find likely sources of hydrocarbons.

Radar

Radar has similar applications to sonar. It is generally an active technique where a signal is sent and then listening antennas find the reflections caused by the targets thus locating them. Radio astronomy is a passive technique where antennas listen for radio emissions from celestial bodies and use the information to map the heavens.

Tomography

Tomography creates cross-sectional images. X-rays are perhaps the most common technique, but non-destructive techniques, ultrasonic and microwave medical imaging and seismic explorations are growing, (Haykin, 1985). Ultrasonics and tomography consider the information given by an array to construct an image of an underlying object. Von Ramm and Smith (1983) review the principles and techniques of phase array ultrasonic scanners giving an analysis of the current techniques including phase compensation, spatial compounding, frequency compounding, and parallel

processing. Chivers (1986) details the use of time-delay spectrometry in ultrasonic transducer characterization. The author reviews the technique emphasizing the measurement parameters and extending its application to miniature hydrophones.

These are the major areas of array research, each uses the array technology to accomplish its goal. The specifics of each application are not of interest here for the aim of this work is to develop the techniques for application to structures.

Chapter 3

Theoretical Application of Sensor Arrays to Structures

3.1 Introduction

While much work exists in both vibration theory and array theory; little has been done to merge them. Many advantages exist in applying array theory to structures. The benefits of arrays apply directly. It is the purpose of this work to show that arrays accomplish the following when applied to structures.

- Noise Reduction – The noise (the uncorrelated content) on a signal can be reduced by the averaging inherent in the array processing, as discussed in chapter 1.

- Angular Beamforming – because of the spatial nature of the arrays, beamforming can be performed to 'listen' in a direction or to determine the direction of the source as explained in chapter 1.

- AOA and Source Localization – the propagation of the wave front can be viewed from the phasing of the waves; this in turn can be exploited to find angle of arrival and source localization information.

- Frequency Beamforming – owing to the dispersive nature of flexural waves, signal processing can be performed to listen to a particular frequency (or frequency range). It will be shown that in tuning to a particular frequency the array behaves similarly to a low pass filter.

This chapter considers the theoretical effect of these aspects of array processing on the output of the array. It also considers the interdependence of processing between these elements; while each can be considered and quantified individually they are interrelated. Further consideration will be given to how the simple beamforming techniques can be applied in a dispersive media. What applies directly? What must be altered? What cannot be used at all? What new things can be done?

Those questions are answered by considering two things. The first is a look at travelling waves. Travelling waves are the propagation that will be seen highly damped media; waves that originate from a source but are fully absorbed so that no reflections – or negligible ones – exist. In lightly damped media, travelling waves are reflected at the boundaries and combine to develop standing waves. Travelling waves will be studied on an experimental, infinite beam (a beam with anechoic terminations that drastically reduce reflections. Harmonic signals will be considered to fully develop the array concepts in structures.

Secondly a broad band response will be analyzed; this will study transient processing and can be applicable to a broad range of structures. Because this technique processes the transient response, it can be used on both highly and lightly damped structures. Standing waves (i.e. steady state response) will not be considered here. Modal analysis is more effective at analyzing that form of vibration.
For the purpose of theoretical study, the array is made of nine sensors equally spaced in a 3 x 3 grid as shown in fig 3.1. The signals considered are sinusoidal.

3.2 Noise Reduction

In chapter two, the noise reducing property of arrays was developed. As a demonstration of this property as it applies to structures, consider a simulation of the response of a classic beamformer with the array geometry shown in figure 3.1 to a sinusoidal excitation. The relationship between sensor responses is somewhat apparent from the figure. The sensors measure a sinusoidal response, but sensors 7,8, and 9 see the wavefront last, after sensors 4, 5, and 6 which see the wave front after sensors 1, 2, and 3. For a single frequency sinusoid, the time delay between these sensors is given by the product of the velocity (wave speed) and distance (separation),

$$\phi(seconds) = \frac{\zeta}{c} = k\zeta/\omega. \tag{3.1}$$

The delay can be expressed in terms of the wavelength (in radians) by the following relationship,

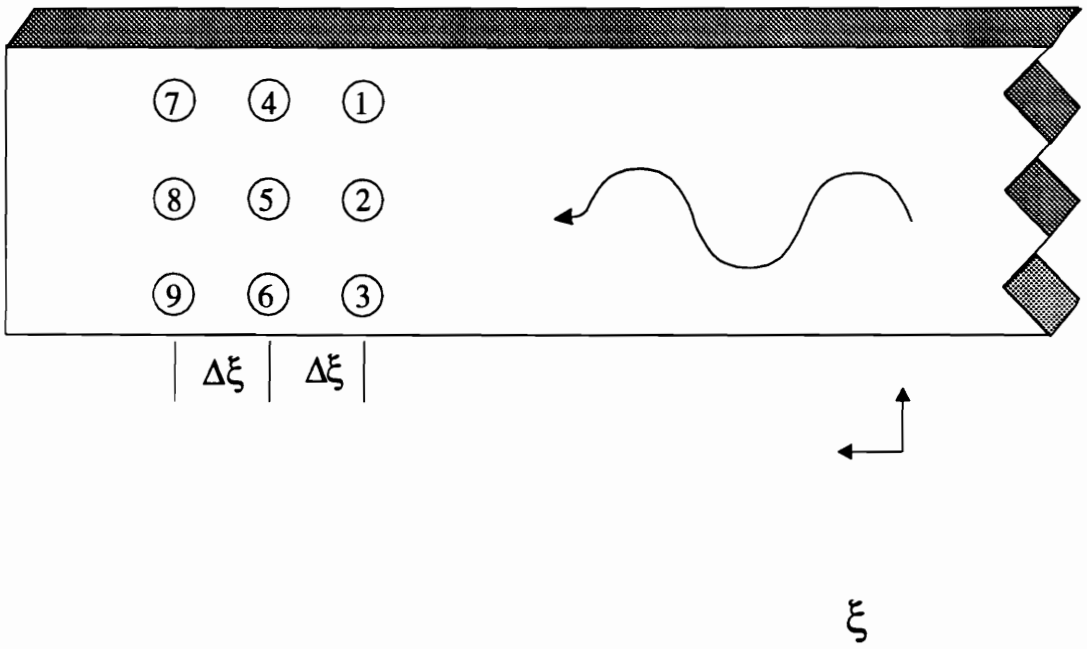

Figure 3.1: Schematic of Rectangular Array

$$\phi(radians) = \frac{\zeta\omega}{c} = k\zeta. \tag{3.2}$$

The relationship between sensors is then given by

$$s(1,2,3) = Asin(\omega t) \tag{3.3}$$

$$s(4,5,6) = Asin(\omega t + \phi) \tag{3.4}$$

$$s(7,8,9) = Asin(\omega t + 2\phi) \tag{3.5}$$

$$\tag{3.6}$$

The signal content viewed by each sensor is the same, simply shifted in phase.

3.2.1 Frequency Domain

By transforming the data into the frequency domain (via the Fourier transform) the amplitude, frequency and phase are extracted. If the output of the array elements are averaged the output is

$$s(array) = Asin(\omega t + \phi_{array}) \tag{3.7}$$

The amplitude and the frequency of the array are the amplitude and frequency of signal. If the output is beamformed to a reference sensor, then the phase of the

array is the phase at that location. If the frequency domain data are uncompensated in phase (perhaps because it is unknown) then the phase of the array is the spatial average of the spectra. If the phase of a signal is random, it is averaged out as noise. If the phase relationship among sensors is unknown it is useful to employ the power spectra to represent the array output. The power spectrum has no phase as it has all real components, eliminating any confusion about phasing when the information is not present. With the frequency spectrum, any signal – if random and uncorrelated between sensors will be reduced, approaching zero in the limit. If power spectrum is used, frequency spectrum is multiplied by the complex conjugate and positive real values are obtained. With zero mean gaussian noise, the noise approaches the variance value, so the SNR is improved by m_s. In this paper the power spectra will be used only where noted.

As an example of the differences in the frequency domain techniques, simulations of the nine element array were conducted. The response of a beam was calculated at the sensor locations depicted in figure 3.1 according to equation A.37. A 310 Hz force of 1 pound located 54 inches from the nearest array element was used along with the beam properties found in table 3.2.1.

Table 3.1: Properties and Measurements of Beam

E	9.5x10e6 psi
Thickness	0.125 in.
Width	3 in.
Density	.098 lbs/$in.^3$

For the beam properties, and forcing function given, the response of the beam at

the sensor location has a magnitude of 3.575×10^{-4} lbs. That corresponds (for a sinusoidal signal) to a $\sigma = 2.52 \times 10^{-4}$and $\sigma^2 = 6.39 \times 10^{-8}$. Significant mean zero, Gaussian noise,$\sigma = 0.5 \times 10^{-2}$, was added to obstruct each signal. The SNR was estimated by comparing the magnitude of the signal content at the forcing function to the magnitude of the signal content at the other frequencies. For an increase to nine elements, an improvement of 2.97 times is seen, this matches (to within statistical tolerance) the predicted value of 3. As the number of elements increases, the effect is more and more dramatic. Figure 3.2 shows how the SNR as defined in equation 2.5 can be improved with averaging. A weak signal is brought out above the noise floor as more and more array elements are used. The frequency spectrum shows the difference in the spectral quality of a signal of 1, 9, and 32 elements. With just one sensor the signal is indiscernible, but is quite readable with added elements. The SNR values are given in table 3.2.1. The SNR should improve by $\sqrt{m_s}$. The comparative improvements also are given in Table 3.2.1.

Table 3.2: Simulated SNR Values for Arrays

SNR of 1 sensor array		2.0705
SNR of 9 sensor array		6.1546
SNR of 32 sensor array		11.6719
	theoretical	*simulated*
9 vs 1	3	2.9725
32 vs 1	5.66	5.6372
32 vs 9	1.89	1.8965

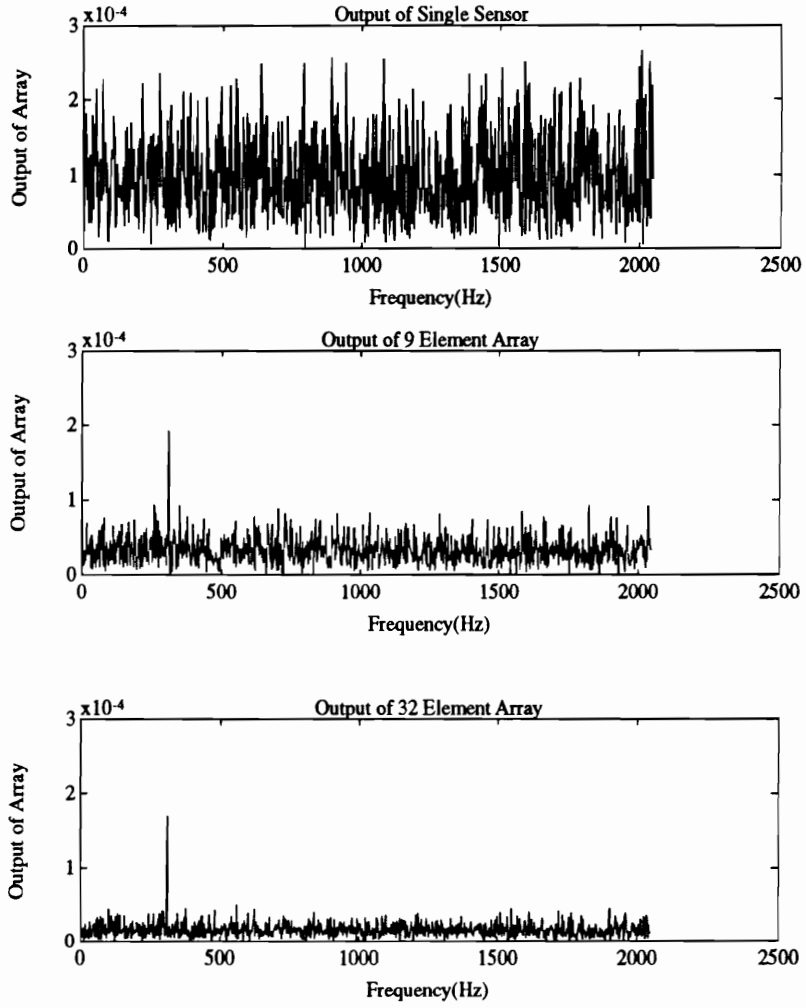

Figure 3.2: Simulated SNR Performance of 1, 9, and 32 Element Arrays – Frequency Domain

3.2.2 Time Domain

The same noise reduction techniques can be demonstrated for time domain analysis. Because of the phase shift between sensors, the signals must be weighted to accomplish phase compensation in the time domain. It is well known that phase shifted signals can destructively interfere to significantly reduce the signal content, so data of each sensor must be shifted so that the signal aligns in phase, and then averaged. The shifting is generally accomplished by weights, the classical beamformer weights are used here. The weight is a phase shift among sensors that is dependent on the geometry of the array and the wave speed or wavenumber as described in equations 3.2 and 3.1. Figure 3.3 demonstrates how time domain signals can be improved with averaging when the signal content is aligned. Again, the response of a beam to sinusoidal excitation was simulated at the sensor locations depicted in figure 3.1. Significant mean zero, Gaussian noise with a variance of 5e-3 was added to obstruct each signal.

The time domain signals were weighted with the appropriate time delay and then averaged, as with the classical beamformer. For example the weight for sensor 1 is given by equation 2.9 for this case $m_s = 0$, d_i = separation from sensor 1 to 2 (2 was the reference sensor) = 1 inch, $\sin\theta = 0$.

$$w_1 = \frac{1}{9} e^{i*k(310Hz)*1in}. \tag{3.8}$$

Each sensor was so weighted and then added to get the output of the array. The SNR values are tabulated for the 1, 9, and 32 element arrays in table 3.2.2. Figure 3.3 shows how the array can reduce the noise so that the signal content can be

easily seen. The amount of that improvement is quantified by the SNR. It can be seen that the noise on the signal is reduced; and the phase of the data is known to be the phase at the reference sensor of the array. This demonstrates the statistical properties of noise reduction developed in basic array theory.

Table 3.3: Simulated SNR Values for Arrays

SNR of 1 sensor array		18.663
SNR of 9 sensor array		55.078
SNR of 32 sensor array		106.94
	theoretical	*simulated*
9 vs 1	3	2.9725
32 vs 1	5.66	5.6372
32 vs 9	1.89	1.8965

3.3 Array Performance

The performance of an array is measured by how well it discriminates against other signals. When the array is tuned to look at a particular frequency and angle, how much do other frequencies impact the response. Usually this is quantified by the beam pattern of the array, which gives the output of the array versus angle, see figure 2.3 and equation 2.7. The array equation is described by more variables for a dispersive media. The beam pattern is still dependent on just AOA and spacing versus wavelength but spacing versus wavelength now changes with frequency (and equivalently k). The output of the 3x3 array is defined by three independent variables.

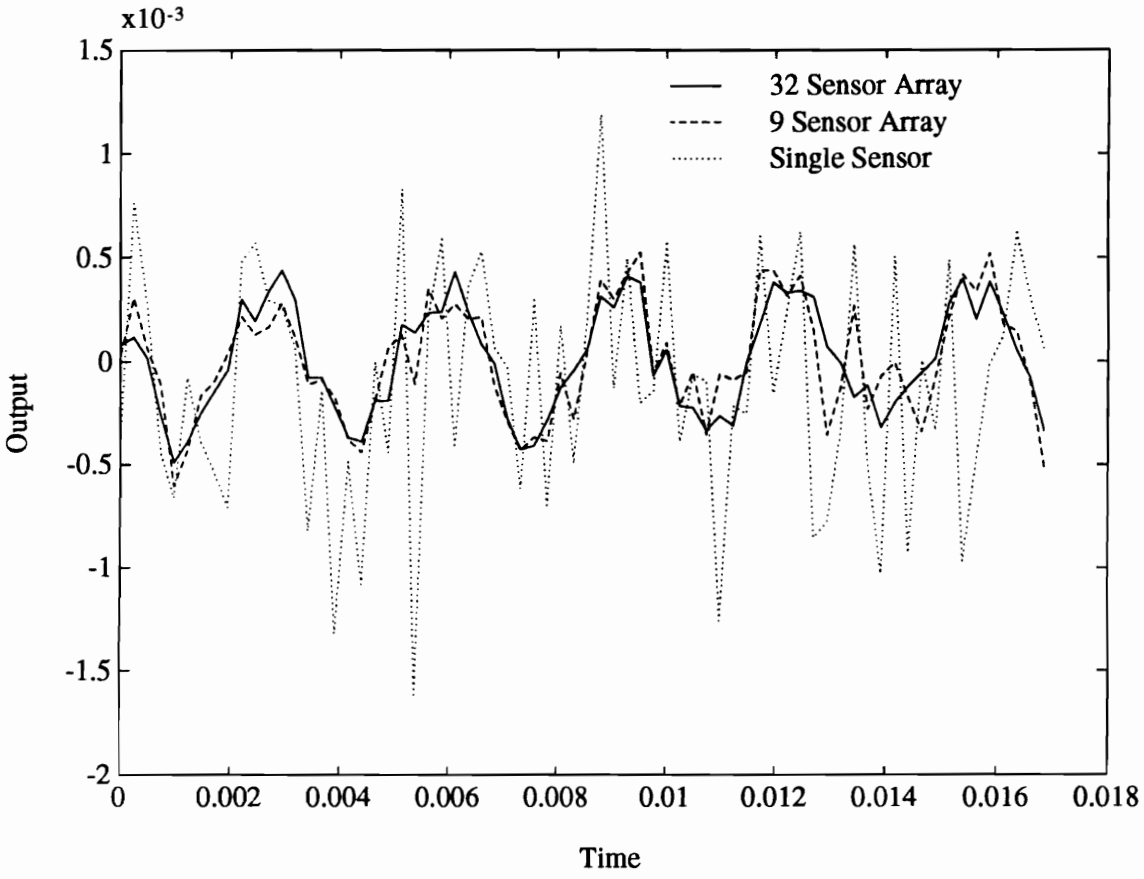

Figure 3.3: Simulated SNR Performance of 1, 9, and 32 Element Arrays – Time Domain

It is impossible to represent a dependency in 3 variables graphically, so descriptions will be give in two variables. These will be interwoven to give the overall impression of the effects of angle, spacing and wavelength on the output of the array.

3.3.1 Angular Beamforming

The weights of the classical beamformer tune an array to an angle, those weights are defined by equation 3.8. The weighting determines the phasing between sensors as noted in equation B.10. It is intuitive that the array has a maximum output when it is beamformed to the angle of arrival, but how is the output of the array affected when signals are present at off angles? What is the beam pattern for this rectangular array?

To quantify the arrays response dependent on the angle or any other variable, a derivation for the relationship between the grid of sensors must be developed. For the grid defined by 3.1, appendix B derives the array response. From equations B.10 and B.11 the array output can be developed for errors in the angle. The output can be expressed as

$$\begin{aligned}\frac{S}{S_{array}} = \frac{1}{9}(&e^{-iks(\sin\theta-\sin\theta_a)} + 1 + e^{iks(\sin\theta-\sin\theta_a} + \\ &e^{iks((\cos\theta-\sin\theta)-(\cos\theta_a-\sin\theta_a))} + e^{iks\cos\theta\cos\theta_a} + \\ &e^{iks((\cos\theta+\sin\theta)-(\cos\theta_a+\sin\theta_a))} + e^{iks((2\cos\theta-\sin\theta)-(2\cos\theta_a-\sin\theta_a))} + \\ &e^{iks2\cos\theta-2\cos\theta_a} + e^{iks((2\cos\theta+\sin\theta)-(2\cos\theta_a+\sin\theta_a)}))\end{aligned}$$

for the array depicted in figure 3.1.

The rather cumbersome equation can be understood by breaking it down into pieces. The first term describes the response of the first element. The array development assumes that the wave consists of only far-field terms so the wave at the reference element can be described by a magnitude, a frequency and a location.

$$S_2 = We^{ikx(2)}e^{-i\omega t} \tag{3.9}$$

The response at sensor one is likewise given by

$$S_1 = We^{ikx(1)}e^{-i\omega t} \tag{3.10}$$

If the output is now multiplied by the weights, the reference sensor is multiplied by $1/m_s$, but sensor 1 output now becomes

$$w_1 S_1 = \frac{1}{9}We^{ik|x(1)|}e^{-i\omega t}e^{i\omega\phi_1} \tag{3.11}$$

$$w_1 S_1 = \frac{1}{9}We^{ik|x(1)|}e^{-i\omega t}e^{i\omega - k_a s_a \sin\theta_a/\omega_a} \tag{3.12}$$

where θ_a, ω_a, k_a, and s_a are the values of θ, ω, k, and s that are used to calculate the weight for the beamformer. If all values but angle are correct, the equation can be rewritten

$$w_1 S_1 = \frac{1}{9} W e^{ik(x(2)+s\sin\theta)} e^{-i\omega t} e^{i\omega\phi_1} \tag{3.13}$$

$$\begin{aligned} \frac{w_1 S_1}{S_2} &= \frac{1}{9} e^{ik(x(2)+s\sin\theta)} e^{-i\omega t} e^{i\omega k_a s_a \sin\theta_a/\omega_a} e^{-ikx(2)} \\ &= \frac{1}{9} e^{iks\sin\theta} e^{i\omega k_a s_a \sin\theta_a/\omega_a} \qquad (3.14) \\ &= \frac{1}{9} e^{iks(\sin\theta-\sin\theta_a)} \end{aligned}$$

Similar analysis can be performed on all array elements, this can be found in appendix B. This leads to equation 3.9, which can evaluate the performance of the array for errors in angle. This equation defines the directivity pattern for the 9 element array. What can be seen from this relationship is that the output of the array is dependent not only on the AOA but also on the value of ks . The derivation of the beam pattern of the linear array showed this also. For small spacings relative to wavelength, the output of the array is omnidirectional; as the spacing between sensors grows, the beam pattern collapses to a main lobe and as ks continues to grow the main lobe thins and side lobes grow.

Mechanically , as the spacing shrinks relative to the wavelength the sensors are effectively located at the point on the beam regardless of the angle of the beamformer. This can be seen in figure 3.4 which depicts the response of the array with changing values of angle and spacing. The response is symmetric, symmetric arrays have symmetric beam patterns, asymmetric arrays have asymmetric patterns. Regardless of the spacing, the array output is maximized for AOA's along the beam – the main lobe.

3.3.2 Frequency Beamforming

The weights of the classical beamformer are also dependent on frequency. Looking back on equation 3.1, the delay between sensors is dependent on the propagating speed. Flexural waves are dispersive, meaning waves of different frequencies propagate at different speeds. When the wavenumber changes with changes in the frequency, the phasing between sensors changes; that change is proportional to the wavenumber, see equation 3.2. From the solution of the wave equation the wavenumber is proportional to the square root of the frequency, $k \propto \sqrt{\omega}$. Substituting this relationship into equation 3.1 yields

$$\phi \propto \sqrt{\omega}\, \zeta. \tag{3.15}$$

All other things being equal, an array tuned to a frequency will measure other frequencies according to relationship 3.15. To quantify the output at other frequencies relative to the tuned frequency, the output of the array must be considered. For the 3x3 grid array, the relationship is derived in Appendix B. From equations B.10 and B.11 the output of the array can be calculated. If no error is assumed in the angle of arrival then the relative output of the array is given by the expression

$$\frac{S}{S_{array}} = \frac{1}{9}(e^{ik(1-k/k_a)((-s)\sin\theta)} + 1 + e^{ik(1-k/k_a)s\sin\theta} +$$

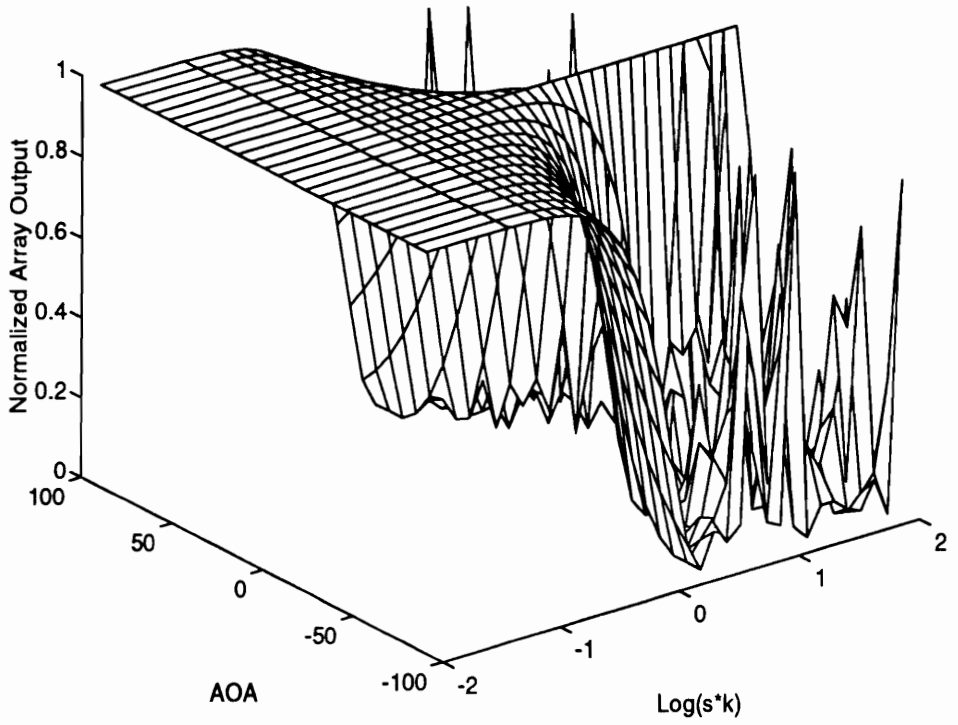

Figure 3.4: Normalized Output of 3x3 Array for off Angle Measurements – Array Tuned at 0 Degrees, Single Frequency

$$e^{ik(1-k/k_a)s(\cos\theta-\sin\theta)} + e^{ik(1-k/k_a)s\cos\theta} + e^{ik(1-k/k_a)s(\cos\theta+\sin\theta)} +$$
$$e^{ik(1-k/k_a)s(2\cos\theta-\sin\theta)} + e^{ik(1-k/k_a)s2\cos\theta} + e^{ik(1-k/k_a)s(2\cos\theta+\sin\theta))} \tag{3.16}$$

for the array depicted in figure 3.1.

Figure 3.5 depicts the response of the array with changing values of the wavenumber and for different values of spacing. The response of the array is fairly flat and near maximum for frequencies below the tuned frequency (and appropriate wavenumber) for those values of wavelength and spacing where the array behaves omnidirectionally.

Attenuation exists for wavenumbers below the tuned frequency if the spacing to wavelength ratio moves the beam pattern out of the omnidirectional region. The maximum output occurs at the tuned frequency for all spacing possibilities as again this is the main lobe of the beam pattern.

When the frequency falls outside the tuned frequency, the shifting done in the "tuning" can cause data to add destructively. If the phasing is sufficiently mistuned, the phasing of some sensors can be at $\approx$ 180 degrees to the reference, such that destructive interference occurs. This occurs at the minimums on the graph. In some respects the array behaves like a low pass filter; but signals that are spatial harmonics of the tuned frequency are not attenuated.

If other estimators are used instead of classical beamforming techniques the response

of array would be characterized by the weighting of the particular estimator. Filtering and higher resolution estimation techniques will reduce out-of-band effects.

3.3.3 Interdependence of Angle and Wavenumber in Classical Beamforming

The output of the array has been parameterized for both errors in wave number and angle of arrival, but these parameters are not easily separated. If the array sees errors in both parameters how does this effect the output of the array? If the array is tuned to a signal of k_1 incident from θ_1; how well will it measure or discriminate a signal of k_2 from θ_2. Returning again to equations B.10 and B.11, the array output can be developed to determine the interdependency of the array on AOA and wavenumber, for the array depicted in figure 3.1.

$$\begin{aligned}\frac{S}{S_{array}} = \frac{1}{9}\Big(&e^{ik((-s)\sin\theta)-i\frac{k^2}{k_a}(-s)\sin\theta_a} + 1 + e^{iks\sin\theta-i\frac{k^2}{k_a}s\sin\theta_a} + \\ &e^{iks(\cos\theta-\sin\theta)-i\frac{k^2}{k_a}s(\cos\theta_a-\sin\theta_a)} + e^{iks\cos\theta-i\frac{k^2}{k_a}s\cos\theta_a} + \\ &e^{iks(\cos\theta+\sin\theta)-i\frac{k^2}{k_a}s(\cos\theta_a+\sin\theta_a)} + \\ &e^{iks(2\cos\theta-\sin\theta)-i\frac{k^2}{k_a}s(2\cos\theta_a-\sin\theta_a)} + \\ &e^{iks2\cos\theta-i\frac{k^2}{k_a}s2\cos\theta_a} + e^{iks(2\cos\theta+\sin\theta)-i\frac{k^2}{k_a}s(2\cos\theta_a+\sin\theta_a)}\Big)\end{aligned}$$

Figures 3.7 through 3.6 show how the array output can be affected by both errors and how those errors are related to one another. These figures represent spacing scheme of $s * k_c = .1$, 1, and 10, where k_c is the tuned wavenumber.

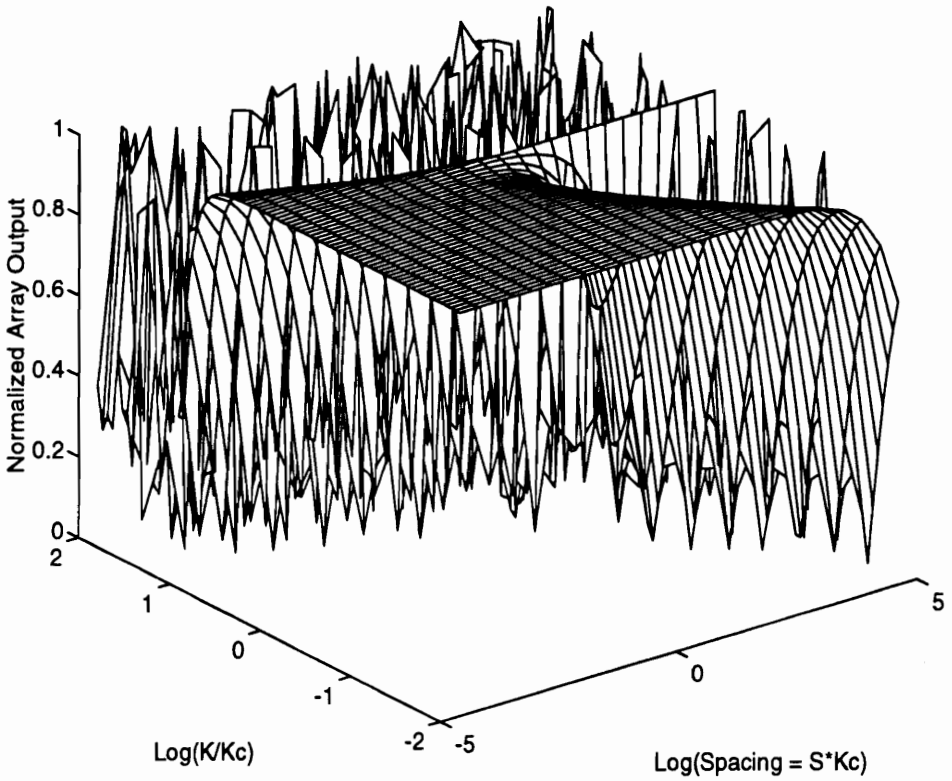

Figure 3.5: Normalized Output of 3x3 Array with Errors in Wavenumber

A flat response region exists at very low relative wavenumbers. The logic is again the same as that developed for frequency beamforming. The output approaches maximum as the frequency approaches values much lower (again by 2 orders of magnitude) than the tuned frequency, regardless of the AOA. As the wavenumbers decrease, the wavelength increases. Once the wavelength is sufficiently long the sensors are essentially located at the same point on the wave regardless of the tuning in either frequency or angle. The region of omnidirectionality changes with the spacing relationship.

The maximum output occurs at the tuned frequency and angle, but the effect of the wrong angle diminishes the signal if tuned to the true frequency/wavenumber. The same is true for the for wavenumber, if the wavenumber is tuned too high, the output can fall into one of the many valleys.

For example, for a signal at 1.43ω and at the tuned AOA, the output of that signal would be 1% of the value it would be if the array were tuned to that frequency. A signal at 1.43ω but at $-44°$ to the tuned AOA would have an amplitude of 11% of its maximum value. In this way signals can be discriminated. This can be an advantage and a disadvantage. If noise exist at a particular angle and frequency, the array can be tuned to 'eliminate' that signal, and other signals will have the amplitudes that correspond to that particular array tuning. It can also be seen that if signals of multiple frequencies and angles exist there is limited ability to beamform the array to listen to incoming signals.

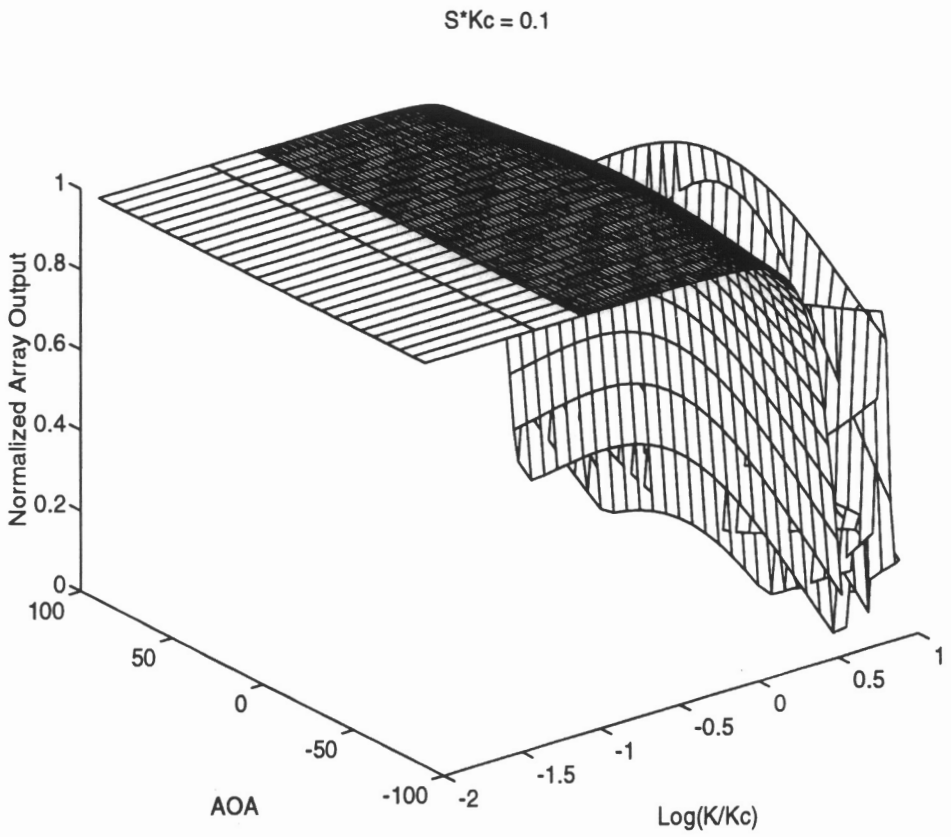

Figure 3.6: Normalized Output of 3x3 Array for Off Angle and/or Off Wavenumber Signals For $k_c s = .1$

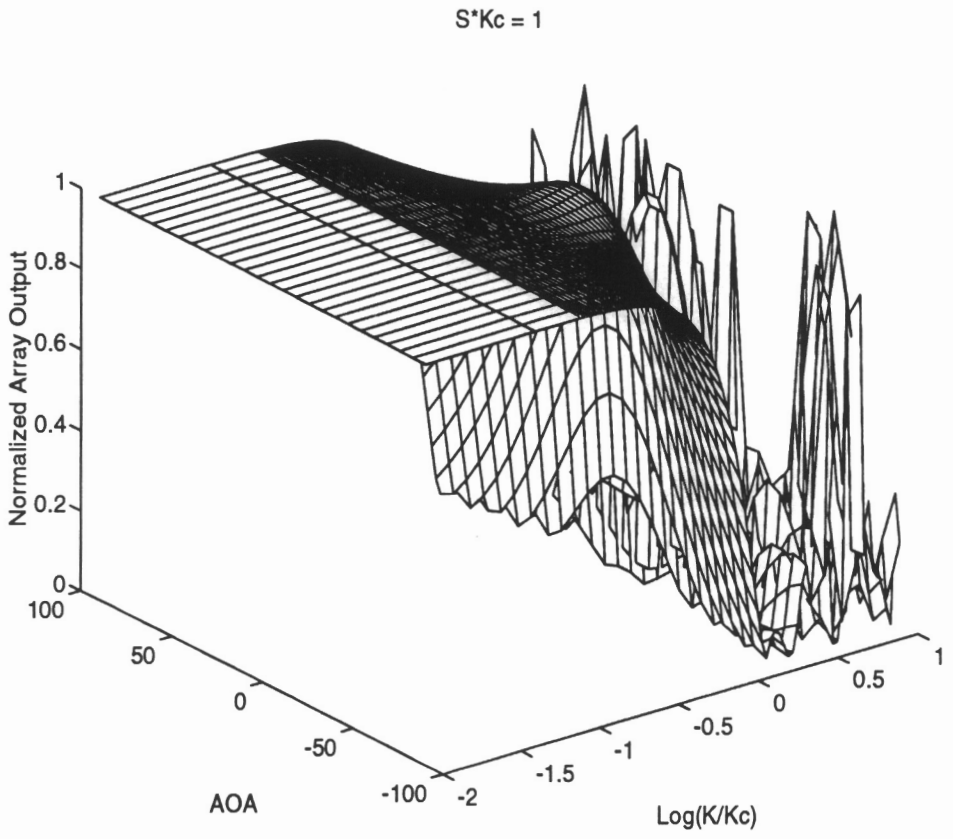

Figure 3.7: Normalized Output of 3x3 Array for Off Angle and/or Off Wavenumber Signals For $k_c s = 1$

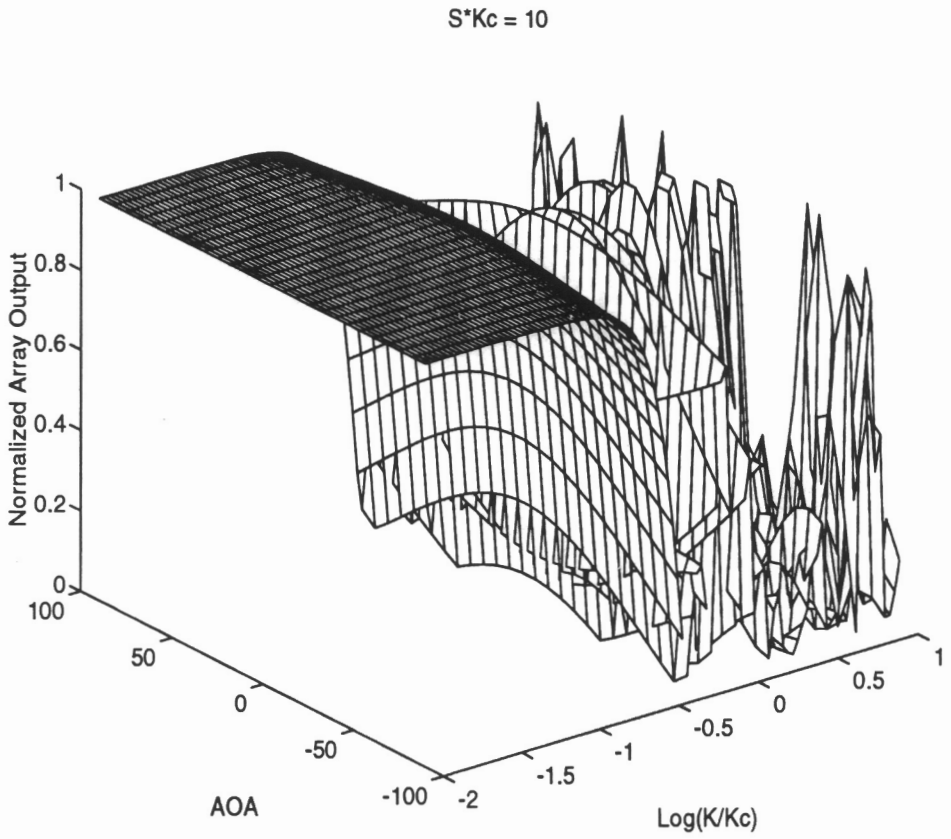

Figure 3.8: Normalized Output of 3x3 Array for Off Angle and/or Off Wavenumber Signals For $k_c s = 10$

3.3.4 The Measurement of Angle of Arrival Based on Phasing

The relationship between phase delay among sensors has been developed to determine its effect on the array output, but what happens if the relationship is used to determine the AOA? Equation 3.1 gives the relationship; and it shows that phase is contingent on the wavenumber, frequency, and the separation of sensors in the propagation direction, which is contingent on θ. Simply, the phasing from sensor to sensor is a measure of the projection of the velocity into the coordinate system of the array. If all other variables are known, then it follows that the AOA can be determined from the phase delay between sensors. Figure 3.9 illustrates how this works. In the top illustration where θ is positive sensor 2 leads sensor 1, but in the bottom illustration where θ is negative sensor 1 leads sensor 2. If the θ were zero there would be no phase shift between sensors. It is evident from this that the phasing indicates the angle of arrival.

Consider the geometry of the array depicted in figure 3.1. The phase between sensor 1 relative to sensor 2 is given by the equation combining equations 3.1 and B.11.

$$\phi_{12} = -ks \sin\theta/\omega$$

Equivalently, knowing the phase, θ can be found,

$$\theta = \sin^{-1}\left(\frac{\phi_{12}\omega}{ks}\right). \tag{3.17}$$

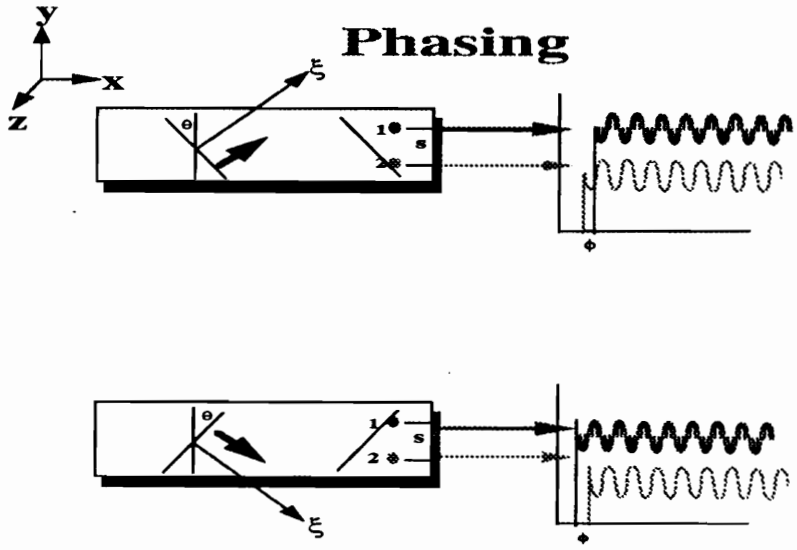

Figure 3.9: Determination of AOA from Phasing

Similarly,

$$\theta = \cos^{-1}\left(\frac{\phi_{52}\omega}{ks}\right). \tag{3.18}$$

While similar relationships can be developed to determine θ, an obvious problem occurs in looking at the relationship between sensors 6 and 2.

$$\phi_{62} = \frac{ks(\sin\theta + \cos\theta)}{\omega} \tag{3.19}$$

$$\sin\theta + \cos\theta = \frac{\phi_{62}\omega}{ks} \tag{3.20}$$

$$\tag{3.21}$$

Equation 3.20 cannot be solved explicitly for θ. While it was convenient to define the separation between sensors relative to sensor 2, it is not so here. It is necessary to write the separation relative to other sensors; ζ_{xy} depicts the separation of sensor x to sensor y. If instead of making the comparison of sensor 6 to 2, the comparison were made between 6 and 3, then θ can be found by the relationship

$$\theta = \cos^{-1}\left(\frac{\phi_{63}\omega}{ks}\right). \tag{3.22}$$

Similar relationships can be made for each sensor.

3.3.5 Error Analysis

The measure of the usefulness of these relationships is the sensitivity of the expressions to errors in k, s, ω and ϕ. The uncertainty of any measurement is given by Taylor's series expansion.

$$u_\theta = \sqrt{\left(u_k \frac{\partial\theta}{\partial k}\right)^2 + \left(u_s \frac{\partial\theta}{\partial s}\right)^2 + \left(u_\omega \frac{\partial\theta}{\partial\omega}\right)^2 + \left(u_\phi \frac{\partial\theta}{\partial\phi}\right)^2} \tag{3.23}$$

It is interesting to note that $\frac{\partial \sin^{-1} u}{\partial x} = -\frac{\partial \cos^{-1} u}{\partial x}$. Thus as regards uncertainty, there is no difference in using cosine or sine relationships. The uncertainty can be evaluated using the following relationships

$$\begin{aligned}
\frac{\partial\theta}{\partial k} &= \frac{\partial\left(\sin^{-1}(\frac{\phi\omega}{ks})\right)}{\partial k} = \frac{\phi\omega/ks}{\sqrt{1-(\frac{\phi\omega}{ks})^2}}(-b^{-1}) \\
\frac{\partial\theta}{\partial s} &= \frac{\partial\left(\sin^{-1}(\frac{\phi\omega}{ks})\right)}{\partial s} = \frac{\phi\omega/ks}{\sqrt{1-(\frac{\phi\omega}{ks})^2}}(-s^{-1}) \\
\frac{\partial\theta}{\partial\phi} &= \frac{\partial\left(\sin^{-1}(\frac{\phi\omega}{ks})\right)}{\partial\phi} = \frac{\phi\omega/ks}{\sqrt{1-(\frac{\phi\omega}{ks})^2}}(\phi^{-1}) \\
\frac{\partial\theta}{\partial\omega} &= \frac{\partial\left(\sin^{-1}(\frac{\phi\omega}{ks})\right)}{\partial\omega} = \frac{\phi\omega/ks}{\sqrt{1-(\frac{\phi\omega}{ks})^2}}(\omega^{-1})
\end{aligned} \tag{3.24}$$

The sensitivity of the AOA measurement is evaluated using the Monte Carlo approach. Owing to the complicated nature of the sensitivity equation, they were evaluated for a range of values of k, s, ϕ, and ω. These evaluations are given in figure 3.10 and show that the sensitivity increases as ϕ and ω increase and as k and s decrease. It is also helpful to note that the sensitivity function does not exist for values of $-1 < \frac{\phi\omega}{ks} < 1$ since the $\sin^{-1}$ and $\cos^{-1}$ functions do not exist there. Furthermore the $\sin^{-1}$ and $\cos^{-1}$ functions assume values of -90 to 90 and 0 to 180 respectively. For the purpose of this work AOA are limited to -90 to 90. The values of $\cos^{-1} > 90$ are reassigned to $\cos^{-1} -180$ to keep it within that range.

The uncertainty can be expressed by substituting the individual sensitivities into the Taylor expansion. This yields

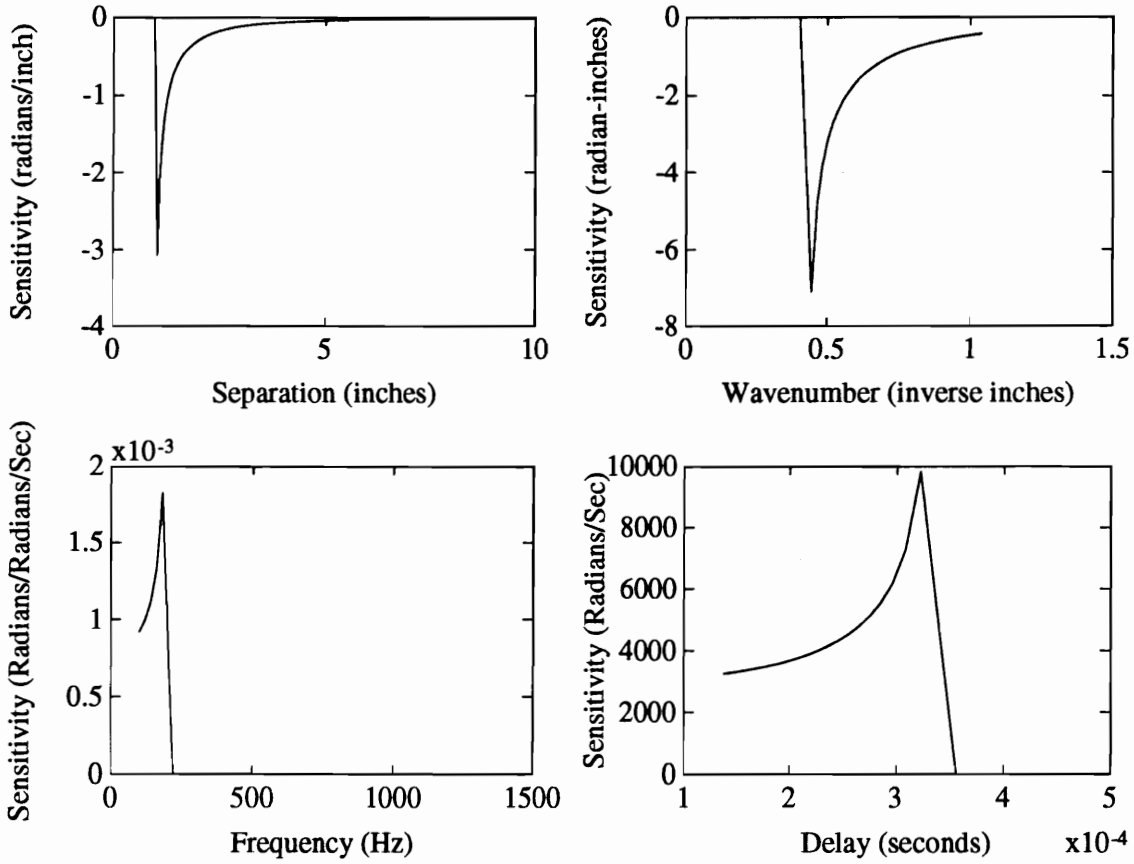

Figure 3.10: Sensitivity of AOA Measurements

$$u_\theta = \frac{\phi\omega/ks}{\sqrt{1-(\frac{\phi\omega}{ks})^2}}\sqrt{\left(\frac{u_\phi}{\phi}\right)^2+\left(\frac{u_\omega}{\omega}\right)^2+\left(\frac{u_k}{k}\right)^2+\left(\frac{u_s}{s}\right)^2} \tag{3.25}$$

As is obvious from the complexity of the uncertainty equation, the uncertainty of the angle of arrival for an uncertainty of a particular variable is dependent on the values of all other variables. For example, an uncertainty in spacing is more significant at shorter wavelengths. If the uncertainty in spacing is .01 inches, that is far less critical for a wavelength of 20 inches (and thus k = .31 (1/inches)) than it is for a wavelength of .2 inches (and thus k = 31 (1/inches)).

Because of this interconnectedness of the variables it is impossible to isolate the impact of a single uncertainty from the other variables. What then can be done to quantify the propagation of errors in AOA determination is to hold all other variables constant while varying one variable and evaluating the uncertainty. Values of s = 1 inch,f = 200 Hz, k = .4243 1/inch, and $\phi = 3.4 \times 10^{-4}$ were assumed for the evaluation. Owing to the nature of the equations, combinations of s, ϕ, k, and f fail to have a solution to the AOA equation. For the sensitivity plots this corresponds to $s < 1$ inches, $k < .4243$ 1/inches , $F > 200$ Hz and $\phi > 3.4 \times 10^{-4}$ seconds.

If one considers the sensitivity plot for spacing, the plot shows that the uncertainty of AOA is greatest for the smallest spacing and decreases with larger spacing. For a spacing of 1 inch (the nominal value) an uncertainty of ± 1 inch yields and uncertainty of $\mp\pi$ radians. But at a spacing of 10 inches 1 inch uncertainty corresponds to .01 radians. For a typical experimental setup with a spacing of 1 inch and an uncertainty in spacing of .01 inches (at f = 200 Hz and $\phi = 3.4 \times 10^{-4}$ sec) this

corresponds to an uncertainty of 0.31 radians or < 2 degrees.

If uncertainty in frequency and wavenumber are considered instead similar conclusions can be drawn. Uncertainty in frequency is more critical at higher frequencies because they signify shorter wavelengths. For an uncertainty of 20 Hz (this corresponds roughly to an uncertainty of .02 (1/inches) in wavenumber) evaluated at 100 Hz an uncertainty of 6.6 degrees in AOA is given while at 400Hz it would correspond to an uncertainty of 9.5 degrees.

For the uncertainty in the phase measurement it can be seen that the equation is most sensitive as the argument of the arc sin approaches 1. For the values assigned in this evaluation the argument of the $\sin^{-1}$ is $\frac{\phi}{3.4 \times 10^{-4}}$. So the sensitivity will increase as it approaches the nominal value.

Chapter 4

Application of Sensor Array to Infinite Beam – Experimental Harmonic Response

4.1 Introduction

Now that the relationships that exist in beamforming data have been established and to some degree predicted by theory, these relationships need to be validated by experiment. This will be done by looking at the propagation of harmonic signals on an infinite beam, so that travelling waves may be isolated. This experiment will be used to confirm the theory and model previously established, it will also show any deviations from theory. This chapter will also illustrate the use of array processing to show improved SNR and AOA determination. Chapter five will deal with the transient analysis.

4.2 Experimental Considerations

4.2.1 Setup

The first series of experiments were performed on an infinite beam so that travelling waves would be the primary phenomenon. An infinite beam model was fabricated

by taking a long thin beam and putting nearly anechoic terminations on both ends. The terminations were built by layering the end of the beam with damping material, the layers thickening toward the ends. The ends of the beam were then imbedded in boxes of sand again growing wider towards the ends. The purpose here is to slowly change the impedance of the beam without creating any discontinuities that could cause reflections.

The beam was then mounted, supported by the boxes at both ends and by strings from the ceiling at three locations along the beam. A shaker was attached at one end, and a sensor array was attached at the other. The first array used was an upper triangular array of 6 accelerometers mounted in a 3x3 grid. The accelerometers were separated by 1 inch. The setup can be seen in figure 4.1.

Data were also collected using the VPI laser. The laser measures velocities; its operating principle is based on the measurement of the Doppler shift frequency. The setup was much the same as the accelerometer arrangement with the laser making measurements as opposed to accelerometers. The setup can be seen in figure 4.2. A grid pattern was setup along the beam that consisted of 750 measurement locations in a 10 row by 75 column matrix. Single frequency, least squares processing was used to determine the amplitude and phase at each location. Time histories were not recorded. The beam had the same properties and measurements as noted previously, see table 3.2.1.

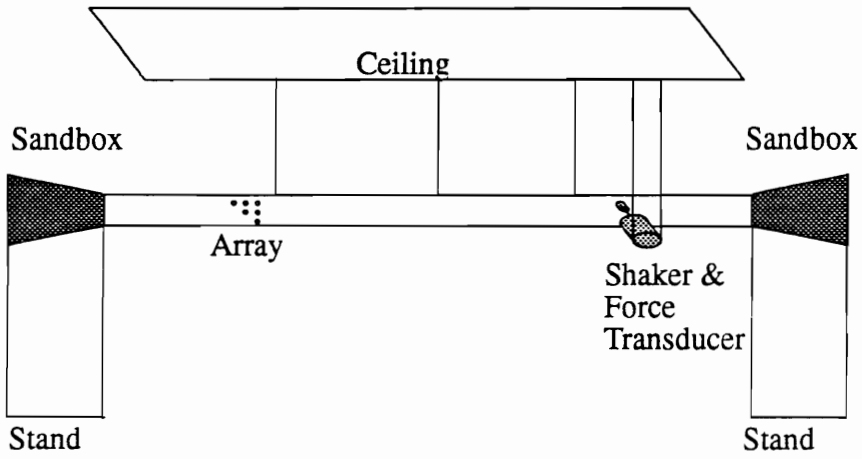

Figure 4.1: Experimental Setup Using Accelerometers

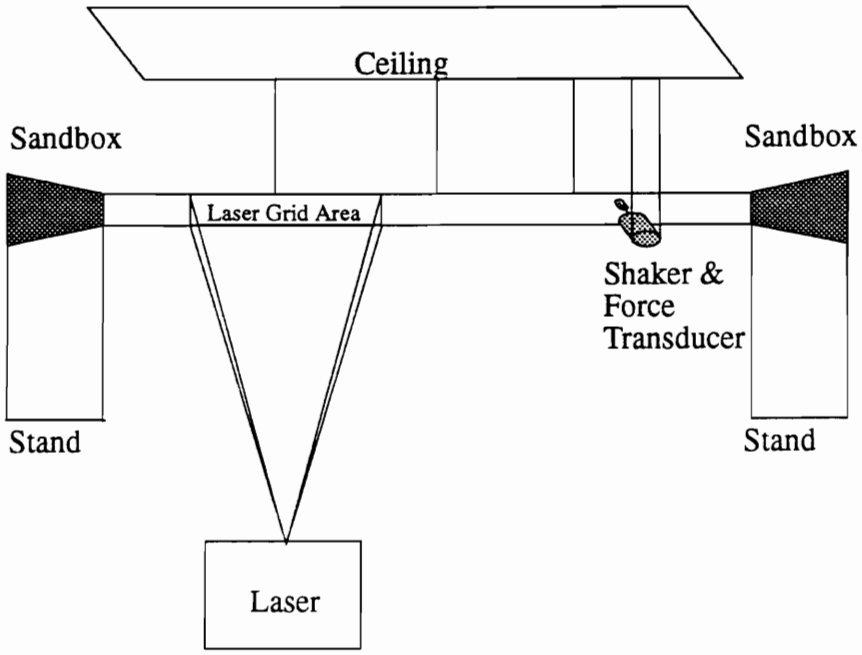

Figure 4.2: Experimental Setup Using Laser

4.2.2 Euler-Bernoulli Analysis Verification

Euler-Bernoulli analysis was used to model the wave behavior of the beam. A comparison of the Euler-Bernoulli equation to a more exact model validates the use of this model. A corrected equation is given below, (Cremer, et al, 1988)

$$\frac{EI}{m'}\frac{\partial^4 y}{\partial x^4} + \frac{\partial^2 y}{\partial t^2} - \left[\frac{J'}{m'} + \frac{EI}{\mathcal{K}}\right]\frac{\partial^4 y}{\partial x^2 \partial t^2} + \frac{J'}{\mathcal{K}}\frac{\partial^4 y}{\partial t^4} = 0 \tag{4.1}$$

where m' = distributed mass (per unit length), J' = distributed mass moment of inertia (per unit length), and $\mathcal{K}$ = shear stiffness.

The first two terms correspond to the uncorrected wave equation; the other terms represent the corrections. The first two of the correction terms correspond to the rotational inertia and shear deformations respectively. Either of these terms would appear if the appropriate correction alone were considered. The last term is a higher-order correction that is negligible even at frequencies where the first two correction terms are significant. In homogeneous structures the second of these correction terms (shear deformations) is more significant (it is 3.12 times greater) than the first (rotational inertia). This follows from the definitions of these terms

$$\frac{J'}{m'} = \frac{I}{A} = \frac{h^2}{12} \tag{4.2}$$

$$\frac{EI}{\mathcal{K}} = \frac{IE\mathcal{X}}{GA}. \tag{4.3}$$

where $\mathcal{X}$ = shear distribution parameter , and G = shear modulus.

The correction term can now be written as

$$-4.12\frac{h^2}{12}\frac{\partial^4 y}{\partial t^2 \partial x^2}. \tag{4.4}$$

These correction terms decrease the value of the propagating speed as the wavelength approaches the thickness of the beam. As that happens, the assumption allowing for the neglect of shear deformation and rotary inertia effects are no longer valid. Assuming that the correction is significant only if it changes the propagation speed by 1% or more, this relationship allows us to determine the range of frequencies for which the Euler-Bernoulli solution is valid. The Monte Carlo evaluation of the uncertainty of wavenumber ($k = \omega/c$) corresponds to an uncertainty of less than 2 degrees at the most sensitive location.

From the solution to the wave equation, it is known that $\frac{\partial^2 y}{\partial x^2}$ = multiplication by $-k^2 = (2\pi/\lambda)^2$, and $\frac{\partial^2 y}{\partial t^2}$ = multiplication by $-w^2$,
making the correction term

$$13.6(\frac{h}{\lambda})^2\frac{\partial^2 y}{\partial t^2},$$

where h = beam thickness.

The equation can then be written

$$\frac{EI}{m'}(\frac{\omega}{c})^4 - \omega^2 \left(1 + 13.6 \left(\frac{h}{\lambda}\right)^2\right) = 0. \tag{4.5}$$

Solving for c yields

$$c = \sqrt[4]{\frac{EI\omega^2}{m'}} \left(1 + 13.6 \left(\frac{h}{\lambda}\right)^2\right)^{-1/4}.$$

Thus the correction term is only necessary for values of

$$\lambda \leq .055h.$$

For the infinite beam in this experiment that corresponds to a frequency range up to 8 kHz (Cremer *et al.*, 1988).

4.2.3 Measurement of Anechoic Termination

It was also a necessary step in checking the apparatus (once the infinite beam was fabricated) to determine the the quality of the infinite beam representation.

It is assumed that the anechoic termination of a sandbox can absorb waves for which the sandbox is $>$ 1.5 to 2 times the wavelength. For the 24 inch box of this experiment and the infinite beam, this corresponds to frequencies above 200 to 300 Hz. To check the performance of the terminations, the reflection coefficients of the sandboxes were calculated according to the analysis presented in Appendix C. Figure 4.3 shows the reflection coefficients for the range of 0 to 1600 Hz, for the left and right sandboxes. It shows that for frequencies above 200 Hz, less than 10 % of the incident power is reflected back.

4.2.4 Measurement Problems

Mass Loading of Accelerometers

The next consideration was to determine the effect of the instrumentation on the beam behavior. The accelerometers behave as a lumped mass located on the beam. From Guigou (1992) and Frampton (1991) the effect of a lumped mass (located at x = 0) on an infinite beam can be expressed

$$\begin{aligned} y(x) &= W[e^{ikx} + (\frac{i\omega^2 m}{4EIk^3 + (1-i)\omega^2 m} - sgn(x)\frac{i\omega^2 J}{4EIk + (1+i)\omega^2 J})e^{ik|x|} \\ &+ (\frac{-i\omega^2 m}{4EIk^3 + (1-i)\omega^2 m} + sgn(x)\frac{i\omega^2 J}{4EIk + (1+i)\omega^2 J})e^{-k|x|}] \end{aligned} \tag{4.6}$$

where W = the initial amplitude of the incoming wave, m is the mass of the lumped mass, and J is its mass moment of inertia.

For $x > 0$ this can be written

$$\begin{aligned} y(x) &= W[e^{ikx} + (\frac{i\omega^2 m}{4EIk^3 + (1-i)\omega^2 m} - \frac{i\omega^2 J}{4EIk + (1+i)\omega^2 J})e^{ikx} \\ &- (\frac{-i\omega^2 m}{4EIk^3 + (1-i)\omega^2 m} + \frac{i\omega^2 J}{4EIk + (1+i)\omega^2 J})e^{-kx}] \end{aligned} \tag{4.7}$$

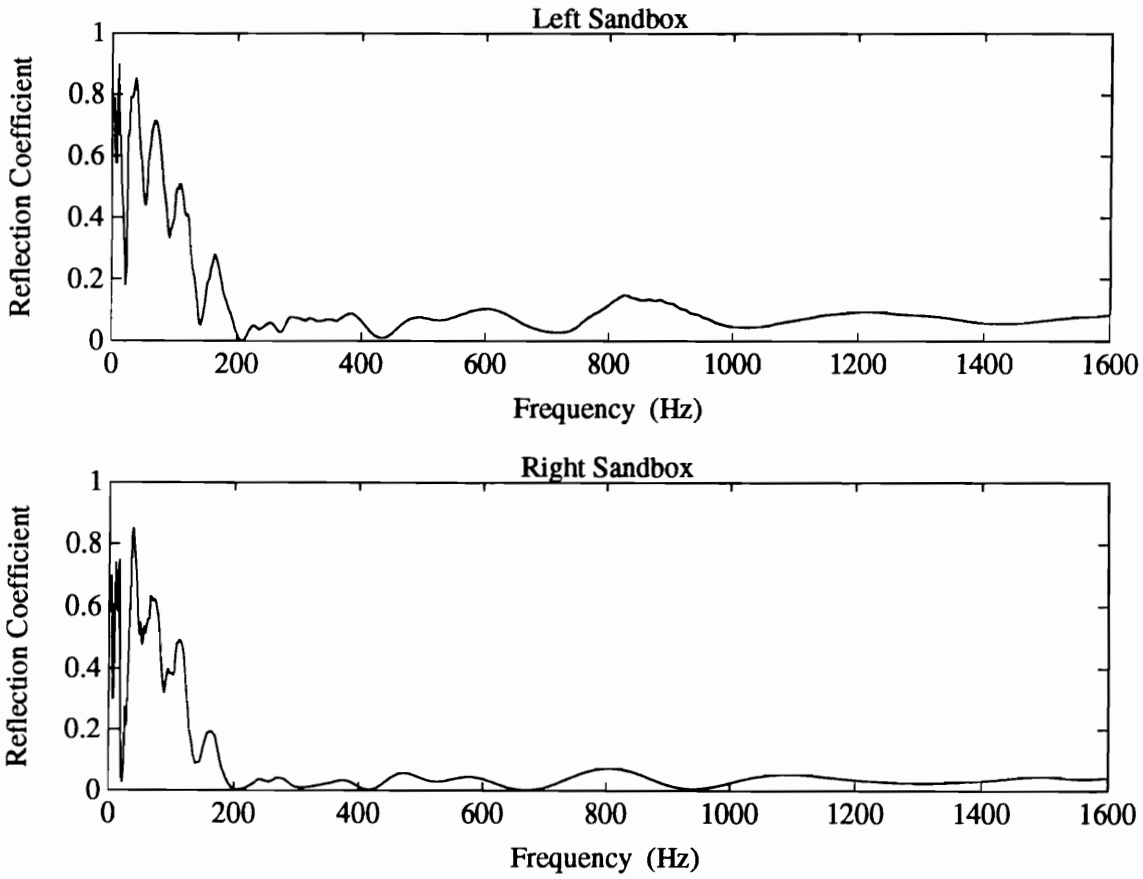

Figure 4.3: Reflection Coefficient of Sandboxes

For $x < 0$ this can be written

$$\begin{aligned} y(x) &= W[e^{ikx} + (\frac{i\omega^2 m}{4EIk^3 + (1-i)\omega^2 m} + \frac{i\omega^2 J}{4EIk + (1+i)\omega^2 J})e^{-ikx} \\ &+ (\frac{-i\omega^2 m}{4EIk^3 + (1-i)\omega^2 m} - \frac{i\omega^2 J}{4EIk + (1+i)\omega^2 J})e^{kx}] \end{aligned} \tag{4.8}$$

Equations 4.8 and 4.9 can be broken down into terms. The first term in the large bracket is the incident wave – the original wave. The terms in the first set of parenthesis (the terms multiplied by $e^{\pm ikx}$ are waves that are transmitted ($x > 0$) and reflected ($x < 0$) by the mass discontinuity. The wave is propagating from the $x < 0$ direction. The terms in the second set of parenthesis correspond to near-field flexural waves transmitted ($x > 0$) and reflected ($x < 0$) by the mass discontinuity.

To quantify the effect of the mass of accelerometers on the wave propagation of the beam, and in particular on the phase of the wave; equations 4.8 and 4.9 were evaluated. Figure 4.4 shows the magnitude and phase of a 200 Hz incident wave with no mass discontinuities, this can be compared theoretically to the response when performing measurements with an accelerometer. The accelerometers each weigh .009 lbs and act as mass discontinuities. The effect of 1 accelerometer can be seen in figure 4.5. At values of ($x < 0$) the magnitude of the wave is no longer constant, exhibiting that there is more in this region than just a travelling wave. The mass reflects part of the wave and the reflected wave combines with the incident wave to create a new waveform. This can be seen in the phase component as well. The phase is no longer a linear function, but is distorted from that of a travelling wave. To quantify how the added mass of the accelerometers can effect the measurement

process, the velocity response of the beam was measured using the laser with 2, 4, and 6 accelerometers. The phase shift per unit distance (the effective wavenumber) between two point was measured at 3 frequencies and compared. The data are given in table 4.2.4. It can be seen that the mass from the accelerometer array can load the measurement of wavenumber by about 15% with two accelerometers and about 50% with six.

Table 4.1: Errors in Measured Wavenumber with Mass Loading

	0 accelerometers	2 accelerometers	6 accelerometers
310 Hz	.54	.63	0.80
410 Hz	.61	.70	0.98
510 Hz	.67	.75	1.05

Laser Alignment

The laser is not a contacting measurement technique, and therefore adds no mass to the system. The system does have inherent measurement problems as well. The laser measures the velocity along the laser axis. As the laser scans an area it moves from being perpendicular to the beam. As the laser moves from perpendicular, the velocity measurement is a measurement of the velocity projection in the plane of the laser beam. For the scans performed in this experiment, the laser scanned a maximum of 37.5 inches of the beam at at distance of 11 feet from the beam. The sharpest angle then is formed at the $\tan^{-1} \frac{\pm 18.75}{132} = 8°$ which corresponds to an error in the velocity magnitude of $\approx 1\%$. The $\cos(8°) = 0.99$. This is considered negligible in all data. The laser was used when more than 6 sensors were required, when

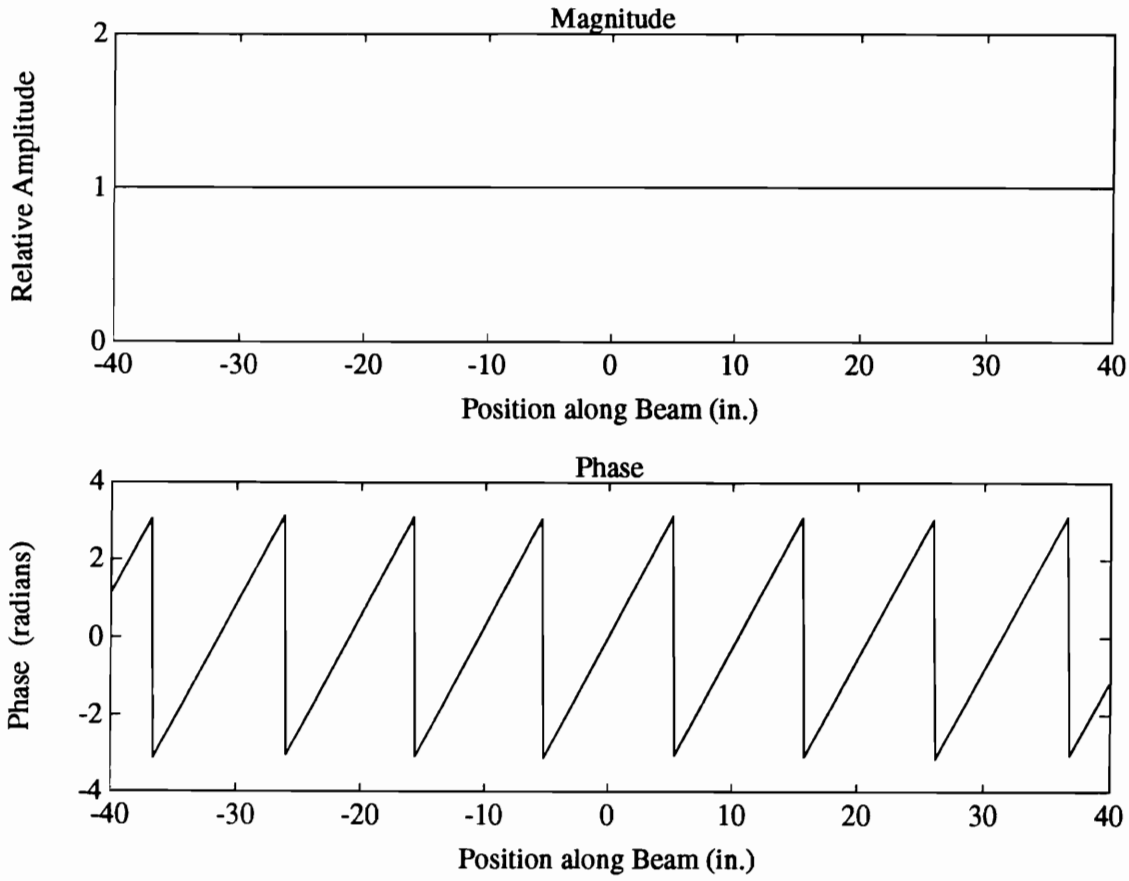

Figure 4.4: Theoretical Magnitude and Phase of Incident Wave Without Mass Discontinuity Located at x = 0

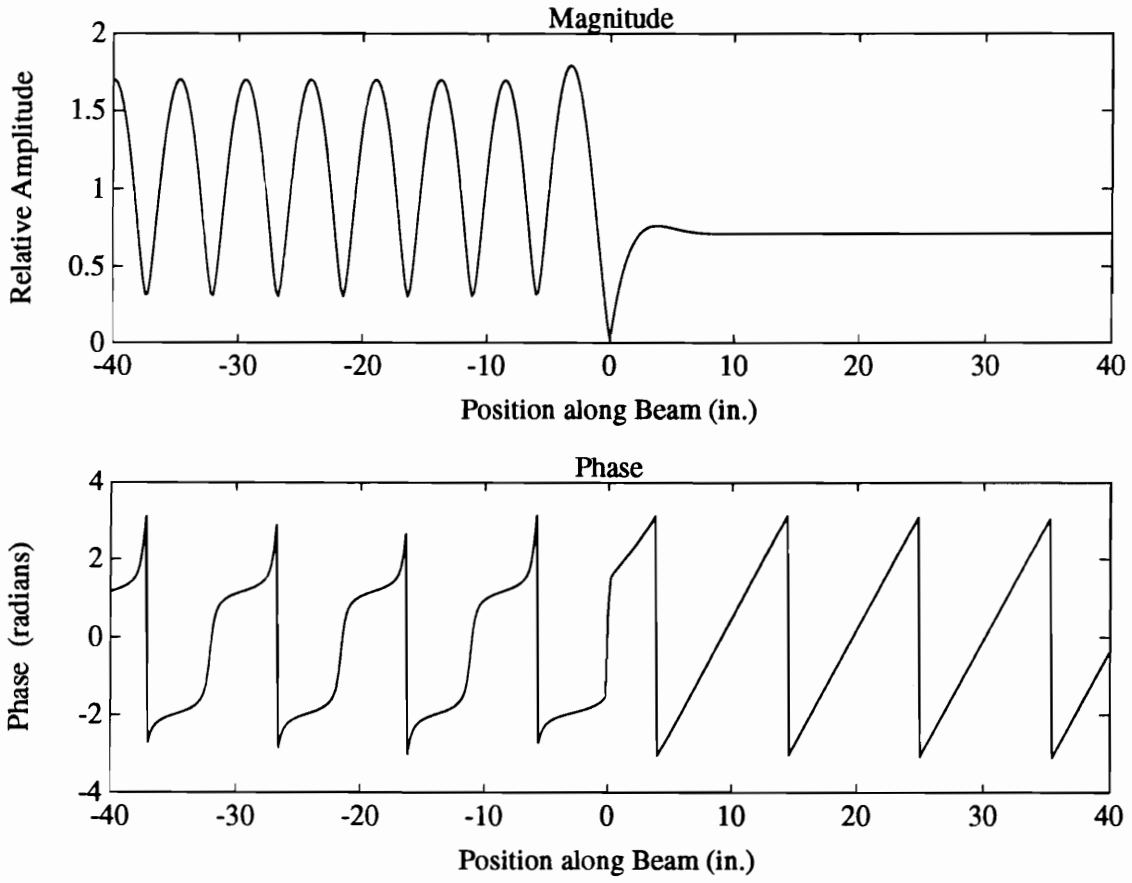

Figure 4.5: Theoretical Magnitude and Phase of Incident Wave With Mass Discontinuity

the mass loading effects of the accelerometers were substantial, or to compare the response of the beam with and without accelerometers.

The laser analysis of the response of the beam velocity was performed using a 64 point linear least squares fit. The input frequency was assumed known. The phase measurement is referenced to the output of the force transducer mounted to the shaker stinger assembly. Although it is assumed that access to the source is not available, this does not cause a loss of generality. The laser measures the response of each point in the scan independently, it is therefore impossible to reference the phase from sensor to sensor without first referencing them to another signal. The force transducer was used because it was an easily accessible signal throughout the scanning process. If simultaneously sampled data were available the phase information would be available between the sensors.

Effects of Terminal Reflections

From the analysis of the mass loading effects, it was seen that reflections can affect the measurements of the traveling waves. To quantify the affects of the $\approx$10% reflections that were found from the reflection coefficient measurements, a simulation was performed in which reflections from the anechoic terminations were added into the displacement. Figure 4.6 shows the theoretical magnitude and phase along the beam for this simulation. Figure 4.7 shows the experimental verification of this phenomenon. Data taken with the laser is displayed and demonstrates the same behavior. The magnitude of the signal is not constant, indicating the presence of more than a single travelling wave.

The phase is of particular interest; the rising line of the phase does not have a constant slope. For an ideal travelling wave propagating down a beam, one would expect to see a constant shift in phase with distance as seen in figure 4.4, with the phase wrapping around from π to $-\pi$. The phase versus position plot should have a linear dependence which wraps around at wavelength intervals (the phase going from -π to π every wavelength). The slope of that linear dependence should remain constant between wraps and it should have a value of k, k = rad/in. If the slope is not constant (as caused by the reflections) it erroneously depicts values of k that are not constant, or phase changes among sensors that are not spatially consistent. k can be estimated from the change in phase divided over the length of beam (from location 1 to location 2),

$$k = \frac{\Phi(x_1) - \Phi(x_2)}{x_1 - x_2}. \tag{4.9}$$

If equation 4.9 is used to measure k, then errors up to 50 % are incurred. Similarly the phase shift from location to location can be erroneous.

From equation 4.9 it is that k is the slope of the phase line; it is the change of the phase (in radians) per inch. While it is obvious from figure 4.6 that the slope changes along the wavelength, the variations in the waveform are consistent from wavelength to wavelength. The wavelength has not changed, but the rate of change of phase varies non-linearly from position to position. In order to minimize the effects of this warble in phase, it is important to use information that is at least a wavelength long

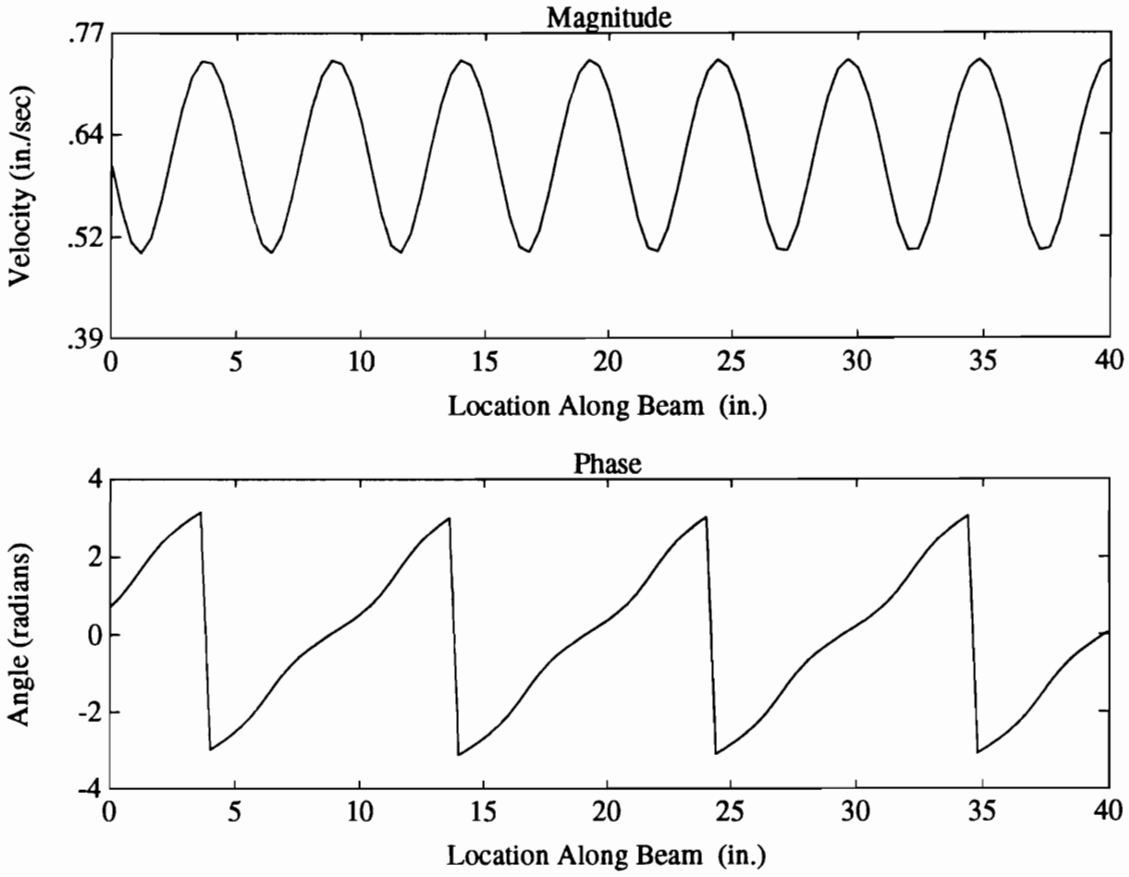

Figure 4.6: Beam Displacements with 10% Reflections - Theoretical

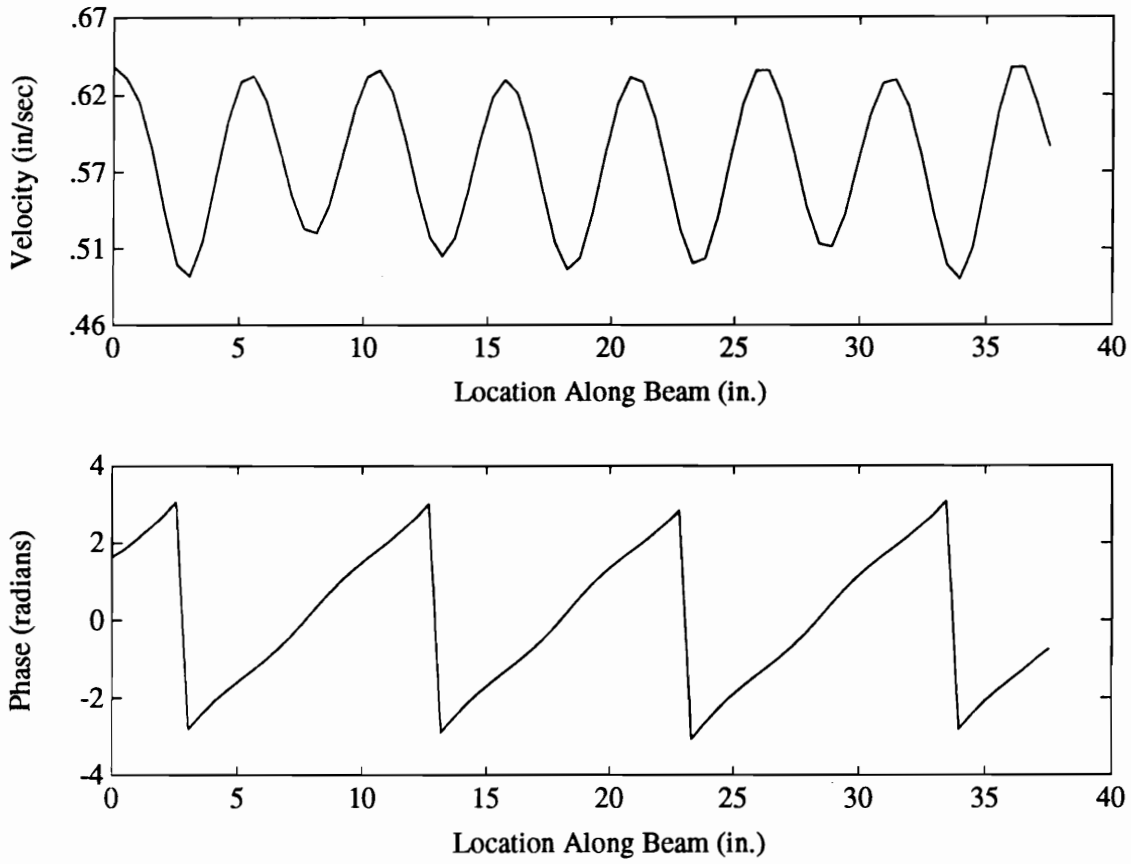

Figure 4.7: Experimental Verification of Beam Displacements with 10% Reflections

so that the warble is effectively averaged out. If sections of the wavelength are used, the phase shift from location to location is a misrepresentation of the wavenumber. Figure 4.8 shows how the values of k vary along the wavelength, but the variation is centered about the theoretical value. The values of k were calculated by measuring the phase at adjacent sensors along the beam and dividing that phase by the separation distance. In this way figure 4.8 calculates the instantaneous, spatial slope of figure 4.7.

4.3 Experimental Results

4.3.1 Noise Reduction

The first task of the experiment was to prove that arrays can improve the SNR. This can be shown in a number of ways; the output of the data in both time domain and frequency domain will be examined.

Time Domain

To examine the performance of the array in the time domain consider the performance of the 6 element array of accelerometers. Figure 4.9 shows the improvement in signal quality with 6 accelerometers. The response of the beam to sinusoidal excitation at 310 Hz was measured using 6 accelerometers. The data were acquired at 26.75 kHz and filtered with a low pass 8 pole 6 zero elliptic filter set at the Nyquist Frequency. The data were normalized by the maximum output to have the same amplitude (because of the small reflective content the amplitude was not constant from sensor to sensor), then combined with white noise, aligned in phase to a ref-

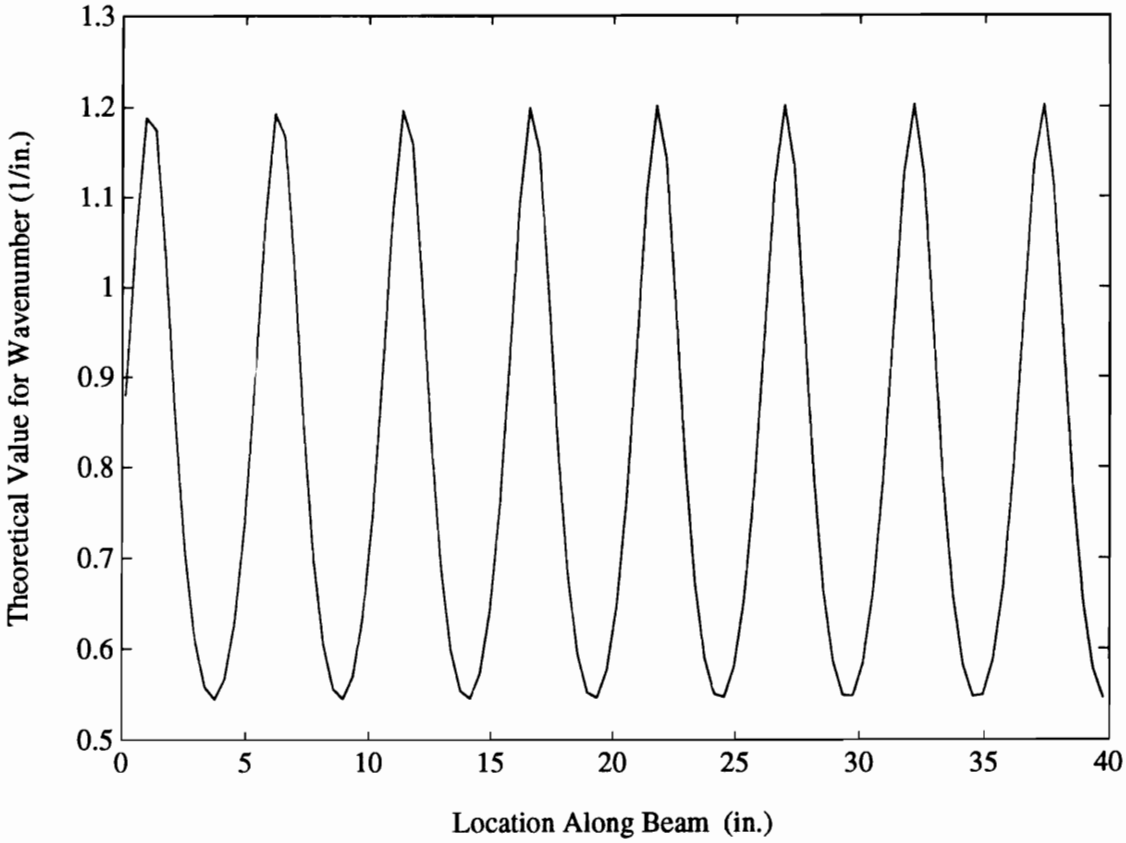

Note: This figure shows the estimation of k based on the instantaneous slope of the phase line. It depicts how a nonlinear phase causes variations in the estimation of k.

Figure 4.8: Estimation of Wavenumber Based on Theoretical Phase (Figure 4.6) from 10% Reflections

erence sensor, then averaged. As larger sensor arrays were fabricated by combining the signals of smaller sensor arrays each group was aligned in phase to a common reference measurement. The improvement in signal to noise ration will be quantified in the frequency domain development.

With larger arrays greater improvement is possible. To generate the larger array, 6 independent data sets were combined. To fabricate the response of a 36 element array. Figure 4.10 shows how SNR improves with large sensor arrays.

It is also important to realize that if these signals are combined arbitrarily (i.e. without compensating for the delay between sensors) the signal can be obscured. Figure 4.11 shows that the signal content can be lost without beamforming. These signals were combined without adjusting for the phase between sensors. The signal has been averaged out along with the noise. This can be seen in the signal strength decrease of 36 averages.

These experiments validate the noise reducing properties of an array. An array can take a noisy signal and decrease the noise level dramatically. There is also a danger of an array obscuring the signal through destructive interference.

Frequency Domain

The frequency domain response of the array will be considered using three different techniques. The same data (as the time domain techniques) is analyzed here. First the average of non-beamformed spectra of the accelerometers will measured. Second the averages of the power spectra will be evaluated. Finally, the spectra of the

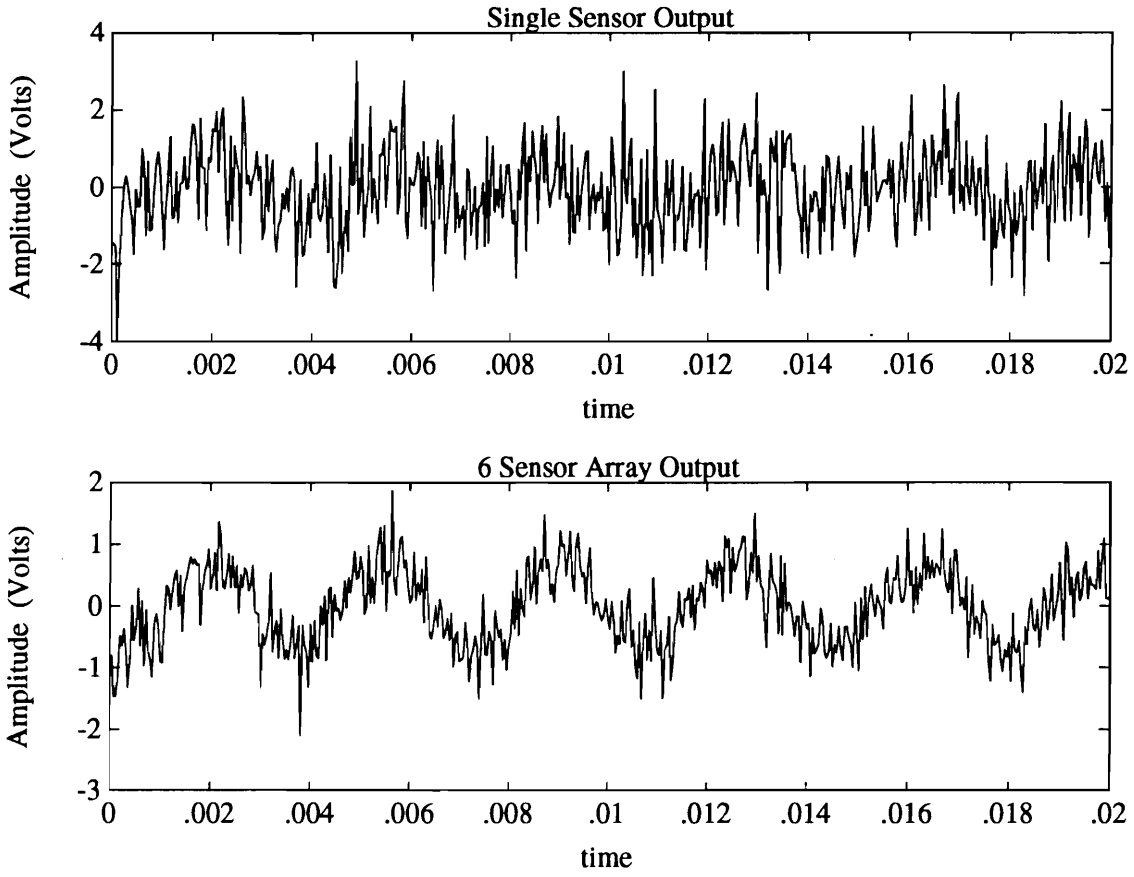

Figure 4.9: Time Domain Response of 6 Element Array – Beamformed

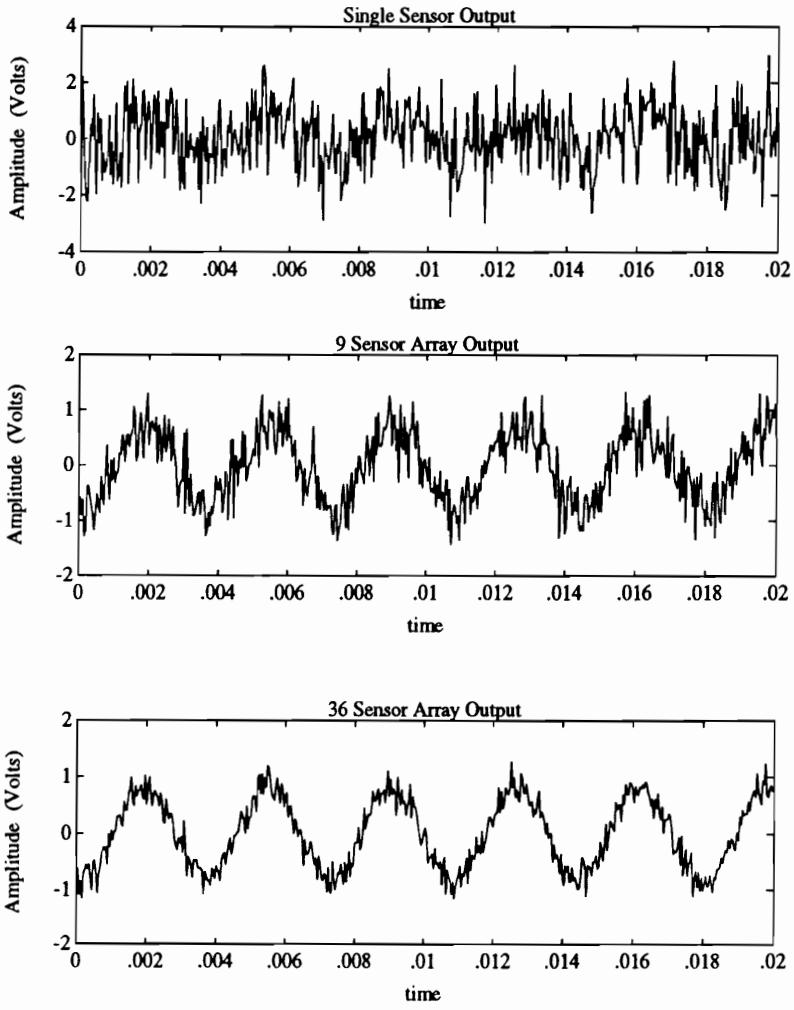

Figure 4.10: Time Domain Response of Infinite Beam Using Beamformed Array

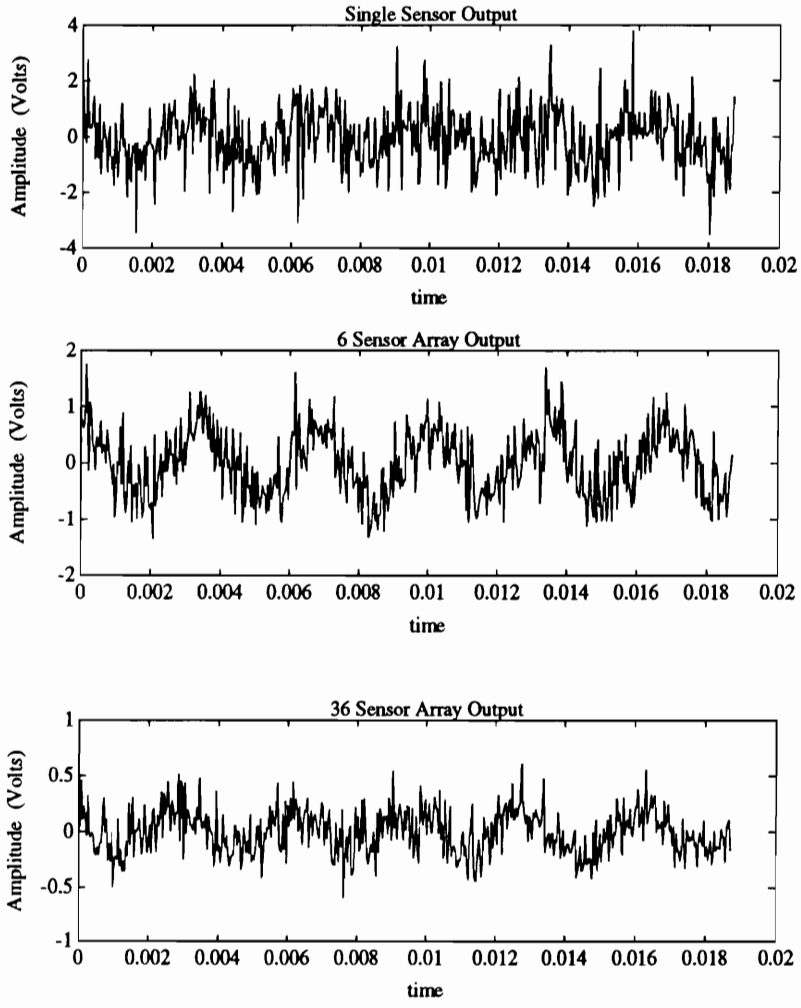

Figure 4.11: Time Domain Response of Infinite Beam Using Non-Beamformed Array

beamformed spectra will be considered.

Averaging the spectral response of the sensors has the same effect as measuring the spectral content of the non-beamformed time data. In either case the phase shifts (measured in either time or frequency) between sensors cause destructive interference. Figure 4.12 illustrates this without added noise.

The second technique prevents the loss of signal in averaging by averaging the autospectra of each sensor. The autospectra is a real only quantity, that cannot lose the signal through destructive interference. The result of this technique can be seen in figure 4.13, again without added noise.

The final technique takes the beamformed data and determines the spectral content. The data are phase shifted so that the measurements are aligned to the reference sensor. Figure 4.14 shows the improvement in SNR for the 6 element array. The improvement of larger array is produced as before and can be seen in figure 4.15. The improvement in SNR can be found in table 4.3.1.

Again, the frequency domain techniques show that arrays can accomplish noise reduction. Just like the time history, the frequency spectra can be averaged destructively and cause a loss of signal content. If phase information is unimportant to the application, then the power spectra can be averaged without any danger of phase cancellations. If the frequency content is important, then the data must be aligned in phase and then analyzed.

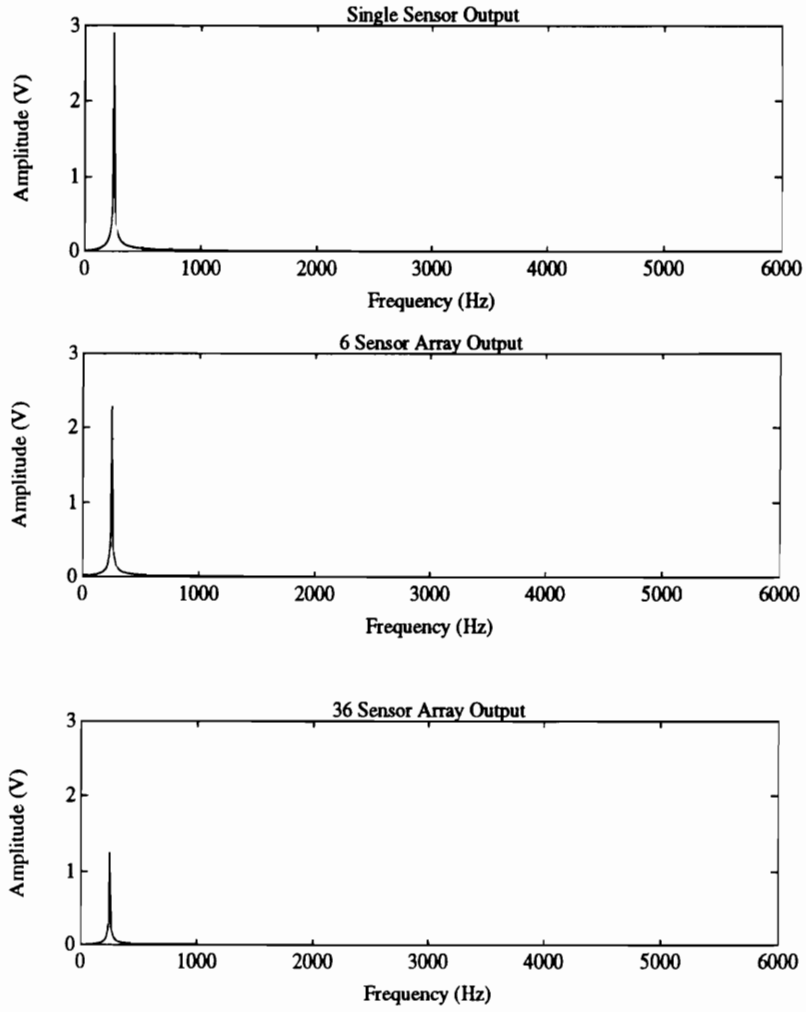

Figure 4.12: Frequency Response on nonbeamformed spectra

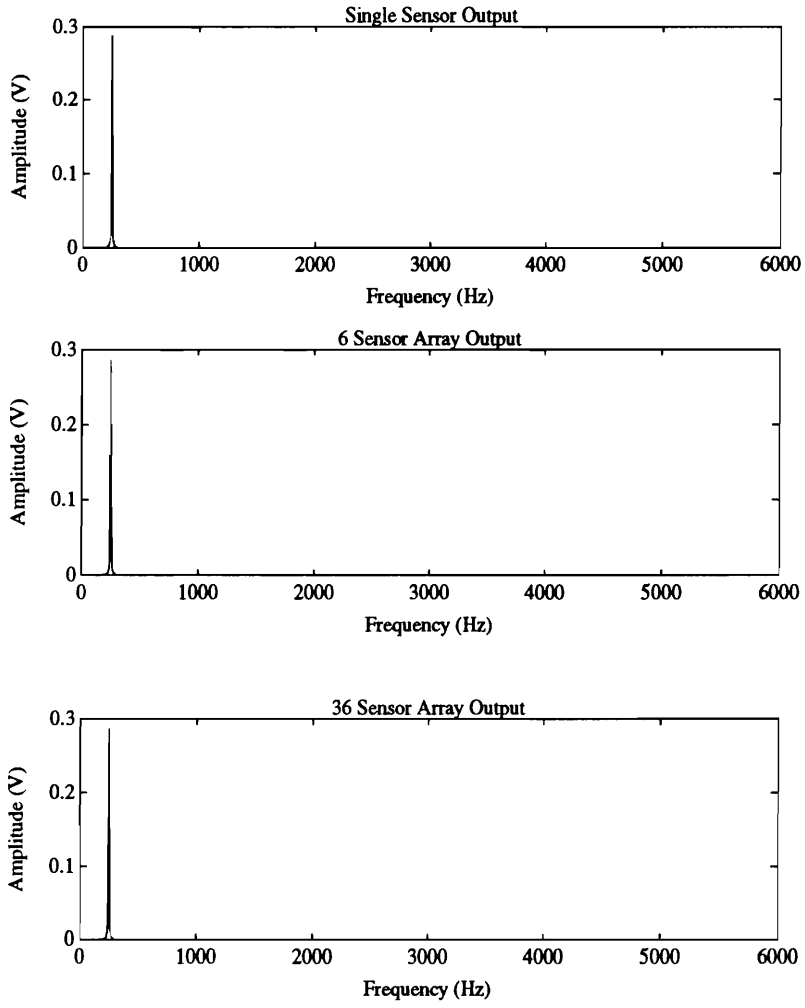

Figure 4.13: Frequency Response of Array – Autospectra

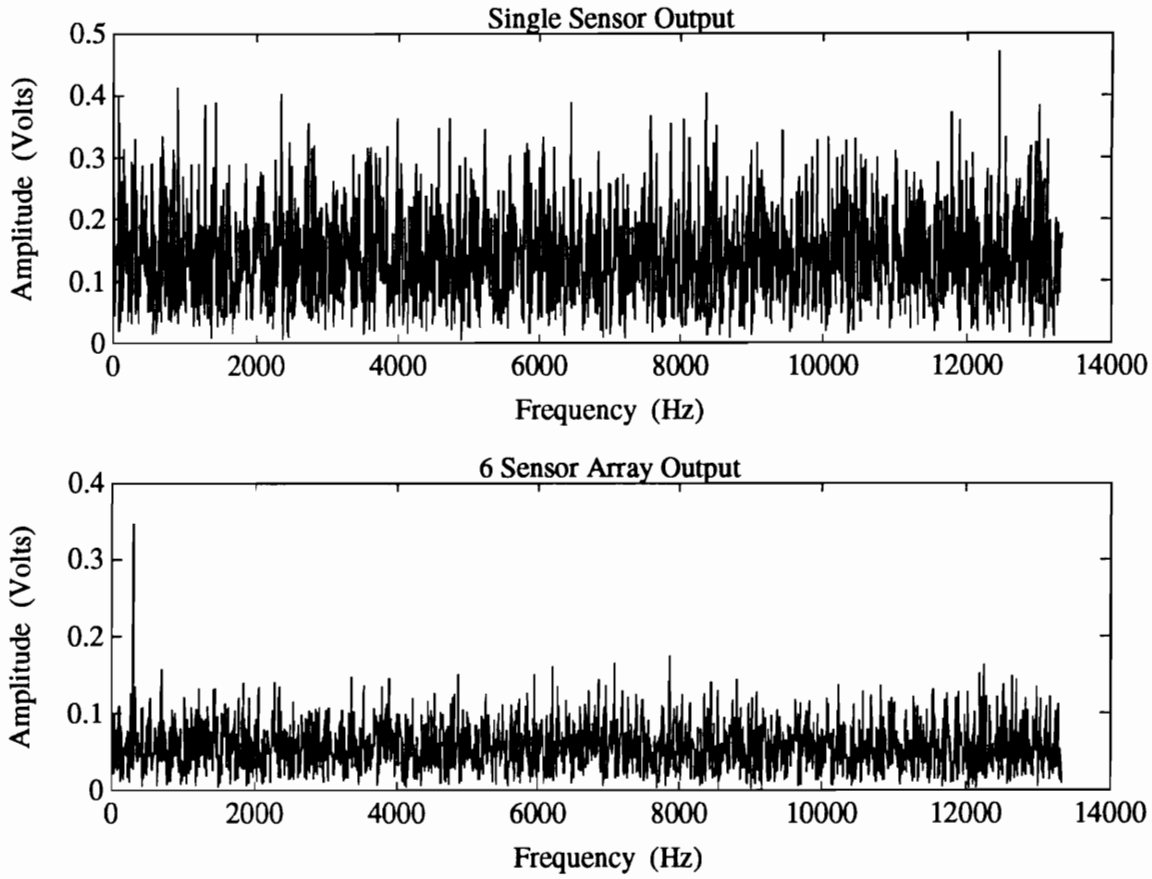

Figure 4.14: Frequency Domain Response of Infinite Beam Using Beamformed Array

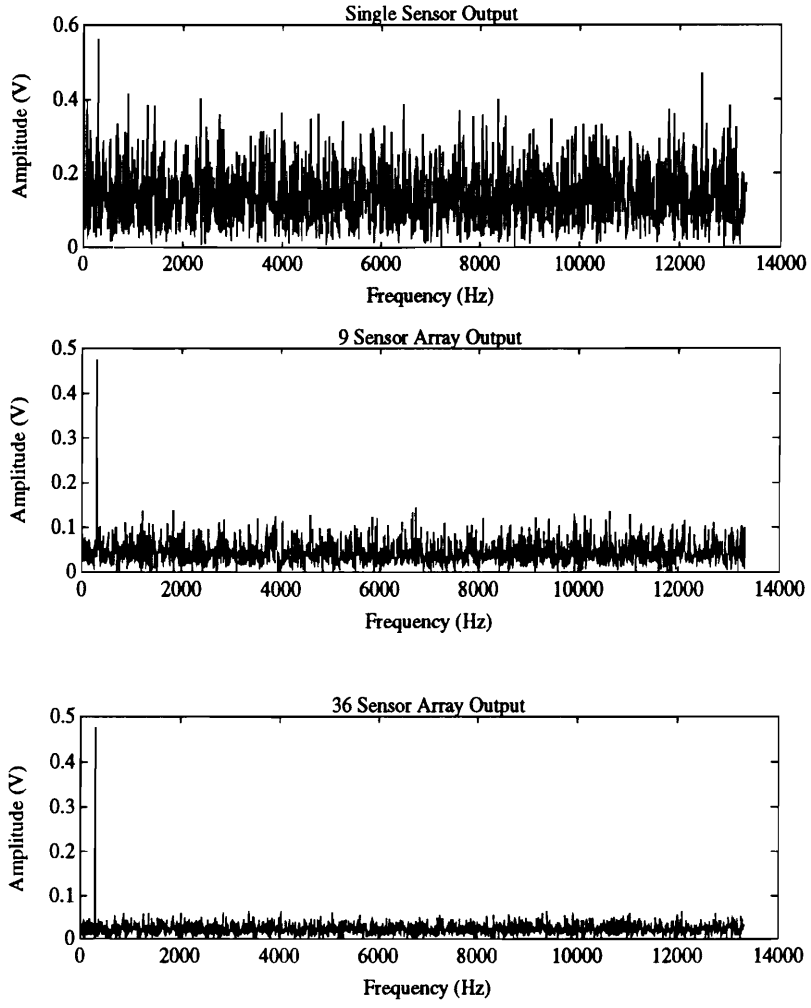

Figure 4.15: Frequency Response of Larger Arrays – Beamformed

Table 4.2: Measured SNR Values for Arrays

SNR of 1 sensor array		1.028
SNR of 9 sensor array		2.672
SNR of 32 sensor array		5.252
	theoretical	*simulated*
9 vs 1	3	2.6
36 vs 1	6	5.11
36 vs 9	2	1.96

4.3.2 Determination of AOA

While the classical beamformer, or any of the other signal processing techniques can be used to provide angle of arrival information, a more direct approach will be taken. Using the relationships between sensors, like the ones given in equations 3.17, 3.18, and 3.22, the AOA can be solved for explicitly. The restriction is that all elements of the grid must be definable (with respect to another) by either a sine or cosine relationship and not a combination of sines and cosines as in equation 3.20.

The beam acts as a one-dimensional structure, and the propagation direction of waves is always along the beam. Since the direction of propagation can not be changed, the array orientation must be changed to demonstrate AOA determination. If the 3x3 grid were mounted on the beam at a 30° angle of rotation it should measure an AOA of $-30°$. Directivity can be demonstrated with arrays skewed from normal on a one-dimensional beam.

The grid of the laser data lends itself to this kind of analysis. Each grid location is a sensor, determining amplitude and phase. By choosing the appropriate geometry

of sensor locations angles from 0 to 90° were measured. Figure 4.16 shows sensor locations for the angles analyzed. Rectangular arrays at 0, 14, 26.6, 45, 63.4, 71.6, and 90 degrees were generated from the grid of laser measurements. A base array of 4 sensor locations exist for each configuration and the array equations are given below. This arrangement stays within the implicit restraint of sines or cosines. The spacing of the grid in x and y coordinates is .5068 in. horizontally and .2534 inches vertically.

$$\phi_{21} = \frac{ks_{21}\sin\theta}{\omega} \tag{4.10}$$

$$\phi_{31} = \frac{ks_{31}\cos\theta}{\omega}$$

$$\phi_{43} = \frac{ks_{43}\sin\theta}{\omega} \tag{4.11}$$

While the laser grid is defined by the x-y coordinate system, each array configuration has its own coordinate system, and the spacing relative to the reference frame changes accordingly. The spacing for the base grid for each angular orientation is given in table 4.3.

Returning to the problem of small amounts of reflectivity causing variances in the delay between sensors along the length of the beam, it is necessary to repeat the unit cell grid down the length of the beam. This also maximizes the information available. Then for each cell group, the expressions of equation 4.12 can be used to solve for the θ, averaging the values to determine the AOA.

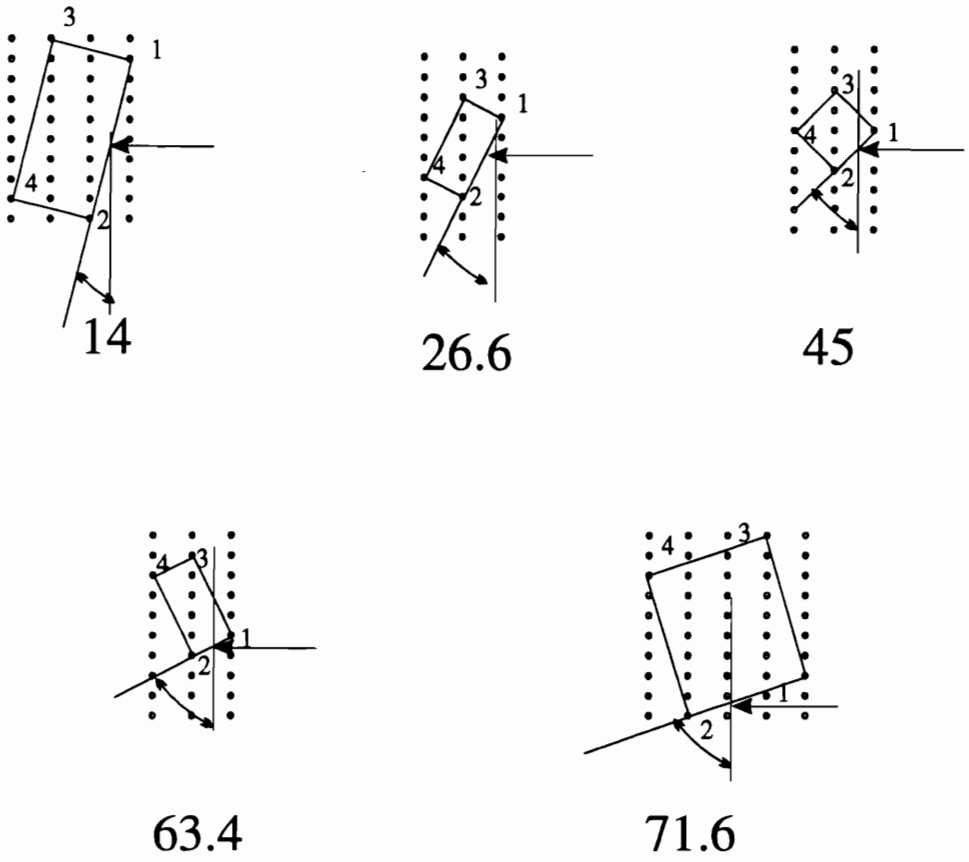

Figure 4.16: Grid Arrangement For AOA Calculations

Table 4.3: Sensor Spacing for Laser Grid

Angle	s_{21}	s_{31}	s_{32}
0	0.2534	0.5068	0.2534
14	2.0894	1.0447	2.0894
26.6	1.1331	0.5666	1.1331
45	0.7167	0.7167	0.7167
63.4	0.5666	1.1331	0.5666
71.6	1.6025	1.6025	1.6025
90	0.5068	0.2534	0.5068

Data were taken with the laser for frequencies between 310 and 710 Hz in 20 Hz increments. The processing algorithm selected the sampling frequencies based on the excitation frequency. These values can be found in table 4.4. All data were filtered with a low pass 8 pole Butterworth filter at the Nyquist frequency.

Least squares processing was performed on the data to determine the magnitude and phase of the response. The values were curve fitted with a two-degree of freedom (5 x 12 order) polynomial (to the 10x75 data set) fit to smooth out dropout from the laser. This program performed a surface fit of a complex matrix using a regression model of Legendre polynomials (for orthogonality) in the form $z(x,y) = (a_0P_0(x) + a_2 * P_1(x) + ...a_{12}P_{12}(x))...(b_0P_0(y) + b_2 * P_1(y) + ...b_5P_5(y))$ with complex coefficients. After the processing the AOA was determined from the phasing of the cells. Figures 4.17 through 4.19 show the determined AOA versus frequency, the line indicates the actual AOA. The agreement between true and measured data is good with the maximum error being less than 3 degrees. Table 4.3.2 gives the values found for

Table 4.4: Table of Sample Rate for Laser Data

Excitation Frequency(Hz)	Sample Frequency (kHz)
310	2.5
330	2.6
350	2.8
370	3.0
390	3.1
410	3.3
430	3.4
450	3.6
470	3.7
490	3.9
510	4.1
530	4.2
550	4.4
570	4.6
590	4.7
610	4.9
630	5.1
650	5.2
670	5.3
690	5.5
710	5.7

each configuration at each frequency. The mean values and the standard deviation of the data are given at the bottom of the table.

From the values of table 4.3.2 it can be seen that the phase can be used to determine the AOA. From the values listed in the table, one can see that the errors worsen as the frequency increases. This is to be expected as was shown by the sensitivity plots in figure 3.10. It can also be seen from the standard deviations that there is more spread as the AOA reaches 0 or 90. This comes from the sensitivity of the sin^{-1} and cos^{-1} as the value of the delay approaches its maximum value as seen in figure 3.10. The spread at 0 and 90 is not as great as it might be because if the argument of sin^{-1} and cos^{-1} exceeded ± 1, (where the function no longer exists, the argument was limited to ± 1.

If one looks at the mean values of the AOA's, there is a bias error in the data. The mean values of AOA are lower than true for most angles. The most likely cause for this is uncertainty in the grid spacing. For the spacings of .5068 and .2534 inches, uncertainties of .004 inches and .002 inches correspond to $\pm$ .5 degrees.

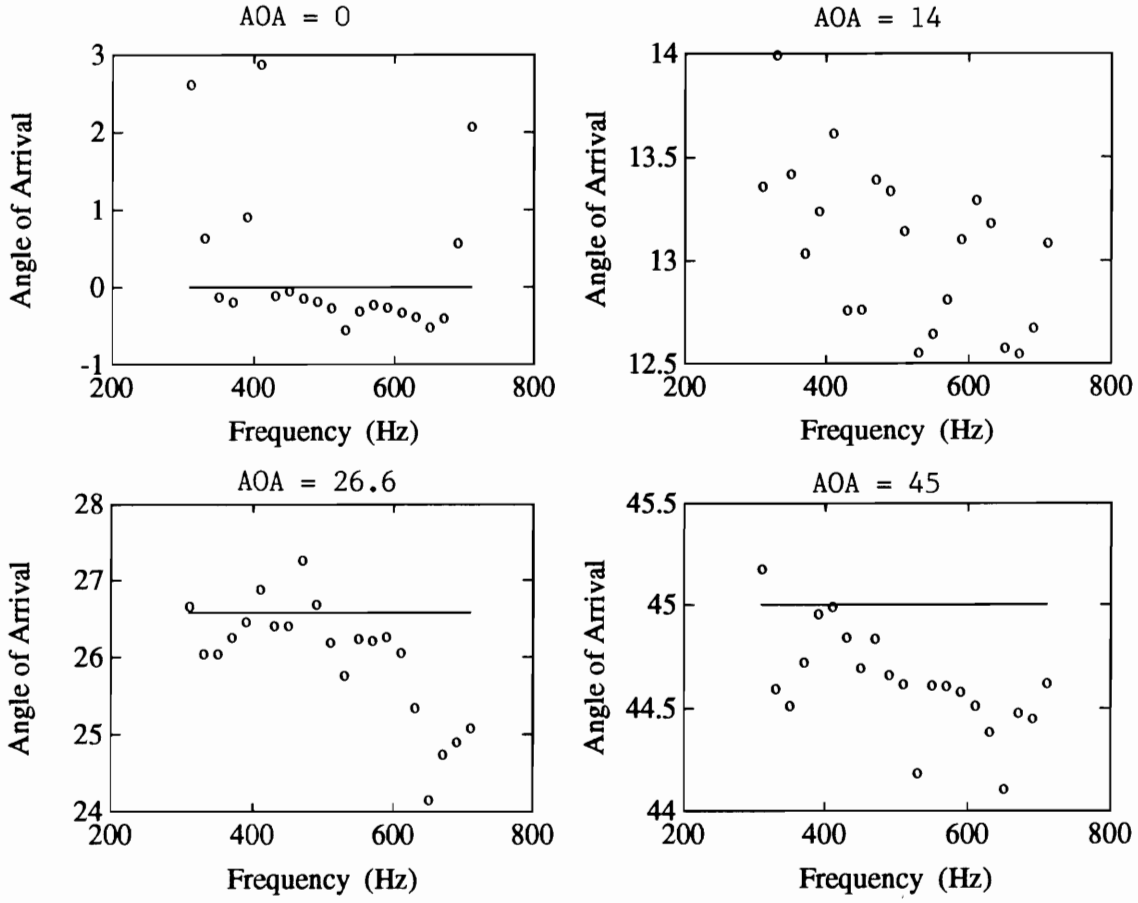

Figure 4.17: Experimentally Determined Angle of Arrival for Infinite Beam

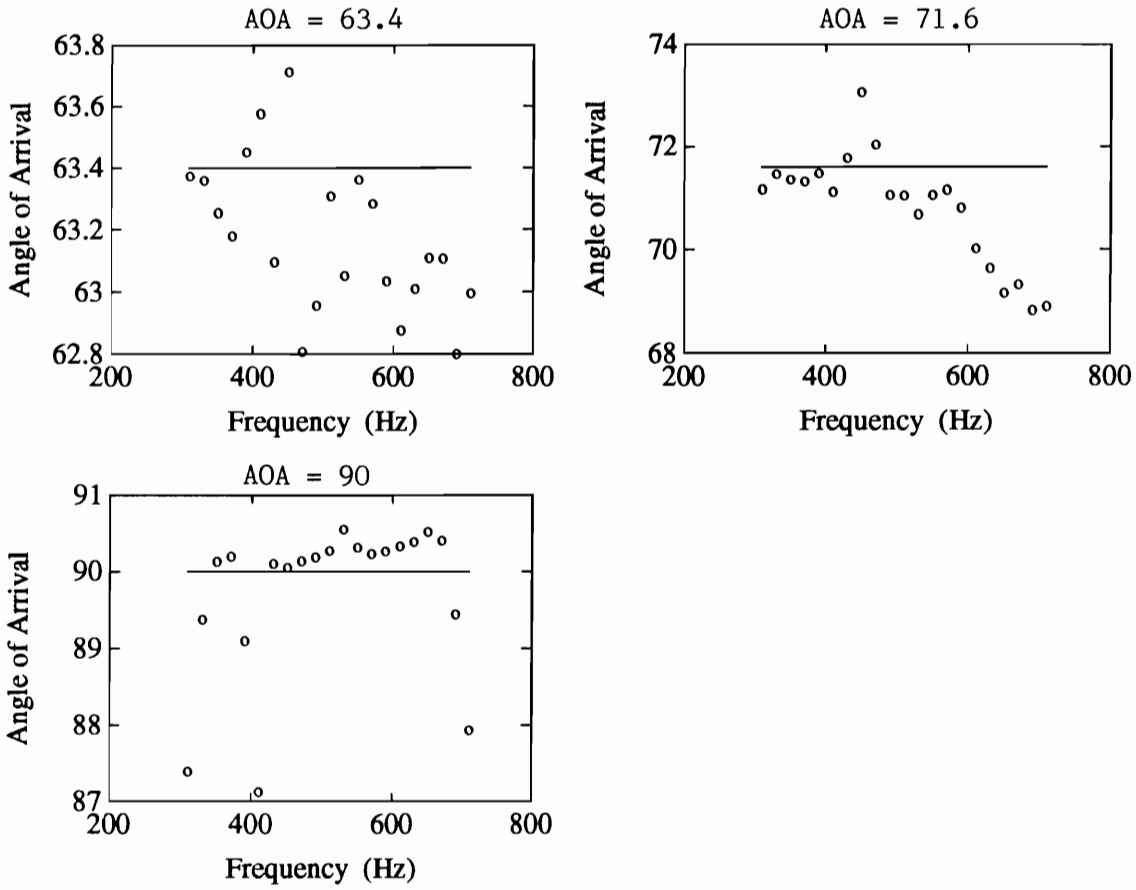

Figure 4.18: Experimentally Determined Angle of Arrival for Infinite Beam – cont.

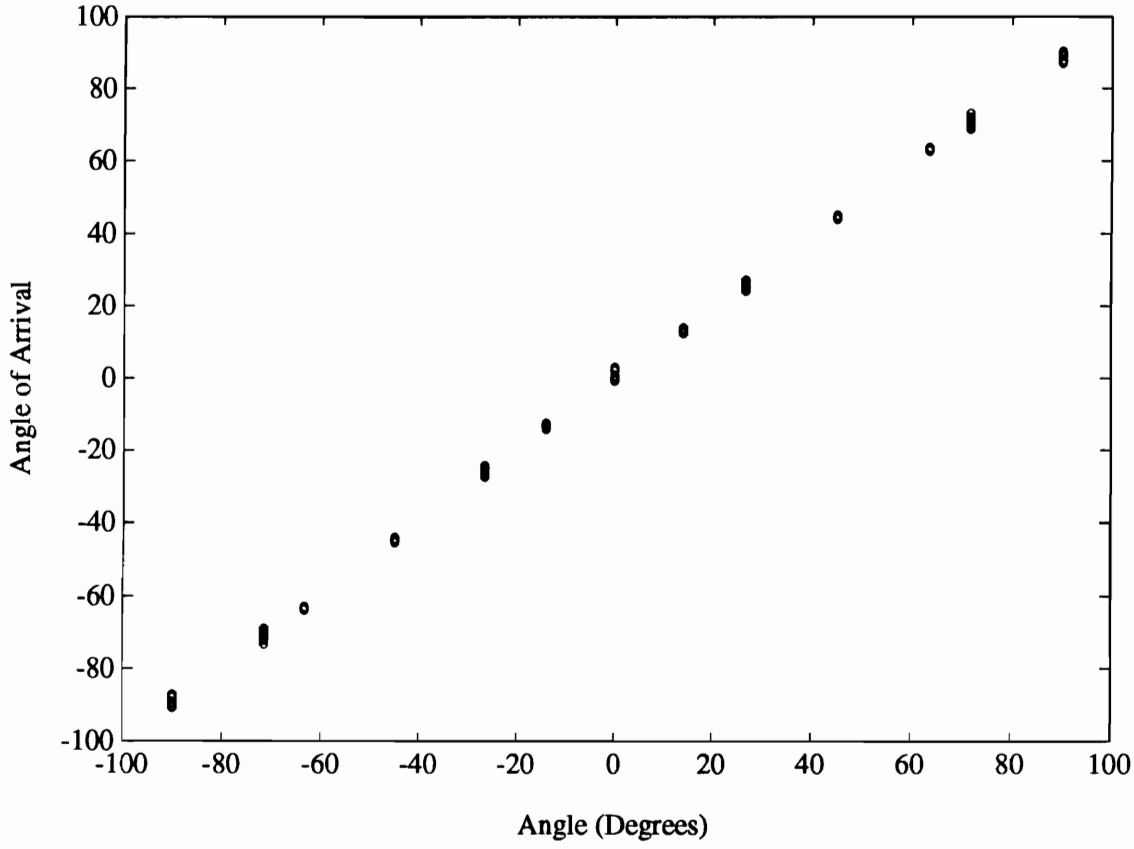

Figure 4.19: Experimentally Determined Angle of Arrival for Infinite Beam vs Angle of Arrival

Table 4.5: AOA Measurements

Hz	0	14	26.6	45	63.4	71.6	90
310	2.60	13.35	26.65	45.17	63.37	71.15	87.39
330	0.62	13.99	26.03	44.59	63.35	71.46	89.37
350	-0.13	13.41	26.03	44.51	63.25	71.33	90.13
370	-0.19	13.03	26.25	44.71	63.17	71.30	90.19
390	0.90	13.23	26.45	44.95	63.45	71.47	89.09
410	2.88	13.61	26.87	44.98	63.57	71.10	87.11
430	-0.10	12.75	26.40	44.84	63.09	71.77	90.10
450	-0.05	12.76	26.40	44.69	63.71	73.05	90.05
470	-0.14	13.39	27.26	44.83	62.80	72.03	90.14
490	-0.18	13.33	26.68	44.65	62.95	71.04	90.18
510	-0.26	13.13	26.19	44.61	63.30	71.03	90.26
530	-0.55	12.55	25.75	44.18	63.05	70.67	90.55
550	-0.31	12.64	26.24	44.60	63.36	71.04	90.31
570	-0.23	12.81	26.20	44.60	63.28	71.14	90.23
590	-0.26	13.10	26.26	44.57	63.03	70.80	90.26
610	-0.32	13.29	26.05	44.51	62.87	70.01	90.32
630	-0.38	13.17	25.34	44.38	63.00	69.62	90.38
650	-0.51	12.57	24.14	44.10	63.10	69.15	90.51
670	-0.40	12.54	24.73	44.47	63.10	69.32	90.40
690	0.55	12.67	24.90	44.45	62.80	68.82	89.44
710	2.00	13.08	25.08	44.61	62.99	68.89	87.92
mean	0.28	13.07	26.00	44.62	63.17	71.73	89.73
std	1.02	1.13	0.98	0.46	0.34	1.38	1.05

Chapter 5

Application of Sensor Array to Finite Beam – Experimental Transient Broad band Response

Now that the performance of the array for narrow band signals has been characterized, the performance under broad band disturbance needs to be analyzed. What happens to the array's performance when the structure is impacted (hit with an impulse)? Can the system be analyzed as before? The development of the SNR, AG, and AOA were all based on the ability to beamform the data. The beamformer uses the delay caused by propagation to determine the proper phasing between sensors. With multiple frequency content in a dispersive media multiple propagating speeds exist. The array cannot beamform for more than one frequency at a time. If the phasing for each frequency can be determined separately, then that information can be used to do the AOA determination.

A logical choice might be to use the FFT to switch the signal into the frequency domain and deal with each frequency separately. For a transient response, the time domain response of the array can be captured by each sensor. Each signal can then

be transferred into the frequency domain. Transfer functions between sensors should show the phase relationship between the sensors and the analysis proceeds as before. This works as long as no reflections are present; but in finite structures reflections can not be avoided.

A likely solution to this would be the truncation of the time domain signal to insure against reflections. For a given frequency range, the maximum propagating speed is known, and thus the length (of time) of data is defined. This procedure would dictate a different length time history for each point. Fourier transforming different length time histories creates leakage and thus destroys the phase information.

While it might be possible to truncate all the sensor signals at the same point in time (as dictated by the shortest one) and insure no reflections, there is no guarantee that all the resulting time histories will have signal content. It is certainly guaranteed that they will not have the same frequency content so that phase comparisons can be made.

Knowing that the frequency domain technique will not describe the phase information, two things are evident. One, power spectra must be used for any frequency domain averaging that is done. Two, time domain techniques must be employed to determine phase information.

While the dispersive property of flexural waves precludes analysis of phasing in the frequency domain, it can be exploited in the time domain. Each point along a beam is temporally and spatially linked. So each point down the beam (in the propagation

direction of the wavefront) will have a different time history.

Imagine an impulse containing frequencies from 0 - 50 Hz acting on a beam. At the source the frequencies are coincidental; they occur nearly simultaneously. As the signals propagate away from the source, the frequency content begins to disperse; the frequencies that existed simultaneously at the source will spread over an increasingly longer time period as they move away from the source. From equation 3.15, it is known that the delay from is proportional to the square root of the frequency. The 36 Hz component will have travelled twice as far as the 9 Hz component. Close to the source the frequencies seem lumped together, but as they propagate away, the spread widens. Once significantly far away from the source (that significance dictated by the frequency content and the propagation characteristics) the frequencies separate.

This behavior can be seen in figure 5.1. This plot shows the difference in time histories as dependent on beam position. The response of the beam to an low frequency impact (a half rectified sine wave of .018 seconds duration) was measured at 4.44 inch intervals along the beam. Data were taken at 50 kHz. Because the laser can only scan one point at a time, a programmed impulse was repeated for each data point and was used as a trigger to simulate simultaneous sampling.

The propagation of the wavefront delays in time as the sensor location moves down the beam; it takes longer to travel farther. Further, the impulse spreads as its travels, the high frequencies being measured first, and the low frequencies arriving last. This can be seen in the data by comparing the time histories for the closest and

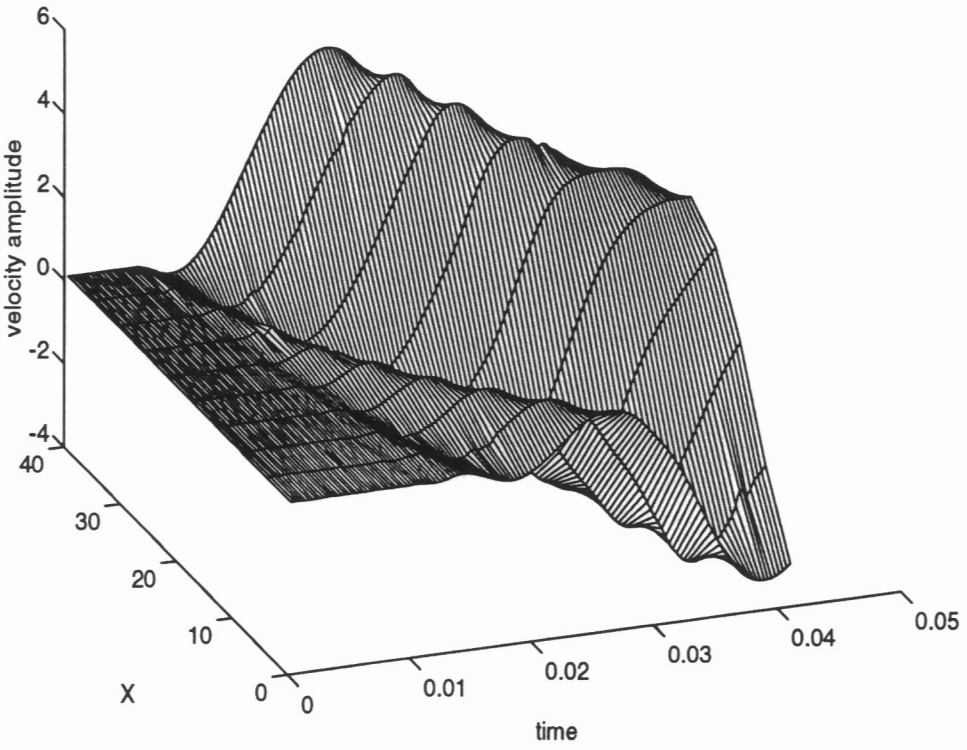

Figure 5.1: Example of Dispersion in Beam – Plot of Time History for Different Sensor Locations in Response to Impact

farthest sensors in figure 5.2. At the farthest sensor it can be seen that the high frequency component has separated from the gathering of other frequencies, as given by the dispersion equation, equation 3.15. This can be seen at time = .015 seconds. No such component is distinguishable in the nearest sensor as the frequencies have not had the time to spread apart.

So it can be seen, as previously stated, points at the same distance along the propagation axis are linked spatially and temporally. The signal content of sensors coplanar in the wavefront should be the same except for noise. They should have experienced the same amount of dispersion. So if the time histories can be quantitatively compared, those with the most similar time histories describe the propagation direction.

The correlation coefficient (CC) is a means to do this quantitative comparison. The CC is a measure of the strength of the relationship between two variables and is defined by

$$CC = \frac{S_{xy}}{\sqrt{S_{xx}}\sqrt{S_{yy}}} \tag{5.1}$$

where $S_{AB} = \sum_{i=1}^{N} AB$.

It is helpful to note that the CC is a normalization of the covariance matrix that bounds the values between -1 and 1. It is expected that the correlation coefficient would be maximized for sensors at the same point along the wave front. This rela-

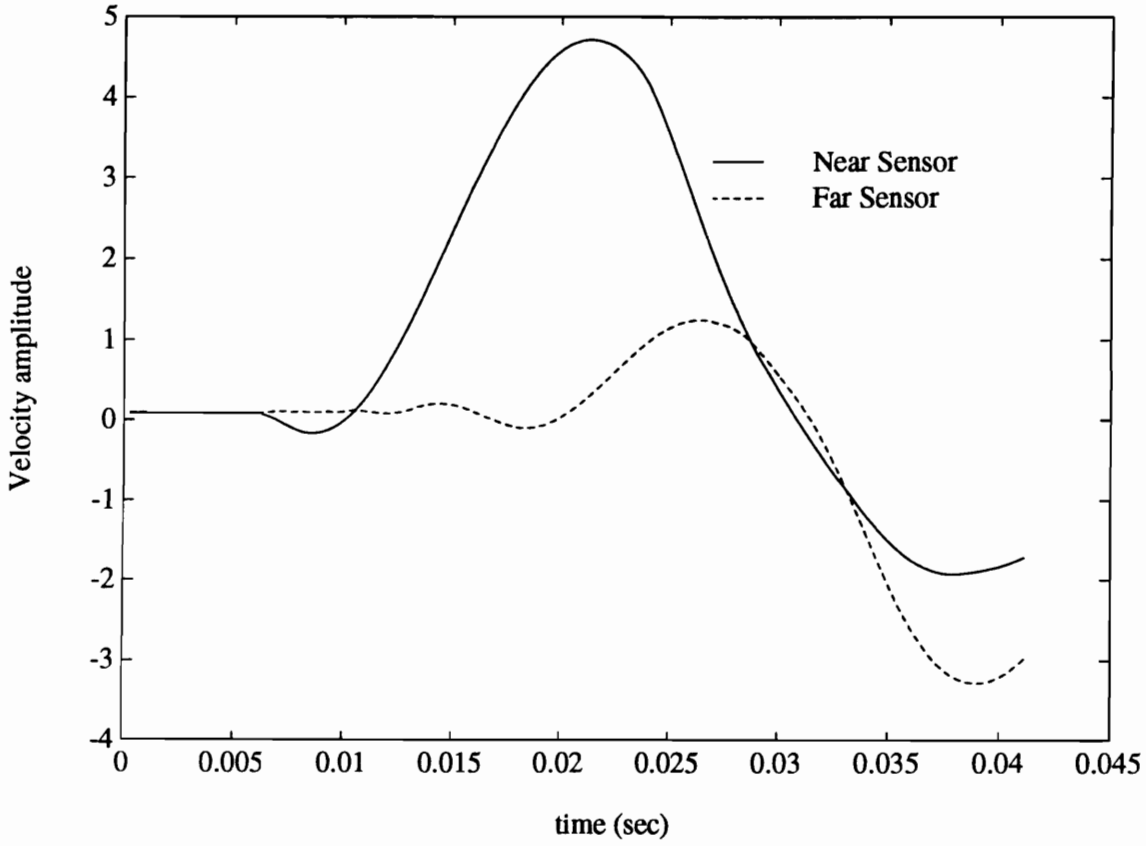

Figure 5.2: Time Histories at Two Different Beam Positions in Response to Impact

tion will be the foundation for AOA determination for broad band sources.

To verify this, transient data were taken using the laser velocimeter. The response of the beam to an impulse was measured for a grid of points on the beam. Arrays measured at 0, 26.6 45, 63.5 and 90 degrees were constructed from the grid and the correlation coefficients were calculated for the sensor locations.

The grid was made of a rectangular matrix of points spaced a third of an inch apart and covering approximately a 3 by 6 inch area. This experiment was set up to produce a worst case scenario result. The impulse has frequency content from 0 to 50 Hz; these low frequencies have low propagating velocities. With the closely spaced grid and slowly propagating waves, the change from sensor to sensor will be small. While this will result in high correlation coefficients for all sensor locations, little change will occur within the array. With faster wave velocities or greater sensor spacing, the change in the correlation coefficient from sensor to sensor is greater. Figure 5.3 shows the excitation sent to the shaker and the signal measured at the force transducer. The excitation signal was used to trigger data collection.

Figure 5.4 shows the array orientation for each configuration and the lines on these show the assumed 0 degree line. The output of each array is calculated by measuring the angles among all the sensors and determining the correlation coefficients among them as well. Sensor pairs of the same angular orientation are averaged to give the CC for that AOA. The maximum CC should occur at the angle matching the AOA.

The results of the experiment are presented in figures 5.6 through 5.10. It can

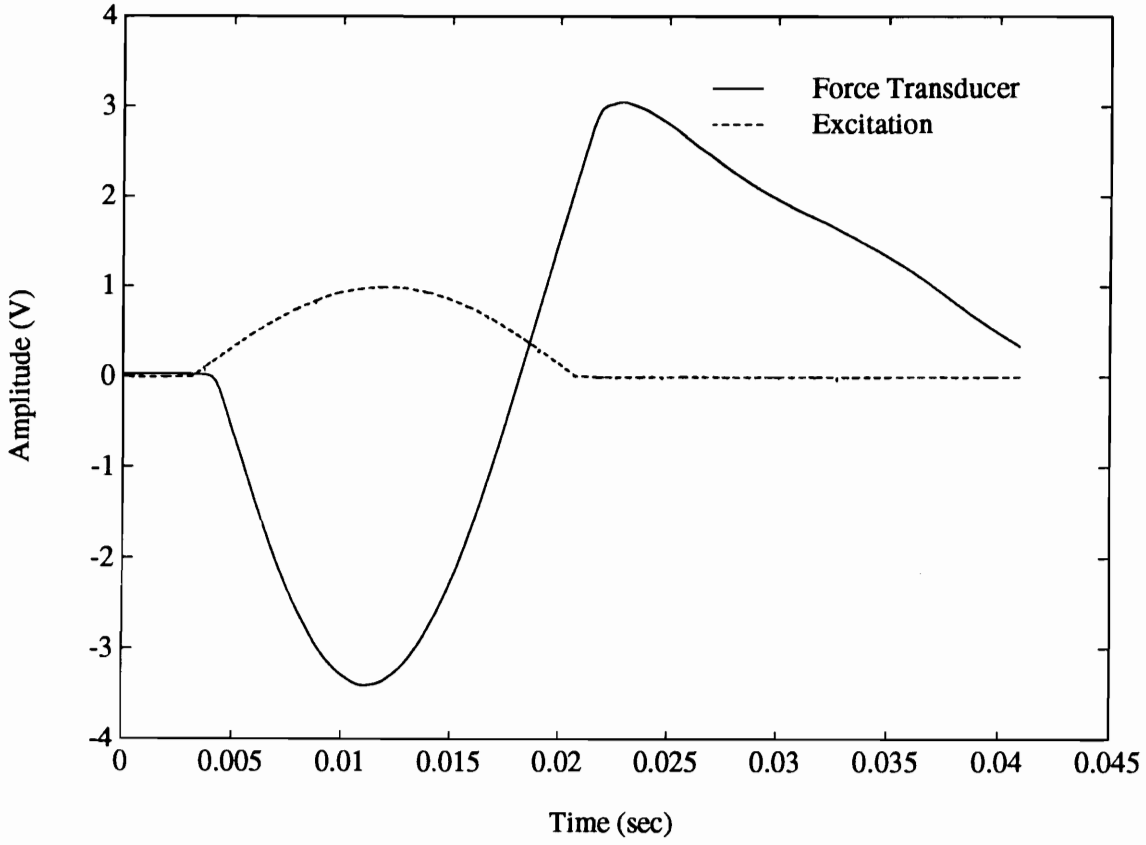

Figure 5.3: Excitation for Transient Response

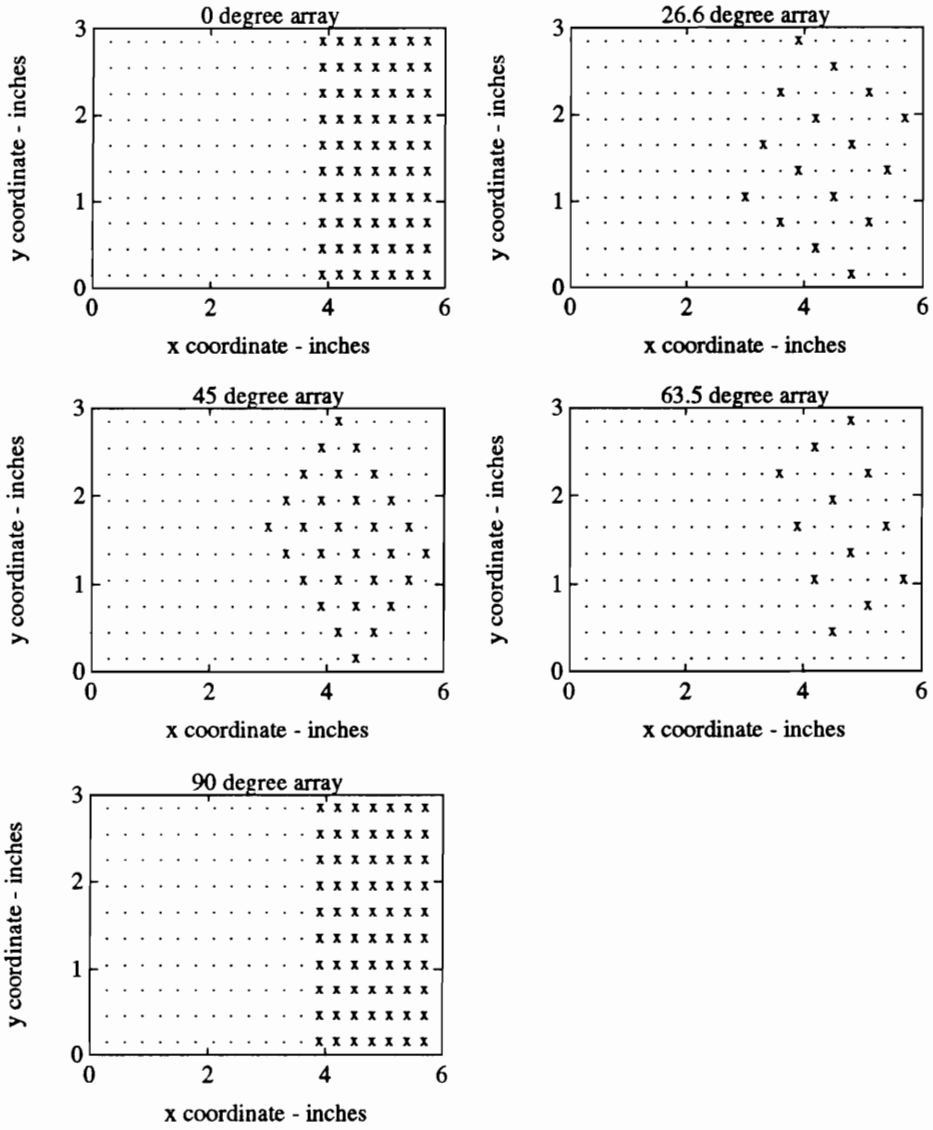

Figure 5.4: Grid Spacing for Transient Experiments

be seen that the maximum value of the correlation coefficient occurs at or near the AOA. This can be used to determine the AOA. It is important that this is purposely an ill-posed setup and with larger area arrays, higher frequencies, greater spacing between sensors more resolution would be evident.

In looking at the data, it can be seen that the values of the correlation coefficients spread out as they get off angle, but vary, little when near the AOA. The reason for this is evident with a study of the geometry of the array. Take the array arrangement of figure 3.1. While the angle between 1 and 3 and between 1 and 2 both measure 90 degrees, the signal from sensor 2 is more correlated to sensor 1 than it is to sensor three. The delay between 1 and 3 is greater, so the dispersion is greater. This is indicated by a lower CC. A spread in the values of CC for an angle will indicate measurement at off angle, while little or no spread can be seen as the angle approaches AOA.

This technique limits the signal processing to consider only those angles for which there is a colinearity of sensors, angles in between those values cannot be evaluated. The evaluated angles are those angles which equal the $\tan^{-1}$ of the possible Δx and Δy combinations. The resolution of this method is then limited by the size of the array. Table 5 shows the difference in the angles that can be evaluated for a 3x3, 4x4, 5x5, and 6x6 uniform array. Note that a 6x6 array has a maximum separation of 5 units in any direction.

Consider figure 5.6, that was generated from the grid pattern denoted in figure 5.4. For simplicity sake, refer to the sensor locations by the numbering depicted in ta-

ble 5. Using the results of figure 5.6 and geometry of reffig:gridt, it can be shown that the values of the correlation coefficients can be predicted by and related back to the beam pattern.

Table 5.1: Numbering of Sensors for 0 Degree Array

61	51	41	31	21	11	1
62	52	42	32	22	12	2
63	53	43	33	23	13	3
64	54	44	34	24	14	4
65	55	45	35	25	15	5
66	56	46	36	26	16	6
67	57	47	37	27	17	7
68	58	48	38	28	18	8
69	59	49	39	29	19	9
70	60	50	40	30	20	10

With frequency content between 0 to 50 Hz the impulse spans wavenumbers from 0 to approximately 0.2 in^{-1}. The midrange frequency of 25 Hz corresponds to a wavenumber of $.15in^{-1}$. For the spacing between adjacent sensors of .33 inches this corresponds to $ks = .05$ for at 25 Hz.

Consider the correlation coefficients evaluated at 90 degrees. This occurs any time an element is compared to the one directly behind it (compare 1 to 11), the one two rows behind it(compare 1 to 21), the one three rows behind it (1 to 31), et cetera. This corresponds to measuring the correlation at spacing of 1/3, 2/3, 1, 4/3, 5/3, and 2 inches. At 90 degrees then there are corresponding values of $ks = 0.05$, 0.1, 0.15, 0.2, 0.25, and 0.3 for the respective spacings. The values of CC correspond to

beampattern values evaluated at 90 degrees for the appropriate values of ks.

The correlation coefficients at $\pm$ 80.5 degrees correspond to comparing sensor 1 to sensor 20 or comparing sensor 10 to 11. The sensor separation is the distance between sensors which is 3.02 inches. The CC correspond to the beampattern evaluation at 80.5 degrees and $ks = .46$.
Similar analysis can be performed for each point, and an estimate of the array output given based on solving equations B.10 and zetas for the k, s, and θ values for each correlation coefficient. This was done for the array at 0 degrees and the beampattern prediction is given in figure 5.5, demonstrating the relationship between the beam patterns and the patterns generated by the correlation coefficients.

It may not be obvious why high resolution methods such as MUSIC are not employed here, so an explanation is necessary. The high resolution models assume that the output of the sensor can be expressed as

$$\mathbf{x}(t) = \mathbf{A}\mathbf{u}(t) + \mathbf{n}(t) \tag{5.2}$$

where $\mathbf{A}$ is a set of weighting vectors that define the phasing from source to sensor. The MUSIC formulation assumes the the weighting is dependent only on θ, but for structures it is also dependent on frequency. This model does not work in a dispersive media for multiple frequencies and thus can not be employed here. It could still be used for a single frequency case.

The same problem exists in employing AR, or ARMA modelling. The z transform

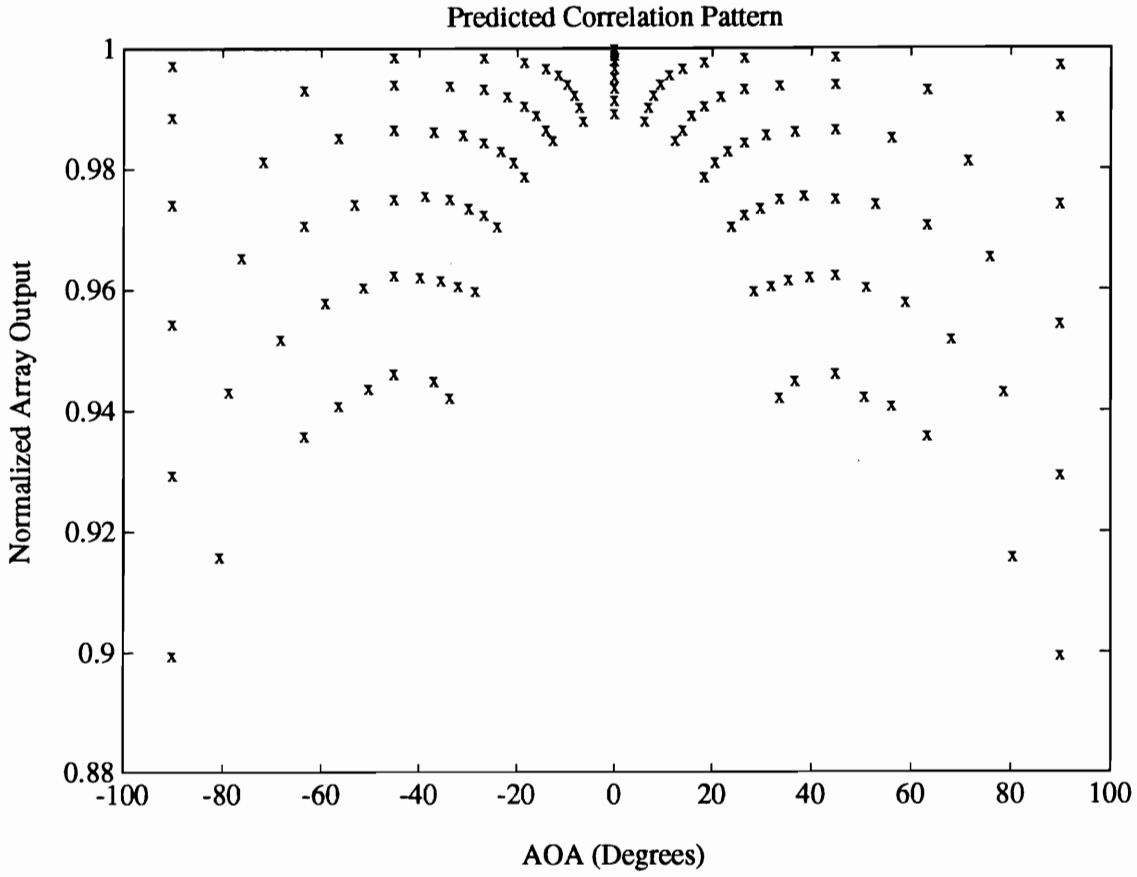

Figure 5.5: Correlation Prediction Based on Beampattern Response

Table 5.2: Resolution of Arrays as a Function of Size

x and y spacing	indicated angle	3x3	4x4	5x5	6x6
2 3 4 5 $\pm\infty$	$\pm$ 90.0	x	x	x	x
$\pm$ 5	$\pm$ 78.7				x
$\pm$ 4	$\pm$ 76.0			x	x
$\pm$ 3	$\pm$ 71.6		x	x	x
$\pm$ 5/2	$\pm$ 68.2				x
$\pm$ 2	$\pm$ 63.4	x	x	x	x
$\pm$ 5/3	$\pm$ 59.0				x
$\pm$ 3/2	$\pm$ 56.3		x	x	x
$\pm$ 4/3	$\pm$ 53.1			x	x
$\pm$ 5/4	$\pm$ 51.3				x
$\pm$ 1	$\pm$ 45.0	x	x	x	x
$\pm$ 4/5	$\pm$ 38.7				x
$\pm$ 3/4	$\pm$ 36.9			x	x
$\pm$ 2/3	$\pm$ 33.7		x	x	x
$\pm$ 3/5	$\pm$ 31.0				x
$\pm$ 1/2	$\pm$ 26.6	x	x	x	x
$\pm$ 2/5	$\pm$ 21.8				x
$\pm$ 1/3	$\pm$ 18.4		x	x	x
$\pm$ 1/4	$\pm$ 14.0			x	x
$\pm$ 1/5	$\pm$ 11.3				x
$\pm$ 0	$\pm$ 0.0	x	x	x	x

model is such that the delay of the z operator is a function of both k and θ. The problem is the same here, the basis assumes a non-dispersive media.

5.1 Summary

So what is seen for the finite case is that the correlation coefficients (the normalization of the covariance matrix) can be used to find AOA for transient signals even in a dispersive media. The correlation coefficients are highest nearest the angle of arrival

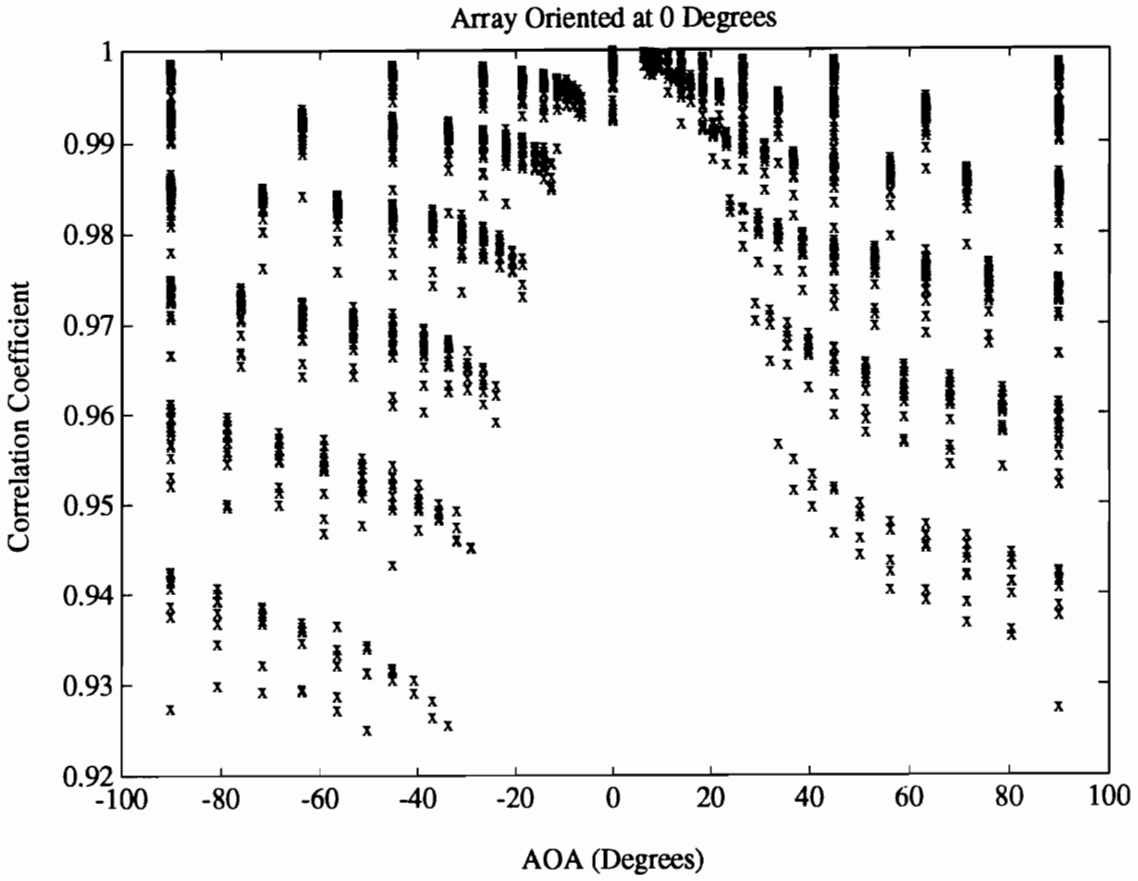

Figure 5.6: Correlation Coefficients for Array Positioned at 0 Degrees

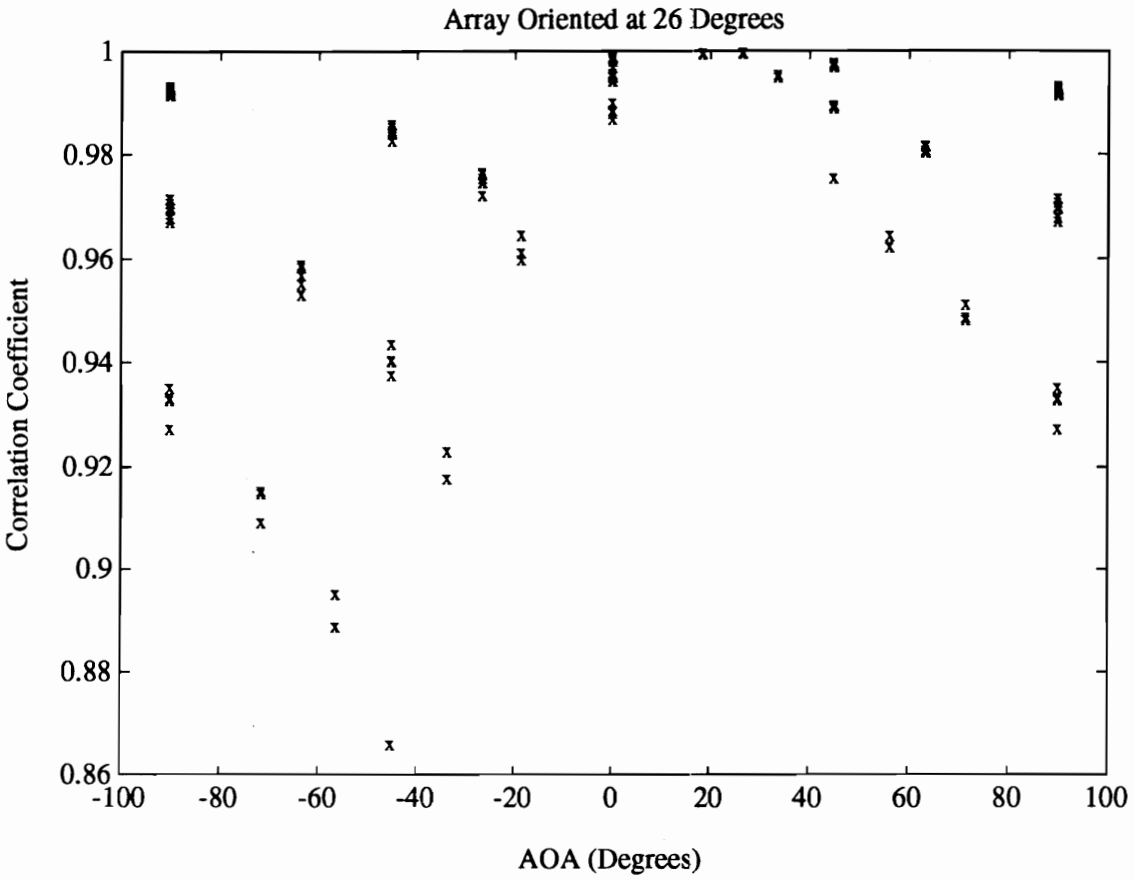

Figure 5.7: Correlation Coefficients for Array Positioned at 26.6 Degrees

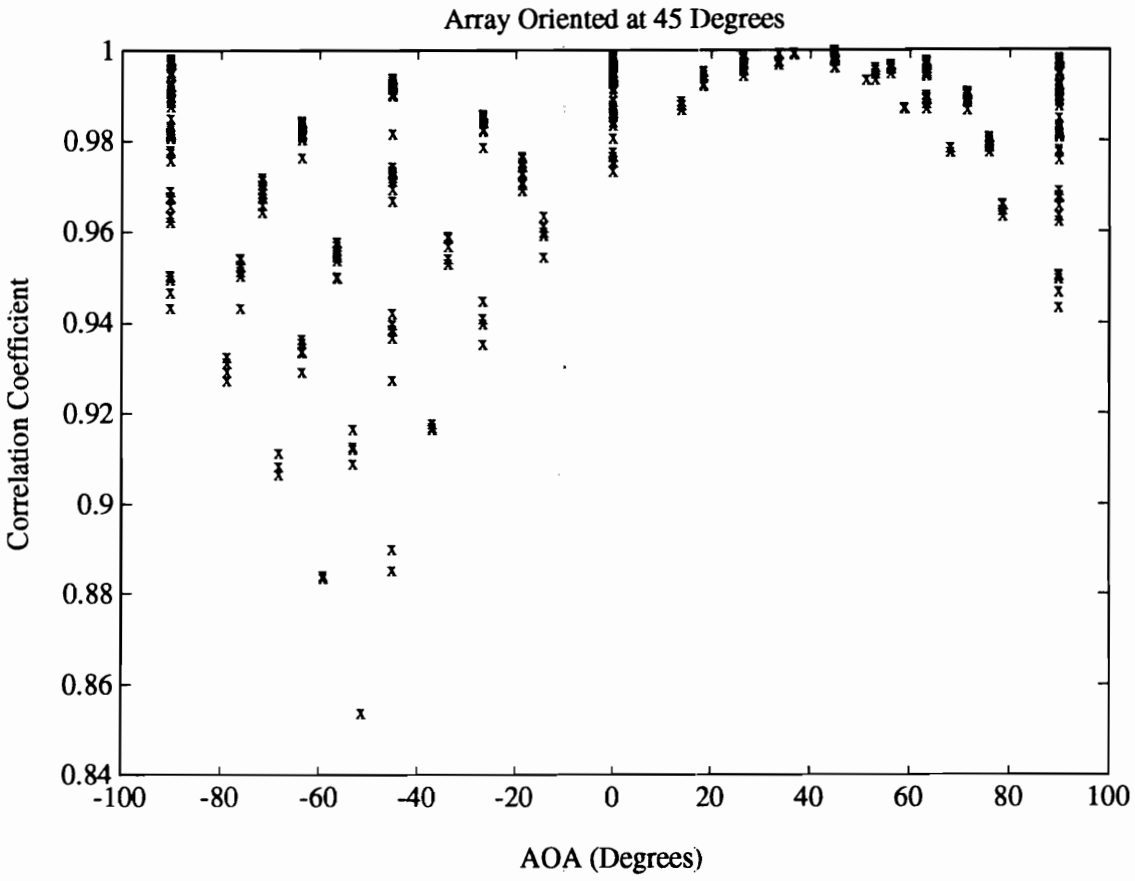

Figure 5.8: Correlation Coefficients for Array Positioned at 45 Degrees

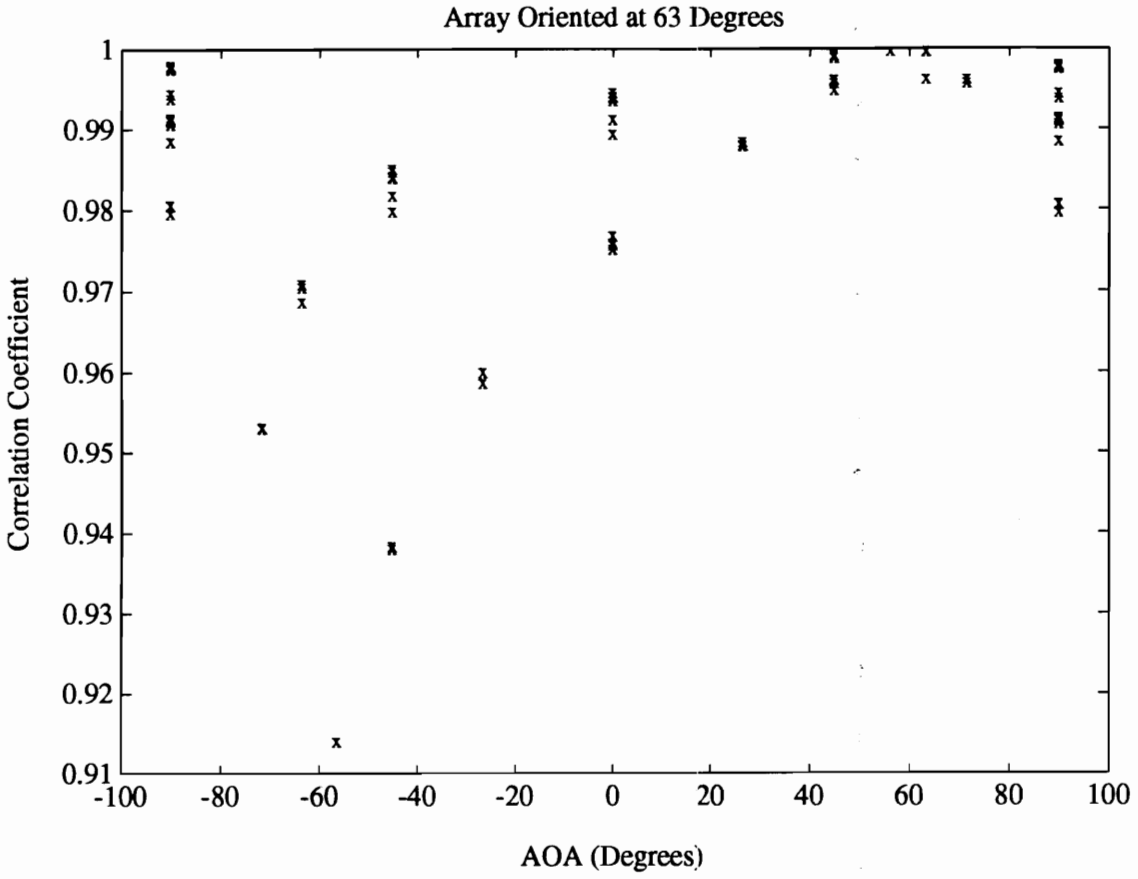

Figure 5.9: Correlation Coefficients for Array Positioned at 63.5 Degrees

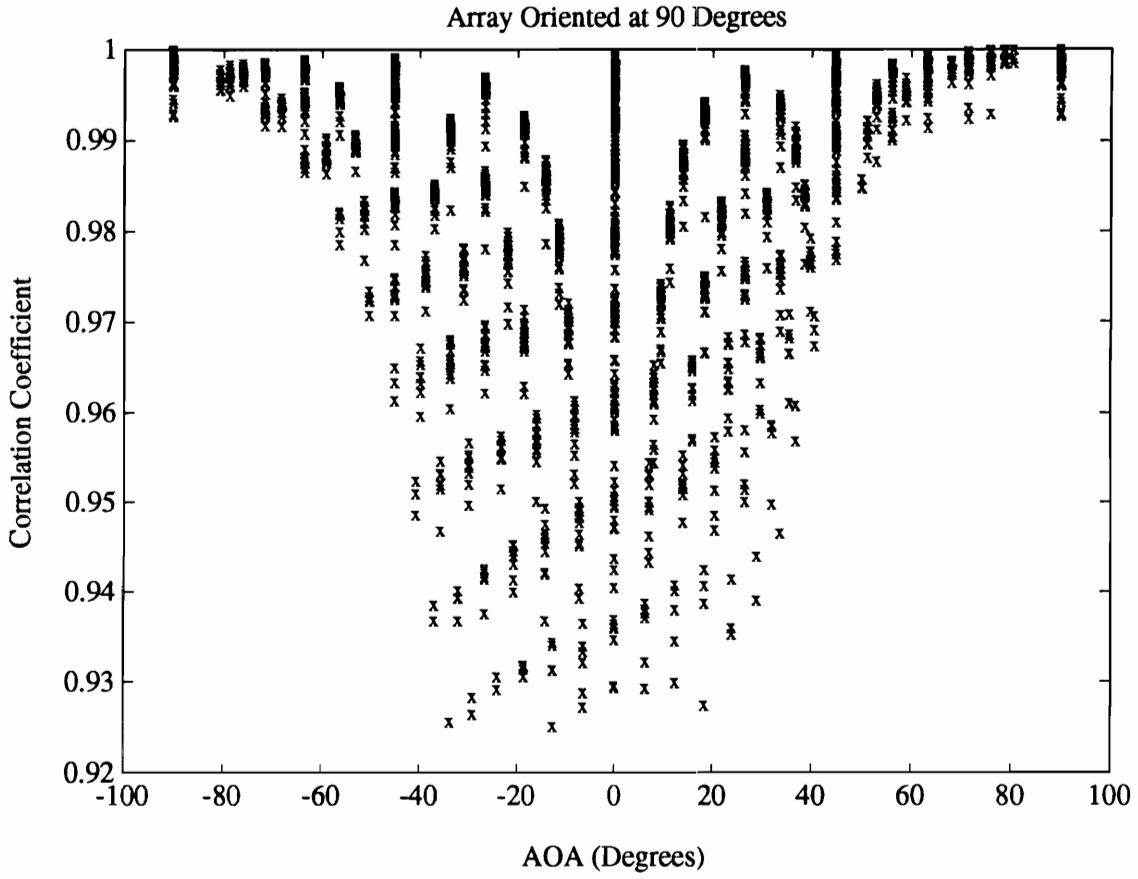

Figure 5.10: Correlation Coefficients for Array Positioned at 90 Degrees

with little spread in the values, but they are lower in off angles and they assume a wider range of values. High resolution techniques often used in other applications can not be employed for a multiple frequency signals in a dispersive media. The resolution of the result is limited by the resolution inherent in the geometry of the array.

This process is very much like the beamformer. The output of the array is measured for the possible angles and the maximum (with the minimum in variance) is evaluated as the AOA. In fact, consider the power of the classical beamformer as given in equation 2.12 is the covariance matrix with some weighting functions. The output here is the covariance weighted by some normalizing factors. The covariance matrix is foundation of array processing techniques because it contains within its elements a measure of the relation between sensors, and the different estimation techniques are simply different ways of getting that information out.

The output could be weighted for a particular frequency, and that would emphasize that frequency in the evaluation. The correlation coefficient is still analyzed for the entire time response, over the entire frequency range. This would cause a skewing in the data unless the tuned frequency were dominant.

Chapter 6

Conclusions and Recommendations for Further Work

6.1 Conclusions

What can be seen with arrays is an improvement in performance that is quantified by the array gain (AG). Generally the AG is $\sqrt{m_s}$. The beam pattern describes the array's performance for all angles of incidence, for a given relationship between wavenumber and spacing. The fact that the array's output is maximized along an axis suggests the array's directivity. This can be exploited to determine the source's direction, relative to the array, demonstrating the array's applicability to source localization problems.

These array techniques have obvious applications to structures. The quality of a vibrational measurement can be improved by array processing techniques, but some adaptations need to be made. The flexural waves of a beam are dispersive; so when beamforming is done, tuning of the array needs to occur both in frequency and in angle. Thus many of the equations of the algorithms have a phase dependency

in two variables. This limits the applicability of the present algorithms to structures. For single frequency vibration, the application is immediate. In broad band applications, phasing is dependent on both frequency and AOA. Many of the high resolution techniques can not be used, for they assume a phasing dependent only on spatial geometry.

For the harmonic applications that measured a single frequency travelling wave all the array concepts were established.The agreement of the AOA measurements data with the true values is demonstrated in figures 4.17 through 4.19 and table 4.3.2. From this it can be seen that the AOA can be determined within 3 degrees. The improvement in signal to noise ratio was also demonstrated.

What was seen for the finite case is that the correlations coefficients can be used to find AOA for transient signals even in a dispersive media. The correlation coefficients are highest nearest the angle of arrival with little spread in the values, but they lower in off angles and they assume a wider range of values. High resolution techniques often used in other applications can not be employed for a multiple frequency signals in a dispersive media. The resolution of the result is limited by the resolution inherent in the geometry of the array.

6.2 Contributions of This Work

This work accomplishes the development of the theory of sensor array processing as it applies to dispersive structures. The theory is validated through experiments in both harmonic and broad band applications. It is done without wave vector fil-

tering or wavenumber vector filtering to separate out single frequency components, but rather is developed for single or multiple frequency applications. The harmonic applications could be used in conjunction with wave vector filtering if so desired.

It has been shown and quantified that sensor arrays can improve the SNR using both frequency domain and time domain techniques. For time domain applications the data must be weighted (phased) to maximize the output, this is determined by the geometry of the array and the propagating field of the medium. In frequency domain techniques power spectra can be used to eliminate destructive interference caused by phasing, or frequency domain transforms can be applied to beamformed data if the phase information is needed.

Harmonic techniques based on the classical beamformer were developed to solve implicitly for AOA based on the phase relationship between sensors. This technique applies to harmonic signals in a highly damped medium. This technique can also be used in conjunction with filtering to apply to data filtered to become harmonic.

A transient technique to determine AOA was developed based on the correlation coefficient. This technique allows for the determination of AOA based on the maximization of correlation coefficient and the amount of data scatter. This robust technique is based on the correlation between measurements along a wave front. It does not assume phase relationships between sensors and is therefore applicable to transient signals in a dispersive media.

6.3 Recommendations for Further Work

The future for this work has several obvious avenues. First, it needs to be applied to more complex structures. The beam was effective for proving the concepts presented here, but now full application to plates, shells, thick beams, et cetera is needed.

Actuation applications also look promising. If sensing can be done so to "look" in a direction, actuation should be practicable by exploiting the phasing as well. An actuator array should be able to send a wave front in a prescribed direction. The applications of this to vibrational and acoustic controls are promising.

For the application to the thin beam, the mass loading caused by the accelerometers caused measurement problems, showing the need for lightweight sensors. Piezoelectrics show promise for the films are lightweight. They also have the added incentive that they can perform as actuators or sensors.

These are the things that seem to be the next step in continuing this work.

List of References

1. Abramson, H.N., "Flexural Waves in Elastic Beams of Circular Cross Section," *The Journal of the Acoustical Society of America*, Volume 29, 215-224, 1957.

2. Abramson, H.N., Plass, H.J., and Ripperger, E.A., "Stress Wave Propagation in Rods and Beams," *Advances in Applied Mechanics*, Volume 5, Academic Press, Inc., New York, 111-194, 1958.

3. Anderson, R.A., "Wave Groups in the Flexural Motion of Beams Predicted by the Timoshenko Theory," *Journal of Applied Mechanics*, Volume 21, 388-394, December, 1954.

4. Baggeroer, A. B., "Sonar Signal Processing," *Applications of Digital Signal Processing* ed. A. V. Oppenheimer, Prentice Hall, Englewood Cliffs, N. J., 1978.

5. Baggeroer, A. B., Kuperman, W. A. and Schmidt, H., "Matched Field Processing: Source Localization in Correlated Noise as an Optimum Parameter Estimation Problem," *The Journal of the Acoustical Society of America*, Volume 83, Number 2, 571-587, February, 1988.

6. Bailey, T., and Hubbard J. E. Jr., "Distributed Piezoelectric-polymer Active Control of a Cantilever Beam," *Journal of Guidance, Control, and Dynamics*,

Volume 8, Number 5, September-October, 1985.

7. Bas Ober, P., Deprettere, E.F., and van der Veen, A., "Efficient Methods to Compute Azimuth and Elevation in High Resolution DOA Estimation", Proceedings on the International Congress on Acoustics, Speech and Signal Processing, Volume 5, 3349-3352, 1991.

8. Bendat, J. S., and Piersol, A. G., *Random Data: Analysis and Measurement Procedures*, 2nd ed., John Wiley and Sons, Inc., 1986.

9. Bienvenu, G. and Owsley, N.L., "High Resolution Passive Away Processing: An Overview of Principles," *Lecture Notes in Control and Information Sciences*, Volume 155, 9-28, 1991.

10. Boley, B.A., and Chao, C.C., "Some Solutions to the Timoshenko Beam Equations," *Journal of Applied Mechanics*, Volume 22, 579-586, December, 1955.

11. Campbell, G. A. and Foster, R. M., *Fourier Integrals for Practical Applications*, D. Van Nostrand Company, Inc., Princeton, New Jersey, 1948.

12. Carroll, G.P., "Structural Response and Power Flow Measurement Utilizing Cross Spectra," Dissertation, The Catholic University of America, 1987.

13. "Challenges to Control: A Collective View," *IEEE Transactions on Automatic Control*, Volume AC-32, Number 4, April, 1987.

14. Champeney, D. C., *Fourier Transforms and Their Physical Applications*, Academic Press inc., London, 1973.

15. Chivers, R. C., "Time-delay Spectrometry for Ultrasonic Transducer Characterization," *The Journal of Physics E: Scientific Instrumentation*, Volume 19,

834-842, 1986.

16. Chou, S.I., "Geometric Characterization of Eigenvalues of Covariance Matrix for Two-Source Array Processing," Proceedings on the International Congress on Acoustics, Speech and Signal Processing, Volume 5, 3337-3340, 1991.

17. Cox, H., Zeskind, R. M., and Myers, M., "A Subarray Approach to Matched-Field Processing," *The Journal of the Acoustical Society of America*, Volume 87, Number 1, 168-178, January, 1990.

18. Cozzens, J.H., and Sousa, M.J., "Non unique Sinusoidal Vandermonde Bases," Proceedings of the 1991 International Conference on Acoustics, Speech, and Signal Processing, Volume 5, 3065-3068.

19. Crawley, E. F., and de Luis, X., "Use of Piezoelectric Actuators as Elements of Intelligent Structures," *AIAA Journal*, Volume 25, Number 10, October, 1987.

20. Cremer, L., Heckl, M., and Ungar, E., *Structure-Borne Sound*, 2nd ed., Springer-Verlag, Berlin, 1988.

21. Dengler, M.A., and Goland, M., "Transverse Impact of Long Beams, Including Rotary Inertia and Shear Effects," *Proceedings of the 1st U.S. National Congress of Applied Mechanics*, ASME, New York, 179-186, 1952.

22. DeVault, G.P., and Curtis, C.W., "Problems of Elastic Bar with Mixed Time-Dependent End Conditions of General Form," *Journal of the Acoustical Society of America*, Volume 31, p. 635, 1959.

23. Fitting, D. W., Schmitt, R. M., Grounds, P., Hansell, G., and Carson, P. L., "Development of Two-dimensional PVDF Arrays for Transmission Computed Tomography of Attenuation," *Proceedings of the 1984 IEEE Ultrasonics Symposium*, 794-797, 1984.

24. Frampton, K. D., "Active Control of Acoutsic Radiation Due to Discontinuities on Thin Beams," MS Thesis, Virginia Polytechnic Institute and State University, 1991.

25. Frichter, G. M., Byrne, C. L., and Feuillade, C. "Sector-Focused Stability Methods for Robust Source Localization in Matched-Field Processing," *The Journal of the Acoustical Society of America*, Volume 88, Number 6, December, 1990.

26. Goland, M., Wickersham, P.D., and Dengler, M.A., "Propagation of Elastic Impact in Beams in Binding," *The Journal of Applied Mechanics*, Volume 22, 1-7, 1955.

27. Gonidou, L., "Active Control of Flexural Power Flow in Elastic Thin Beams," Masters Thesis, Virginia Polytechnic Institute and State University, February, 1988.

28. Goryn, D., and Kaveh, M., "Direction Finding Networks Based on the Approximate Maximum Likelihood and Covariance Fit Formulations," Proceedings on the International Congress on Acoustics, Speech and Signal Processing, Volume 5, 3045-3048, 1991.

29. Guigou, C. "Active Control of Sound Radiation Due to Subsonic Wave Scattering from Discontinuities on Thin Elastic Beams," Dissertation, Virginia

Polytechnic Institute and State University, 1992.

30. Hagood, N. W., Chung, W. H., and von Flotow, A., "Modelling of Piezoelectric Actuators Dynamics for Active Structural Control," *AIAA Paper* Paper Number 90-1087-CP.

31. Hamson, R. M., and Heitmeyer, R. M., "Environmental and System Effects on Source Localization in Shallow Water by the Matched-Field Processing of a Vertical Array," *The Journal of the Acoustical Society of America*, Volume 86, Number 5, 1950-1959, November, 1989.

32. Haykin, S., editor., Justice, J. H., Owsley, N. L., Yen, J. L., and Kak , A. C.*Array Signal Processing* Prentice-Hall, Inc., New Jersey, 1985.

33. Haykin, S., editor, *Array Processing Applications to Radar* Dowden, Hutchinson & Ross, Inc., Staoudsburg, Pennsylvania, 1980.

34. Hinich, M. J., "Maximum-likelihood Signal Processing for a Vertical Array," *The Journal of the Acoustical Society of America*, Volume 54, Number 2, 499-503, 1973.

35. Hosseini, S., Harrold, S. O., and Reeves, J. M., "Computer Controlled Focused Ultrasonic Transmitting Array," *IEEE Transactions on Sonics and Ultrasonics*, Volume SU-31, Number 4, July, 1984.

36. Ide, M., and Ohdaira E., "Measurement of Diagnostic Electronic Linear Arrays by Miniature Hydrophone Scanning," *IEEE Transactions on Ultrasonics, Ferroelectrics, and Frequency Control*, Volume 35, Number 2, March, 1988.

37. Im, S., and Atluri, S., N., "Effects of a Piezo-Actuator on a Finitely Deformed Beam Subjected to General Loading," *AIAA Journal*, Volume 27, Number 12, October, 1987.

38. Jones, R.P.N., "Transient Flexural Stresses in an Infinite Beam," *Quarterly Journal of Mechanics and Applied Mathematics*, Volume 8, 373-384, 1955.

39. Kirlin, R.L., "A Maximum Likelihood Score-function with Optimal Eigenvector Weights for Bearing Estimation," Proceedings on the International Congress on Acoustics, Speech and Signal Processing, Volume 5, 3057-3060, 1991.

40. Kock, W. E., *Radar, Sonar, and Holography; An Introduction* Academic Press, New York, 1973.

41. Lamb, H., "On Waves in an Elastic Plate," *Proceedings of the Royal Society*, Volume 93, Ser. A, 2231-2251, 1917.

42. LeCadre, J.-P., and Ravazzola, P., "Extension of High-Resolution Methods to Realistic Cases," *Lecture Notes in Control and Information Sciences*, volume 155, pp. 31-80, 1991.

43. Lee, C. K., "Piezoelectric Laminates for Torsional and Bending Modal Control: Theory and Experiment," PhD Dissertation, Cornell University, May, 1987.

44. Leitch, R. R., Tokhi, M. O., "Active Noise Control Systems," *IEE Proceedings*, Volume 134, Part A, Number 6, June, 1987.

45. Lin, S., and Barkat, M., "Maximum Likelihood Estimation of Direction-of-Arrival for Broad-Band Sources Via Dynamic Programming," *Midwest Sym-*

posium on Circuits and Systems, Volume 1, 311-314, 1991.

46. Livingston, E. and Diachok, O., "Estimation of Average Under-ice Reflection Amplitudes and Phases Using Matched-field Processing," *The Journal of the Acoustical Society of America*, Volume 86, Number 5, 1909-1919, November, 1989.

47. Love, A. E. H., *The Mathematical Theory of Elasticity*, Cambridge, 1927.

48. McGarrity, J.S., Soraghan, J.J. Durrani, T.S., and Mayrargue, S., "The ESPRIT and MUSIC Algorithms Using the Covaviance Matrix," Proceedings on the International Congress on Acoustics, Speech and Signal Processing, Volume 5, 3285-3288, 1991.

49. Meirovitch, L., *Elements of Vibration Analysis*, McGraw-Hill, Inc., 1975.

50. Meirovitch, L., *Analytic Methods in Vibrations*, The Macmillan Company, New York, 1967.

51. Meirovitch, L., and Baruh, H., "Control of Self-adjoint Distributed-parameter Systems," *Journal of Guidance, Control, and Dynamics*, Volume 5, Number 1, Jan.-Feb., 1982.

52. Meirovitch, L., Baruh, H., Montgomery, R.C., and Williams, J.P., "Nonlinear Natural Control of an Experimental Beam," *Journal of Guidance, Control, and Dynamics*, Volume 7, Number 4, 437-442, 1984.

53. Meirovitch, L., Baruh, H., and Oz, H., "A Comparison of Control Techniques for Large Flexible Systems," *Journal of Guidance, Control and Dynamics*, Volume 6, Number 4, 302-310, 1983.

54. Meeks, S. W., and Ting, R. Y., "Effects of Static and Dynamic Stress on the Piezoelectric and Dielectric Properties of PVF_2," *The Journal of the Acoustical Society of America*, Volume 74, Number 6, Dec., 1983.

55. McNab, A. and Stumpf, I., "Monolithic Phased Array for the Transmission of Ultrasound in NDT Ultrasonics," *Ultrasonics*, Volume 24, 148-155, May, 1986.

56. Miklowitz, J., "Flexural Wave Solutions of Coupled Equations Representing the More Exact Theory of Bending," *The Journal of Applied Mechanics*, Volume 20, 511-514, 1953.

57. Miklowitz, J., "Recent Development in Elastic Wave Propagation," *Applied Mechanics Reviews*, Volume 13, Number 12, 865-878, 1960.

58. Mindlin, R.D., and Fox, E.A., "Vibrations and Waves in Elastic Bars of Rectangular Cross Section," *Journal of Applied Mechanics*, Volume 27, 152-158, March, 1960.

59. Mindlin, R.D., and Niven, H.D., "Axially Symmetric Waves in Elastic Rods," *Journal of Applied Mechanics*, Volume 27, 145-151, March, 1960.

60. Nicholas, P., and Vezzosi, G., "Localisation of Broadband Sources with an Array of Unknown Geometry," *Lecture Notes in Control and Information Sciences*, Volume 155, 81-125, 1991.

61. Oberhettinger, F., *Tables of Fourier Transforms and Fourier Transform of Distributions*, Springer-Verlag, Berlin, 1990.

62. Odell, D., and Meador, J., "A Versatile Integrated Acoustic Beamforming System," *Proceedings of the IEEE Pacific Rim Conference on Communications,*

Computers and Signal Processing, 635-638, 1991.

63. Oh, S.K., and Un, C.K., "Fast Initialization Procedure of the Alternating Projection Algorithm for Maximum Likelihood Localization of Multiple Sources," *Signal Processing*, Volume 25, Number 3, 381-389, Dec, 1991.

64. Oliver, J., "Elastic Wave Dispersion in a Cylindrical Rod by a Wide-Band Short-Duration Pulse Technique," *The Journal of the Acoustical Society of America*, Volume 29, 189-194, February, 1957.

65. Perkins, J. S., and Kuperman, W. A., "Environmental Signal Processing: Three-dimensional field processing with vertical array," *The Journal of the Acoustical Society of America*, Volume 87, Number 4, April, 1990.

66. Pillai, S. U. and Burrus, C. S. consulting editor, *Array Signal Processing*, Springer-Verlag, New York, 1989.

67. Plass, H.J., Jr., "Some Solutions of the Timoshenko Beam Equation for Short Pulse-Type Loading," *Journal of Applied Mechanics*, Volume 25, 379-385, September, 1958.

68. Preston, J. R., Akal, T. and Berkson, J., "Analysis of Backscattering Data in the Tyrrhenian Sea," *The Journal of the Acoustical Society of America*, Volume 87, Number 1, 119-134, November, 1990.

69. Preston, R. C., " The NPL Ultrasound Beam Calibrator," *IEEE Transactions on Ultrasonics, Ferroelectrics, and Frequency Control*, Volume 35, Number 2, March, 1988.

70. Rayleigh, J.W.S., *Theory of Sound*, Macmillan, London, 1894.

71. Ross, C. F., "An Algorithm for Designing a Broadband Active Sound Control System," *Journal of Sound and Vibration*, Volume 80, Number 3, 1982.

72. Sakarya, F.A., and Hayes, M.H., "Estimating 2-D Angles of Arrival Using Overlaping Volume Arrays," Proceedings on the International Congress on Acoustics, Speech and Signal Processing, Volume 5, 3353-3356, 1991.

73. Sato, T., Ishikawa, H. and Ikeda, O., "Multilayered Deformable Mirror Using PVDF Films," *Applied Optics*, Volume 21, Number 20, October, 1982.

74. Schaechter, D.B., "Hardware Demonstration of Flexible Beam Control," *Journal of Guidance, Control, and Dynamics*, Volume 5, Number 1, 48-53, 1982.

75. Schmidt, H., Baggeroer, A. B., Kuperman, W. A., and Scheer, E. K., "Environmentally Tolerant Beamforming for High-Resolution Matched Field Processing: Deterministic Mismatch," *The Journal of the Acoustical Society of America*, Volume 88, Number 4, 1851-1862, October, 1990.

76. Schmidt, R. O., "Multiple Emmiter Location and Signal Parameter Estimation," in *Proceedings RADC Spectral Estimation Workshop*, 243-258, October,1979.

77. Schweppe, F. C., "Sensor-Array Data Processing for Multiple-Signal Sources," *IEEE Transactions on Information Theory*, Volume IT-14, Number 2, 294-305, March, 1968.

78. Seto, William W., *Schaum's Outline of Theory and Problems of Mechanical Vibrations*, McGraw-Hill Book Company, New York, 1964, 136-150.

79. Seybert, A.F., and Ross, D.F., "Experimental Determination of Acoustic Properties Using a Two-microphone Random-excitation Technique," *Journal of the Acoustical Society of America*, Volume 61, Number 5, 1362-1370, May, 1977.

80. Shaulov, A. A., Smith W. A., and Ting, R. Y., "Modified-Lead-Titantate/Polymer Composites or Hydrophone Applications," *Ferroelectrics*, Volume 93, 1989.

81. Shang, E. C., "An Efficient High-resolution Method of Source Localization Processing in Mode Space," *The Journal of the Acoustical Society of America*, Volume 86, Number 5, 1960-1964, November, 1989.

82. Shaw, H. J., Weinstein, D., Zitellli, L. T., Frank C. W., DeMattei, R. C., and Fesler, K., "PVF_2 Transducers," *Proceedings of the 1980 IEEE Ultrasonics Symposium.*

83. Smith, C.R., and Erickson, G.J., "Multisensor Data Fusion: Concepts," *Proceedings of the 1991 IEEE Pacific Rim Conference on Communications, Computers and Signal Processing*, 235-237, 1991.

84. Stein, P. J., "Interpretation of a Few Ice Transients," *The Journal of the Acoustical Society of America*, Volume 83, Number 2, 617-622, February, 1988.

85. Stergiopoulos, S., and Sullivan, E., "Extended Towed Array Processing by an Overlap Correlator," *The Journal of the Acoustical Society of America*, Volume 86, Number 1, 158-171, July, 1989.

86. Takeuchi, H., Jyomura, S., Ishikawa, Y., and Yamamoto, E., "A 7.5 MHz

Linear Array Ultrasonic Probe Using Modified $PbTiO_3$ Ceramics," *Proceedings of the 1982 IEEE Ultrasonics Symposium*, 849-853, 1982.

87. Timoshenko, S.P., "On the Correction for Shear of the Differential Equation for Transverse Vibration of Prismatic Bars," *Phil. Magazine*, Volume 41, Ser. 6, 744-746, 1921.

88. Timoshenko, S.P., "On the Transverse Vibrations of Bars of Uniform Cross Section," *Phil. Magazine*, Volume 43, Ser. 6, 125-131, 1922.

89. Tran, J. Q. D., and Hodgkiss, W. S., "Matched-field Processing of 200-Hz Continuous Wave (CW) Signals," *The Journal of the Acoustical Society of America*, Volume 89, Number 2, 745-755, November, 1991.

90. Uchino, E., "Electrostrictive Actuators: Materials and Applications," *Ceramics Bulletin*, Volume 65, Number 4, 1986.

91. Uflyand, Y.S., " The Propagation of Waves in the Transverse Vibration of Bars and Plates," *American Mechanics Review*, Volume 3, Review 33, 1950.

92. Urick, R. J. *Principles of Underwater Sound*, McGraw-Hill, Inc., New York, 1975.

93. Von Flotow, A. H., and Schafer, B., "Wave-Absorbing Controllers for a Flexible Beam," *Journal of Guidance, Control, and Dynamics*, Volume 9, Number 6, November-December, 1986.

94. Von Ramm, O. T., and Smith, S. W., "Beam Steering with Linear Arrays," *IEEE Transactions on Biomedical Engineering*, Volume BME-30, Number 8, August, 1983.

95. Wahlberg, B., Ottersten, B., and Viberg, M., "Robust Signal Parameter Estimation in the Presence of Array Perturbations," Proceedings on the International Congress on Acoustics, Speech and Signal Processing, Volume 5, 3277-3280, 1991.

96. Wang, C. and Cadzow, J., "Direction-Finding with Sensor Gain, Phase, and Location Uncertainty," Proceedings on the International Congress on Acoustics, Speech and Signal Processing, Volume 2, 1429-1432, 1991.

97. Watanabe, H., Suzuki, M. Nagai, N. and Miki, N., "Maximum Likelihood Estimation by Quasi-Newton Method Using a Uniform Linear Array," Proceedings on the International Congress on Acoustics, Speech and Signal Processing, Volume 5, 3325-3328, 1991.

98. Wax, M., "Detection of Coherent and Noncoherent Signals Via the Stochastic Signals Model," Proceedings on the International Congress on Acoustics, Speech and Signal Processing, Volume 5, 3541-3544, 1991.

99. Wheeler, D.A., and Atkins, P.R., "Estimation of Source Bearings at a Randomly Deformed Array by Signal Space Transformation," Proceedings on the International Congress on Acoustics, Speech and Signal Processing, Volume 5, 3345-3348, 1991.

100. Widrow, B., and McCool, J. M., "A Comparison of Adaptive Algorithms Based on the Methods of Steepest Descent and Random Search," *IEEE Transactions on Antennas and Propagation*, Volume AP-24, Number 5, September, 1976.

101. Withers, Jr., L., "Piecewise Root-MUSIC," Proceedings on the International Congress on Acoustics, Speech and Signal Processing, Volume 5, 3305-3308,

1991.

102. Wu, Y.W., "Estimating Directions of Arrival with Generalized MUSIC Using a Linear-Interpolated Array Manifold," Proceedings on the International Congress on Acoustics, Speech and Signal Processing, Volume 5, 3333-3336, 1991.

103. Xu, G., Silverstein, S.D., Roy, H., and Kailath, T., "Parallel Implementation and Performance Analysis of Beamspace ESPIRIT," Proceedings of the 1991 International Conference on Acoustics, Speech and Signal Processing, Volume 2, 1497-1500, 1991.

104. Yang T. C., "A Method of Range and Depth Estimation by Modal Decomposition," *The Journal of the Acoustical Society of America*, Volume 88, Number 4, 1736-1745, October, 1990.

105. Zeytinoglu, M., and Foda, S. *Proceeding of the 1991 IEEE Pacific Rim Conference on Communications, Computers and Signal Processing*, 819-822, 1991.

106. Ziskind, I, and Bar-Ness, Y., "Localization by Narrow-Band Autoregressive Sources by Passive Sensor Arrays," *IEEE Transactions on Signal Processing*, Volume 40, Number 2, 484-487, February, 1992.

107. Zoltowski, M.D., Kautz, G.M., and Silvestein, S.D., "Development, Performance Analysis, and Experimental Evaluation of Beamspace Root-MUSIC," Proceedings on the International Congress on Acoustics, Speech and Signal Processing, Volume 5, 3049-3052, 1991.

Appendix A

Analysis of Infinite Beam

The analysis of the infinite beam uses Bernoulli-Euler beam theory of bending. This elementary theory has been developed by many sources (Thompson, 1981; Cremer *et al.,* 1988; Meirovitch, 1967, Guigou 1992; Abramson *et al.,* 1958) and is valid for the following assumptions:

- cross-sectional dimensions are small compared to the length
- transverse sections remain planar and normal to the length in bending
- rotary inertia effects are negligible
- shear deformations are small compared to flexural deformations.

A.1 Equations of Motion

To determine the differential equation that governs the motion of the beam, consider a free body diagram of an element of the beam, see figure A.1 Further, all beam parameters are considered constant along the length of the beam. From mechanics of materials the following relationships are known.

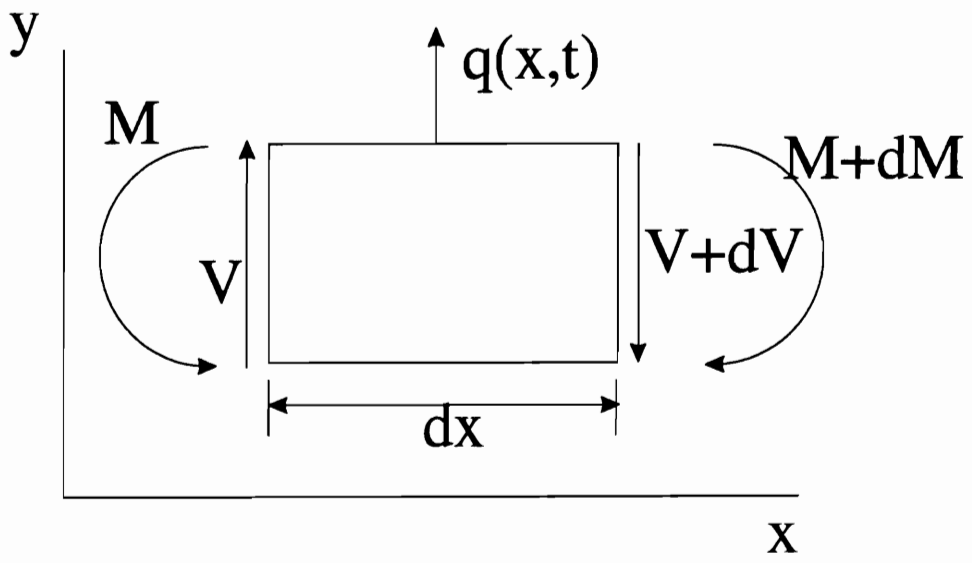

Figure A.1: Free Body Diagram of Differential Element of Beam

$$\frac{\partial V}{\partial x} = -q(x,t); \tag{A.1}$$

$$\frac{\partial M}{\partial x} = -V. \tag{A.2}$$

These equations can be equivalently written

$$\frac{\partial^2 M}{\partial x^2} = -\frac{\partial V}{\partial x} = q(x,t) \tag{A.3}$$

The bending moment can be expressed in terms of beam coordinates by the equation

$$M = -EI\frac{\partial^2 y(x,t)}{\partial x^2} \tag{A.4}$$

where E is Young's modulus and I is the cross-sectional area moment of inertia. From Newton's first law, the free body diagram yields the following relationship for a summing of forces.

$$\partial V + q(x,t)dx = \rho A dx\frac{\partial^2 y(x,t)}{\partial t^2} \tag{A.5}$$

If the relationship between shear and moment is used, (equation A.3) this can be rewritten

$$-\frac{\partial^2 M}{\partial x^2} + q(x,t) = \rho A\frac{\partial^2 y(x,t)}{\partial t^2} = 0 \tag{A.6}$$

where A is the cross-sectional area, and ρ is the volumetric density of the beam. Substituting the relationship between moments and the flexural stiffness (equation A.4) the equation can be written in terms of cartesian coordinates.

$$EI\frac{\partial^4 y(x,t)}{\partial x^4} + \rho A\frac{\partial^2 y(x,t)}{\partial t^2} = q(x,t) \tag{A.7}$$

This equation can be further simplified, if a harmonic time dependence, $e^{i\omega t}$, is assumed. For

$$y = Ae^{i\omega t} \quad \frac{\partial^2 y(x,t)}{\partial t^2} = -A\omega^2 e^{i\omega t} \tag{A.8}$$

Substituting A.8 into equation A.7 yields

$$EI\frac{\partial^4 y(x,t)}{\partial x^4} - \rho A\omega^2 y(x,t) = q(x,t) \tag{A.9}$$

If the applied force is a point force applied at the location x=a on the beam, it can be expressed by

$$F\delta(x-a)e^{i\omega t} \tag{A.10}$$

where F is the magnitude of the forcing function and $\delta(x-a)$ is the spatial Dirac delta function. Replacing the forcing term $q(x,t)$ in equation A.9 with equation A.10 gives

$$EI\frac{\partial^4 y(x,t)}{\partial x^4} - \rho A\omega^2 y(x,t) = F\delta(x-a)e^{i\omega t} \tag{A.11}$$

which can be rewritten

$$\frac{\partial^4 y(x,t)}{\partial x^4} - k^4 y(x,t) = \frac{F}{EI}\delta(x-a)e^{i\omega t}. \tag{A.12}$$

k is known as the structural wave number and is defined by the following relationship:

$$k = (\frac{\rho A\omega^2}{EI})^{\frac{1}{4}}. \tag{A.13}$$

A.1.1 Fourier Transform Solution

Equation A.12 can be solved by using spatial Fourier transforms.

The spatial Fourier transform of equation A.12 is

$$\int_{-\infty}^{+\infty} \frac{\partial^4 y(\omega,t)}{\partial x^4} e^{-i\nu x}dx - k^4 \int_{-\infty}^{+\infty} y(x,t)e^{-i\nu x}dx = \int_{-\infty}^{+\infty} F\delta(x-a)e^{-i\omega t}e^{-i\nu x}dx \tag{A.14}$$

From Fourier transform tables (Campbell and Foster, 1948; Champeney, 1973; and Oberhettinger, 1990) the spatial Fourier transform of

$$y(x,t) = \int_{-\infty}^{+\infty} y(x,t)e^{-i\nu x}dx \tag{A.15}$$

and it is likewise known that

$$\int_{-\infty}^{+\infty} \delta(x-a)e^{-i\nu x}dx = e^{-ia\nu}. \tag{A.16}$$

Assuming

$$\frac{\partial^3 y}{\partial x^3} = \frac{\partial^2 y}{\partial x^2} = \frac{\partial y}{\partial x} = 0 : x = \pm\infty \tag{A.17}$$

equation A.12 can be written

$$\nu^4 y(\nu,t) - k^4 y(\nu,t) = Fe^{-i\omega t}e^{i\nu t} \tag{A.18}$$

or equivalently

$$y(\nu,t) = \frac{Fe^{-i\nu a}}{EI(\nu^4-k^4)}e^{i\omega t}. \tag{A.19}$$

Solving for $y(x,t)$ can be done with the inverse Fourier Transform

$$y(x,t) = \mathcal{F}^{-1}[y(\nu,t)] \quad = \int y(\nu,t)e^{i\nu t}d\nu \tag{A.20}$$

$$= \frac{\int Fe^{i\nu a}e^{-i\omega t}e^{i\nu x}}{EI(\nu^4-k^4)} \tag{A.21}$$

$$= \frac{Fe^{-i\omega t}}{EI}\int \frac{e^{i\nu(x-a)}}{\nu^4-k^4}d\nu \tag{A.22}$$

$$\tag{A.23}$$

Using partial fraction expansion

$$y(x,t) = \mathcal{F}^1[y(\nu,t)] = \frac{Fe^{-i\omega t}}{EI} e^{i\nu(x-a)}[\frac{A}{\nu^2+k^2} + \frac{B}{\nu^2-k^2}] \tag{A.24}$$

where:

$$A = \frac{-1}{2k^2} \quad B = \frac{1}{2k^2}$$

$$y(x,t) = \frac{Fe^{-i\omega t}}{2EIk^2}[\int \frac{-e^{i\nu(x-a)}}{\nu^2+k^2}dz + \int \frac{e^{i\nu(x-a)}}{\nu^2-k^2}dz] \tag{A.25}$$

from Fourier analysis theory

$$\frac{2a}{a^2+\omega^2} \iff e^{-a|t|} \tag{A.26}$$

for the component:

$$\int \frac{-e^{i\nu(x-a)}}{\nu^2+k^2}dz \tag{A.27}$$

if we let

$$\begin{aligned} a &= k \\ \omega^2 &= \nu^2 \\ t &= (x-a) \end{aligned}$$

$$\int \frac{-e^{i\nu(x-a)}}{\nu^2+k^2}dz = \frac{-1}{2k}\int \frac{2k}{\nu^2+k^2} e^{i\nu(x-a)}dz \tag{A.28}$$

$$= \frac{-1}{2k} e^{-k|x-a|} \tag{A.29}$$

for the other component:

$$\int \frac{e^{i\nu(x-a)}}{\nu^2 - k^2} dz \tag{A.30}$$

if we let

$$\begin{aligned} a &= -ik \\ \omega^2 &= \nu^2 \\ t &= (x-a) \end{aligned}$$

$$\int \frac{e^{i\nu(x-a)}}{\nu^2 - k^2} dz = \frac{-1}{2ik} \int \frac{2ik}{\nu^2 - k^2} e^{i\nu(x-a)} dz \tag{A.31}$$

$$= \frac{-1}{2ik} e^{ik|x-a|} \tag{A.32}$$

Substituting A.29 and A.32 into A.25:

$$y(x,t) = \frac{F e^{-i\omega t}}{2EIk^2} \left[\frac{-1}{2k} e^{-k|x-a|} + \frac{-1}{2ik} e^{ik|x-a|} \right] \tag{A.33}$$

$$y(x,t) = \frac{F}{4EIk^3} \left[\frac{-1}{i} e^{ik|x-a|} - e^{-k|x-a|} \right] e^{-i\omega t} \tag{A.34}$$

$$y(x,t) = \frac{iF}{4EIk^3}\frac{-1}{i}\left[ie^{ik|x-a|} - e^{-k|x-a|}\right]e^{-i\omega t} \tag{A.35}$$

$$y(x,t) = \frac{iF}{4EIk^3} - i\left[ie^{ik|x-a|} - e^{-k|x-a|}\right]e^{-i\omega t} \tag{A.36}$$

$$y(x,t) = \frac{iF}{4EIk^3}\left[e^{ik|x-a|} - ie^{-k|x-a|}\right]e^{-i\omega t} \tag{A.37}$$

Appendix B

Derivation for Phase Relationship Between Sensors

The output of a sensor is assumed to be proportional to the deflection, velocity, and acceleration of the beam at the sensor location and can be written

$$s = \frac{iF}{4EIk^3}\{e^{ik|x-\alpha|} + ie^{-k|x-\alpha|}\}e^{-i\omega t} \tag{B.1}$$

With the sensors located sufficiently far from the source, nearfields are negligible. The source is located at $\alpha = 0$ yielding

$$s(i) = \frac{iF}{4EIk^3}(e^{ik|x(i)|})e^{-i\omega t}. \tag{B.2}$$

The output of each sensor is delayed so that the signal aligns yielding

$$s(i) = \frac{iF}{4EIk^3}(e^{ikx(i)})e^{-i\omega(t+\phi(i))}. \tag{B.3}$$

The output of the array is the average output of the sensors and is then given by

$$\frac{iF}{4EIk^3}\frac{1}{m_s}\sum_{i=1}^{m_s} s(i) = e^{ikx(i)}e^{-i\omega t}e^{i\omega\phi(i)}. \tag{B.4}$$

To quantify the output of the sensor array with errors in frequency or angle, the output of a correctly tuned array can be compared to an incorrectly tuned one.

The assumed values of a variable are denoted as follows

ω_a = assumed frequency
k_a = assumed wavenumber
θ_a = assumed angle of arrival
ϕ_a = assumed delay

For a correctly tuned array, the delays are all matched to the reference sensor, $\phi = 0$.

$$S_{ideal} = \frac{iF}{4EIk^3}\frac{1}{m_s}\sum_{i=1}^{m_s} s(r) = \frac{iF}{4EIk^3}\frac{1}{m_s}\sum_{i=1}^{m_s} e^{ikx(r)}e^{-i\omega t}. \tag{B.5}$$

Thus the output of the array over the ideal output is given by

$$\frac{S}{S_{ideal}} = \frac{\frac{iF}{4EIk^3}\frac{1}{m_s}\sum_{i=1}^{m_s} e^{ikx(i)}e^{-i\omega t}e^{i\omega\phi(i)}.}{\frac{iF}{4EIk^3}\frac{1}{m_s}\sum_{i=1}^{m_s} e^{ikx(r)}e^{-i\omega t}.} \tag{B.6}$$

This can be simplified to

$$\frac{S}{S_{ideal}} = \frac{1}{m_s}\sum_{i=1}^{m_s} e^{ik(x(i)-x(r))}e^{i\omega\phi_a(i)}. \tag{B.7}$$

$\phi_a(i)$ is the assumed delay based on the tuning of array. Using equation 3.2, equation

B.7 can be rewritten

$$\frac{S}{S_{ideal}} = \frac{1}{m_s}\sum_{i=1}^{m_s} e^{ik(x(i)-x(r))}e^{i\omega\zeta_a(i)*k_a/\omega_a}. \tag{B.8}$$

where ζ_a is the assumed separation between sensors in the wave propagation direction. From the wave equation

$$\frac{w}{w_a} = \frac{k^2}{k_a^2}. \tag{B.9}$$

Equation B.9 can be substituted into equation B.8 giving

$$\frac{S}{S_{ideal}} = \frac{1}{m_s}\sum_{i=1}^{m_s} e^{ik(x(i)-x(r))}e^{-i\frac{k^2}{k_a}\zeta_a(i)} \tag{B.10}$$

Ideally the difference in $e^{x(i)-x(r)}$ is equal but opposite to $e^{-\frac{k^2}{k_a}\zeta_a(i)}$. Error is incurred in the difference between the assumed values of ω_a, k_a, θ and $\zeta_a(i)$ and the tuned values ω, k, and $\zeta(i)$.

Using sensor 2 as the reference sensor, the separation between sensors are

$$\begin{aligned}
\zeta_1 &= -s\ \sin\theta \\
\zeta_2 &= 0 \\
\zeta_3 &= s\ \sin\theta \\
\zeta_4 &= \zeta_1 + s\ \cos\theta \\
\zeta_5 &= s\ \cos\theta \\
\zeta_6 &= \zeta_3 + s\ \cos\theta \\
\zeta_7 &= \zeta_4 + s\ \cos\theta \\
\zeta_8 &= 2s\ \cos\theta \\
\zeta_9 &= \zeta_6 + s\ \cos\theta
\end{aligned} \tag{B.11}$$

To find the assumed values of $\zeta(i)$ the assumed value of θ is used. If there is an

error between the assumed and actual value of an array parameter, the output of the array will come off the maximum output. Equations B.10, and B.11 can be used to determine the output of the array for errors in the parameters.

Appendix C

Experimental Analysis of Infinite Beam

To prove that the infinite beam equations are valid for the laboratory setup, it is necessary to prove the non-reflectivity of the beam termini. To accomplish this, the power reflection coefficient of each termination is measured. The technique used here follows the approach taken by Seybert and Ross (1977) and Gonidou (1988).

The power reflection coefficient is a measurement of the reflected power over the incident power. It measures the power of the waves propagating from the sand box over the waves propagating into the box. Fig C.1 shows the setup of the the equipment used to determine the reflection coefficient. Two accelerometers were used, so the acceleration at those two points is to be considered.

The acceleration from the incoming wave can be written

$$A_i = W_i(t)(e^{ikx} - ie^{-k|x|})e^{-i\omega t}.$$

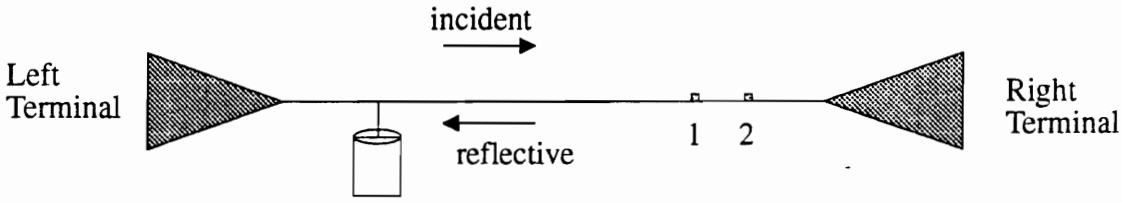

Figure C.1: Apparatus Setup To Measure Reflection Coefficient of Right Sandbox

The acceleration from the outgoing (relected) wave can be written

$$A_o = W_o(t)(e^{-ikx} - ie^{-k|x|})e^{-i\omega t}.$$

By placing the accelerometers sufficiently far enough away from the shaker, the near-field term,$e^{-k|x|}$, is negligible. The acceleration at the location for the two accelerometers can be written

$$A_i = W_i(t)e^{ikx}e^{-i\omega t} \tag{C.1}$$

$$A_o = W_o(t)e^{-ikx}e^{-i\omega t}. \tag{C.2}$$

$$\tag{C.3}$$

Using the frequency spectra from the accelerometers the spectra can be be expressed

$$\begin{aligned} P_{11} &= P_{AA} + P_{BB} + 2(real(P_{AB})\cos(2kx_1) \\ &\quad -imag(P_{AB})\sin(2kx_1)) \end{aligned} \tag{C.4}$$

$$\begin{aligned} P_{22} &= P_{AA} + P_{BB} + 2(real(P_{AB})\cos(2kx_2) \\ &\quad -imag(P_{AB})\sin(2kx_2)) \end{aligned} \tag{C.5}$$

$$\begin{aligned} real(P_{12}) &= P_{AA} + P_{BB}\cos(k\Delta x) \\ &\quad +2(real(P_{AB})\cos(k\Delta x) \\ &\quad -imag(P_{AB})\sin(k\Delta x)) \end{aligned} \tag{C.6}$$

$$imag(P_{12}) = (P_{AA} - P_{BB})\sin(k\Delta x) \tag{C.7}$$

where P_{AA} and P_{BB} are the power spectra of A and B respectively, and P_{AB} is the cross spectra.

The reflection coefficient can be expressed as the reflected power over the incident power or

$$r = \frac{P_{BB}}{P_{AA}}$$

by substituting equations C.5 through C.7 to solve for P_{AA} and P_{BB} the reflection coefficient can be expressed

$$r = \frac{P_{11} + P_{22} - 2Real(P_{12}\cos(k\Delta x) + 2Imag(P_{12})\sin(k\Delta x)}{P_{11} + P_{22} - 2Real(P_{12}\cos(k\Delta x) - 2Imag(P_{12})\sin(k\Delta x)}. \qquad \text{(C.8)}$$

Thus with the output of two accelerometers, the reflection coefficient could be determined.

Vita

Carol Jaeger Wynn was born in Fort Belvoir, Virginia in June of 1963 to Jerome and Clara Jaeger. She was reared in Wisconsin, Florida and Virginia. She graduated from Midlothian High School in 1981. She attended Virginia Tech from 1981 to 1985 when she received her Bachelor of Science in Mechanical Engineering. She worked for a year at Norfolk Naval Shipyard in Portsmouth and then returned to Virginia Tech in the Fall of 1986. She received her Master of Science in Mechanical Engineering in the Spring of 1988. She married Dr. Robert H. Wynn, Jr. in December of that year.